Geomorphology

Middle-late Pleistocene chronology of palaeoshorelines and uplift history in the low-rising to stable Apulian foreland: overprinting and reoccupation

--Manuscript Draft--

Manuscript Number:	GEOMOR-12002R3
Article Type:	Research Paper
Keywords:	synchronous correlation method; palaeoshorelines; MIS 5.5; MIS7.3.
Corresponding Author:	Vincenzo De Santis University of Bari Bari, ITALY
First Author:	Vincenzo De Santis
Order of Authors:	Vincenzo De Santis
	Giovanni Scardino
	Giovanni Scicchitano
	Marco Meschis
	Paolo Montagna
	Edwige Pons-Branchu
	Josè Eugenio Ortiz
	Yolanda Sanchez-Palencia
	Massimo Caldara
Abstract:	To refine knowledge about terrace phases and uplift history for a tectonically poor deformed region, we apply the synchronous correlation method to reconstruct the chronology of a poorly constrained sequence of raised palaeoshorelines on the Apulian foreland, southern Italy. This work uses new chronological constraints obtained by amino acid racemisation (AAR) and isoleucine/alloisoleucine epimerisation (IE) on Patella spp., Thetystrombus latus (Gmelin), Glycymeris sp., and ostracods and U-series dating on corals Hoplangia durotrix Gosse and Cladocora caespitosa Linneo. This procedure provides a quantitative estimate of the vertical movements and associated rates within a region of the Apulian foreland. The synchronous correlation method uses sea-level highstands and uplift rate(s) as inputs; in particular, for sea-level highstands, the inputs are the age of the highstands and the sea-level elevation of the highstands relative to the present-day sea level. The output is a set of currently expected elevations of each sea-level highstand (the present elevations of palaeoshorelines). We then used regression analysis to assess the robustness between our observed palaeoshorelines and expected elevations of sea-level highstands. Our results show that the best fitting scenario is obtained using the sea-level curves of (i) Waelbroeck et al. (2002) from present to 410 ky BP and (ii) Rohling et al. (2014) from 410 to 590 ky BP as inputs for our synchronous correlation method, with uplift rates ranging from 0.09 mm/y to 0.07 mm/y with a mean value of 0.08 mm/y from 590 ky BP onwards. We recognised palaeoshorelines in the field belonging to the following highstands: 120 ky BP (MIS 5.5, second peak), 127 ky BP (MIS 5.5, first peak), 212 ky BP (MIS 7.3), 330 ky BP (MIS 9.3), 410 (MIS 11), 525 ky BP (MIS 13.3), and 590 ky BP (MIS 15). Our results show field observations of the reoccupation effect of younger palaeoshorelines over older ones due to the relatively slow uplift rates measured in the investigated area as predicted by our synchronous correlation method. In particular, we show a well-mapped and described reoccupation of the MIS 5.5 palaeoshoreline over the MIS 7.3 palaeoshoreline, constrained by new absolute dating. In addition, the data from the Apulian foreland suggest an MIS 7.3 highstand close to the present sea level.

We are very grateful to the reviewers for their suggestions to further improve the manuscript. In this R2 version, all suggestions made by the reviewers have been accepted

We apply the synchronous correlation method in order to reconstruct palaeoshorelines

Three palaeoshorelines dating back to two highstand of MIS 5.5

Re-occupation of older ~~younger~~ palaeoshorelines by younger ~~over older ones~~ due to low uplift rates

Sea level for the MIS 7.3 highstand close to the present sea level

Abstract

To refine knowledge about terrace phases and uplift history for a tectonically poor deformed region, we apply the synchronous correlation method to reconstruct the chronology of a poorly constrained sequence of raised palaeoshorelines on the Apulian foreland, southern Italy. This work uses new chronological constraints obtained by amino acid racemisation (AAR) and isoleucine/alloisoleucine epimerisation (IE) on Patella spp., *Thetystrombus latus* (Gmelin), *Glycymeris* sp., and ostracods and U-series dating on corals *Hoplangia durotrix* Gosse and *Cladocora caespitosa* Linneo. This procedure provides a quantitative estimate of the vertical movements and associated rates within a region of the Apulian foreland. The synchronous correlation method uses sea-level highstands and uplift rate(s) as inputs; in particular, for sea-level highstands, the inputs are the age of the highstands and the sea-level elevation of the highstands relative to the present-day sea level. The output is a set of currently expected elevations of each sea-level highstand (the present elevations of palaeoshorelines). We then used regression analysis to assess the robustness between our observed palaeoshorelines and expected elevations of sea-level highstands. Our results show that the best fitting scenario is obtained using the sea-level curves of (i) Waelbroeck et al. (2002) from present to 410 ky BP and (ii) Rohling et al. (2014) from 410 to 590 ky BP as inputs for our synchronous correlation method, with uplift rates ranging from 0.09 mm/y to 0.07 mm/y with a mean value of 0.08 mm/y from 590 ky BP onwards.

We recognised palaeoshorelines in the field belonging to the following highstands: 120 ky BP (MIS 5.5, second peak), 127 ky BP (MIS 5.5, first peak), 212 ky BP (MIS 7.3), 330 ky BP (MIS 9.3), 410 (MIS 11), 525 ky BP (MIS 13.3), and 590 ky BP (MIS 15). Our results show field observations of the reoccupation effect of younger palaeoshorelines over older ones due to the relatively slow uplift rates measured in the investigated area as predicted by our synchronous correlation method. In particular, we show a well-mapped and described reoccupation of the MIS 5.5 palaeoshoreline over the MIS 7.3 palaeoshoreline, constrained by new absolute dating.

In addition, the data from the Apulian foreland suggest an MIS 7.3 highstand close to the present sea level.

Revised manuscript with changes marked

Middle-late Pleistocene chronology of palaeoshorelines and uplift history in ~~a~~ the low-rising to stable Apulian foreland: overprinting and reoccupation

Vincenzo De Santis [a*], Giovanni Scardino [a], Giovanni Scicchitano [a] Marco Meschis [b], Paolo Montagna [c], Edwige Pons-Branchu [d]

José E. Ortiz [e], Yolanda Sánchez-Palencia [e], Massimo Caldara [a]

[a] Dipartimento di Scienze della Terra e Geoambientali, Università degli Studi di Bari "Aldo Moro", Via Orabona 4, 70125 Bari, Italy;

[b] Istituto Nazionale di Geofisica e Vulcanologia, Sezione di Palermo, via Ugo La Malfa, 153, 90146 Palermo, Italy;

[c] Istituto di Scienze Polari (ISP), Consiglio Nazionale delle Ricerche (CNR) Via Gobetti 101, 40129 Bologna, Italia

[d] LSCE/IPSL, UMR 8212, CEA-CNRS-UVSQ, Université Paris-Saclay, Chemin de Saint Aubin - RD 128, F-91191 Gif sur Yvette Cedex, France

[e] Biomolecular Stratigraphy Laboratory, Madrid School of Mines, C/Rios Rosas 21, E-28003 Madrid, Spain.

[*]Corresponding author. Tel.: 0039 080 5442471; Fax: 0039 080 5442625
E mail address: vincenzo.desantis@uniba.it

Abstract

To refine knowledge about terrace phases and uplift history for a tectonically poor deformed region, we apply the synchronous correlation method to reconstruct the chronology of a poorly constrained sequence of raised palaeoshorelines on the Apulian foreland, southern Italy. This work uses new chronological constraints obtained by amino acid racemis~~z~~ation (AAR) and isoleucine/alloisoleucine epimeris~~z~~ation (IE) on Patella spp., *Thetystrombus latus* (Gmelin), *Glycymeris* sp., and ostracods and U-series dating on corals *Hoplangia durotrix* Gosse and *Cladocora caespitosa* Linneo. This procedure provides a quantitative estimate of the vertical movements and associated rates within a region of the Apulian foreland. The synchronous correlation method uses sea-level highstands and uplift rate(s) as inputs; in particular, for sea-level highstands, the inputs are the age of the highstands and the sea-level elevation of the highstands relative to the present-day sea level~~-~~. The output is a set of currently expected elevations of each sea-level highstand (the present elevations of palaeoshorelines). We then used regression analysis to assess the robustness between our observed palaeoshorelines and expected elevations of sea-level highstands. Our results show that the best fitting scenario is obtained using the sea-level curves of (i) Waelbroeck et al. (2002) from present to 410 ky BP and (ii) Rohling et al. (2014) from 410 to 590 ky BP as inputs for our synchronous correlation method, with uplift rates ranging from 0.09 mm/y to 0.07 mm/y with a mean value of 0.08 mm/y from 590 ky BP onwards.

We recognised palaeoshorelines in the field belonging to the following highstands: 120 ky BP (MIS 5.5, second peak), 127 ky BP (MIS 5.5, first peak), 212 ky BP (MIS 7.3), 330 ky BP (MIS 9.3), 410 (MIS 11), 525 ky BP (MIS 13.3), and 590 ky BP (MIS 15). Our results show field observations of the reoccupation effect of younger palaeoshorelines over older ones due to the relatively slow uplift rates measured in the investigated area as predicted by our synchronous correlation method. In particular, we show a well-mapped and described reoccupation of the MIS 5.5 palaeoshoreline over the MIS 7.3 palaeoshoreline, constrained by new absolute dating.

In addition, the data from the Apulian foreland suggest an MIS 7.3 highstand close to the present sea level.

Keywords: synchronous correlation method, palaeoshorelines, MIS 5.5, MIS7.3, reoccupation, overprinting,

1 INTRODUCTION

Past interglacial periods have attracted the scientific community because they are used to study the climate system during warm intervals, and this is crucial for understanding the interaction mechanisms between natural climatic and anthropogenic forcings. Some of the most prominent evidences of past interglacial periods are raised marine terraces and palaeoshorelines, which result from the interactions between sea-level changes and tectonic processes (uplift) during the Quaternary (Lajoie, 1986). Among the assessments of past sea-level changes, the study of these geomorphic features is fundamental to understanding vertical land movements (Grant et al., 2014; Murray-Wallace and Woodroffe, 2014; Marra et al., 2016, 2019, 2020; Cerrone et al., 2021a) and the associated rates of crustal uplift or subsidence (Ferranti et al., 2006; Caputo et al., 2010; Meschis et al., 2020).

Our study area is located in the southern part of the Apulian foreland (southern Italy), the Salento Peninsula. Although the extensive presence of preserved marine terraces has been documented throughout the central-southern Apulian foreland, that is, in the Murge and Salento highlands (Ciaranfi et al., 1992), there is a lack of knowledge about their ages and the associated rates of crustal uplift over time. Indeed, the chronology of uplifted palaeoshorelines is still a matter of debate within the investigated area, where only a few works have associated preserved palaeoshorelines with specific highstands (Antonioli et al., 2018; De Santis et al., 2021a). This also supplements the ongoing debate on whether regional uplift rates affecting the Apulian foreland are constant or fluctuatinged over time (Ferranti and Oldow, 2006; De Santis et al., 2021a, b). The Apulian foreland shows slow uplift rates, suggesting that processes of reoccupation and overprinting of older palaeoshorelines by younger ones can be fairly common (Westaway, 1993; Ascione and Romano, 1999; Roberts et al., 2013). If this process is not taken into account, geoscientists may be likely to (i) assign erroneous ages to undated marine terraces, and, consequently, (ii) estimate inaccurate uplift rates (e.g., Roberts et al., 2013). For instance, when a sequential correlation approach is applied to model sequences of preserved marine terraces (see Roberts et al., 2013 for a critical analysis of this approach) without considering the reoccupation problem, unrealistic uplift rate changes may be reconstructed (e.g., Roberts et al., 2013; Meschis et al., 2018). The sequential correlation method is based on the idea that, given a dated paleoshoreline, the next higher and older paleoshoreline is likely to belong to the next older sea-level highstand (e.g., Armijo et al., 1996; Bianca et al., 2011; Gallen et al., 2014). Unrealistic variations in uplift rates result from not taking into account the “reoccupation problem” (e.g., Roberts et al. 2013 and Robertson et al. 2019) and have not been reported in the vicinity of active seismogenic sources worldwide to date (Cowie and Roberts, 2001; Cowie et al., 2012; Meschis et al., 2020).

Therefore, applying a synchronous correlation method and overcoming the reoccupation problem, becomes crucial when raised palaeoshorelines are used for a better assessment of tectonic and geodynamic implications, as shown by previous studies (e.g., Roberts et al., 2013; Meschis et al., 2018; Robertson et al., 2019; Meschis et al., 2020). For this reason, we have undertaken an in-depth study of uplifted palaeoshorelines and their associated sedimentary deposits within a coastal sector of the Salento Peninsula (Fig. 1) to provide new insights into their morphology and chronology. Our study aims to (i) map the palaeoshoreline elevations, (ii) provide new chronological constraints for undated palaeoshorelines, and (iii) refine the uplift history of the region. We carried out intensive field surveys and detailed topographic analysis using Digital Terrain Models (DTMs) obtained from high-resolution Light Detection And Ranging (LiDAR) data. Thus, we mapped palaeoshorelines (e.g., Armijo et al., 1996; Roberts et al., 2013) and ground-truthed them in the field with the associated deposits, whereif present. We then applied a synchronous correlation method to correlate multiple uplifted palaeoshorelines unevenly spaced in elevations uplifted palaeoshorelines and multiple unevenly spaced in time sea-level highstands (Waelbroeck et al., 2002; Rohling et al., 2014) by iterating uplift rates driven by new chronological constraints, obtained using amino acid racemis~~z~~ation (AAR), isoleucine/alloisoleucine epimeris~~z~~ation (IE), and U-series dating. We then assessed the robustness of our correlations between multiple GIS and field-mapped palaeoshoreline elevations and multiple predicted sea-level highstand elevations iteratively calculated through linear regression analysis. ~~Our results reveal very similar uplift rates (0.09 mm/y from 590 to 130 ky BP and 0.07 mm/y from 130 ky BP onwards), with a mean value of 0.08 mm/y since 590 ky BP.~~ Finally, we discuss our results in terms of local and regional tectonic implications within the -almost tectonically undeformed Apulian foreland.

2 GEOLOGICAL SETTING AND PREVIOUS RESEARCH

The Apulian foreland, which is composed of Mesozoic limestone (Fig. 1A) overlain by Plio-Pleistocene coastal deposits, has experienced uplifting since the middle-late Pleistocene (Azzaroli, 1968; Iannone and Pieri, 1979; Ciaranfi et al., 1992; Ricchetti et al., 1992; Doglioni et al., 1994, 1996; De Santis and Caldara, 2016; Valenzano et al., 2018; De Santis et al., 2020 a, b)

To date, the Apulian foreland has been characterised by a scarcity of reliable documentation of palaeoshorelines and chronological data concerning their formation during the middle-late Pleistocene (Cerrone et al., 2021b). Indeed, for this period, the well constrained chronological data are those related to some areas with extensive presences of Quaternary terrace deposits (Brückner, 1980; Boenzi et al., 1986; Hearty and Dai Pra, 1992; Belluomini et al., 2002; Caldara et al., 2003; Zander et al., 2006; Caldara et al., 2013; Amorosi et al., 2014; De Santis et al., 2010, 2013, 2014a, b, 2018, 2020c, 2021b; Negri et al., 2015). In particular, close to the city of Gallipoli, several marine and aeolian geological units with interbedded palaeosols, all dating back to MIS 5.5, have been described (Hearty and Dai Pra, 1992). Similarly, stratigraphic deposits revealing sea-level oscillations during the Last Interglacial Maximum (LIM) have been described in other localities in Italy (Hearty and Dai Pra, 1987), Mallorca (Hearty, 1987), Spain (Hearty et al., 1987), and Tunisia (Hearty et al., 1986).

In any case, except fo~~t~~r the investigations by De Santis et al. (2021a), all the above-mentioned studies describe and date preserved marine terrace deposits; yet their correlations with associated palaeoshoreline locations and elevations are poorly constrained and, therefore, a ~~-~~reliable possibility of reconstructing the current position of the past sea-level highstands lacks.

As a consequence of this lack of knowledge, most uplift rates of the Apulian foreland have been estimated only for the late Pleistocene and almost exclusively along the Ionian coast based on the elevations of the marine terrace deposits related to the LIM (MIS 5.5) (Hearty and Dai Pra, 1992; Belluomini et al., 2002; Ferranti et al., 2006). These data show a decreasing uplift rate from northwest to southeast, from a maximum uplift rate of 0.31 mm/yr northwest of Taranto (Ponte del Re locality) to a subsidence rate ~~minimum~~ of ~~-~~0.03 mm/yr at Torre Castiglione.

2.1 Geological and geomorphological setting of the study area

The study area is a ca. 30 km long coastal stretch (Figs. 1B, 2A), lying close to the city of Gallipoli and located along the Ionian coast of the Salento Peninsula, which forms the southern portion of the Apulian foreland. The morpho-structural setting of the Salento Peninsula is identified by the Serre Salentine domain, which consists of NW–SE-oriented horsts and grabens~~,~~ (Ricchetti and Ciaranfi, 2013; Fig. 1B); the horsts, whose top surfaces are flat and slightly tilted towards the SW, consist of Mesozoic or Palaeogene-Miocene carbonate units; the grabens contain Plio-Pleistocene deposits belonging to the Bradanic Trough cycle and marine terrace deposits, suggesting middle-late Pleistocene regional tectonic uplift.

From geological and geomorphological points of view, the study area can be divided into two main sectors: a sector from Montagna Spaccata (included) northwards and a sector to the south of the Montagna Spaccata locality (Fig. 2A, B). The sector from Montagna Spaccata northwards coincides with a flank of a horst that represents one of the few coastal stretches with high rocky coasts on the entire Apulian Ionian side. It is characterised almost exclusively by outcrops of Mesozoic limestone (Fig. 1C), with small patches of marine terrace deposits, which have never been mapped to date. Only in the coastal stretch between Santa Caterina and Santa Maria al Bagno, Miocene-aged calcarenites and sands crop out (Fig. 1C) (~~;~~ more inland, Plio-Pleistocene calcarenites crop out (Largaiolli et al., 1969; Ciaranfi et al., 1992; Boenzi et al., 2010).

The sector south of Montagna Spaccata coincides with the terminal part of a graben, characterised by very gentle slopes. Here, Quaternary marine terrace deposits crop out overlying regressive calcarenite deposits of the Bradanic Trough cycle (Caldara et al.,1981; Hearty and Dai Pra, ~~(~~1992). These regressive deposits are well documented in some quarries on the Gallipoli-Alezio ridge (Fig. 2A, B). They constitute the local substrate of the terrace deposits.

Figure 1

3 METHODS

3.1 Field survey and digital terrain model (DTM)

We mapped palaeoshorelines and their associated deposits (see Table 1, Section 4.1) by combining field mapping and GIS analysis using high-resolution Digital Terrain Models (2-m resolution along the coastline and 8-m resolution farther inland). DTMs were extracted by high-resolution Light Detection And Ranging (LiDAR) provided by the "Ministero dell'Ambiente e della Tutela del Territorio e del Mare" (Fig. 2A, B)~~,~~ and acquired during the years 2008-2009. The elevations of LiDAR data were reported on the geodetic reference datum ITALGEO2005~~,~~ and showed a vertical accuracy of ±0.15 m (*Progetto PST - Dati Lidar*, 2021). The tidal datum is referred to the Mean Low Water Springs (MLWS) that, for the study area, presents an uncertainty of ±0.151 m. Considering the different resolutions of the cell width for the two different DTMs (on the coast and inland), the vertical uncertainty of the DTM with 2-m resolution resulted equal to ±0.30 m, while the vertical uncertainty of the DTM with 8-m resolution resulted equal to ±1.0 m.

Elevations of palaeoshorelines were obtained using a Global Position System Real-Time Kinematic (GPS-RTK) receiver, with an accuracy ranging between 0.05 and 0.1 m.

A survey with total stations was performed to assess the elevations of the palaeoshorelines located on the steep slopes, where it was difficult to use the GPS-RTK receiver. The accuracy of the total station ranged between 0.001 and 0.005 m, depending on atmospheric perturbations. Field geological/geomorphological indicators used to identify palaeoshorelines include inner_margins, notches, sea caves, bands of lithophagid borings, marine deposits on wave- cut platforms (Ferranti et al., 2006; Vacchi et al., 2016; Robertson et al. 2020), and relict littoral ridges (*sensu* Ricchetti and Ciaranfi, 2013).

The margin of error related to the palaeoshoreline elevations mapped in the field is prominently linked to the uncertainty of associated markers. Lithophagids colonis~~z~~e calcareous rocky coasts down to deeper than 30 m below the sea level of ~~calcareous rocky coasts~~ and can be detected up to 2 m below sea level (~~Pirazzoli *et alii*, 1999;~~ Ferranti et al.~~*ii*~~, 2006). However, if the upper limit of *Lithophaga* populations is clearly visible and well recognised, it can represent a reliable sea-level indicator (Evelpidou et al., 2012), and the margin of error associated with lithophagid borings was assumed to be ± 2 m at the upper limit (Kershaw, 2000; Ferranti et al., 2006;~~ Kershaw, 2000;~~ Scicchitano et al., 2011; Rovere et al., 2015~~; Scicchitano et al., 2011~~)

The margin of error associated with the tidal notches, when used as palaeo-sea-level benchmarks in the Mediterranean depend~~en~~s on the local tidal range, which is ~0.4 m (Antonioli et al., 2015, 2018). Indeed, the base of a tidal notch is considered the best and most precise marker of the average palaeo-sea-level because its width is closely linked to the local tidal phase (Antonioli et al., 2015; Rovere et al., 2016; Lorscheid et al., 2017).

The elevation of beach facies with the presence of *Thetystrombus latus* (Gmelin) (previously known as *Strombus bubonius*) and senegalensis fauna (Gignoux, 1913; Zazo et al., 2003; Taviani, 2014; Benjamin et al., 2017) can indicate a palaeo-beach deposit (Benjamin et al., 2017), yet they do not always indicate a well-approximated palaeo-sea-level.

Formatted: Font: Italic

Formatted: Font: Not Italic

Figure 2

3.2 Chronological analyses

Chronological analyses were performed on deposits that~~which~~, from field observations, seem to be associated with palaeoshorelines ~~recognised~~ and, where present, on substrate deposits.

3.2.1 Amino acid racemis~~z~~ation (AAR) and isoleucine/alloisoleucine epimeris~~z~~ation (IE) analyses

We applied amino acid racemis~~z~~ation and isoleucine/alloisoleucine epimeris~~z~~ation to shells of (see Table 2, Section 4.3):

1) ostracods for lacustrine and marine deposits where no marine bivalve *Glycymeris* spp. were present;
2) marine bivalve *Glycymeris* spp. (where present) for marine deposits;
3) continental gastropod Helicidae for palaeosols.

For IE applied to *Glycymeris* sp., a hollow diamond drill was used to remove a discoid sample (8 mm in diameter) from the apexes of shells. Outer layers (approximately 20-30%) were removed after chemical etching with 2 N HCl. Afterward, 10-20 mg of sample was collected~~,~~ and ~~in turn~~ divided into a certain number of subsamples (Tab.2A).

For AAR applied to ostracods, sediment samples were washed with running water and sieved. After drying, the sediment remnant (>0.062 mm) was analysed under a binocular microscope, and ostracod carapaces were picked with a needle. The ostracod shells were carefully sonicated and cleaned with water to remove sediment and left for 2-3 hours in hydrogen peroxide to remove organic matter. Only translucent individuals were selected for the analysis, giving a certain number of specimens (subsamples; Tab 2A) for each sample of sediment.

For both *Glycymeris* sp. and ostracods, amino acid concentrations were quantified using Reverse Phase-High Performance Liquid Chromatography (RP-HPLC) following the sample preparation protocol described in Kaufman and Manley (1998) and Kaufman (2000). This procedure involves hydrolysis, performed under an N_2 atmosphere in 20 µl/mg 7 N HCl. The hydrolysates were evaporated to dryness in vacuo and then rehydrated in 10 µl/mg 0.01 N HCl with 1.5 mM sodium azide and 0.03 mM L-homoarginine (internal standard).

Samples were injected into an Agilent HPLC-1100 equipped with a fluorescence detector. Excitation and emission wavelengths were programmed at 335 and 445 nm, respectively. A Hypersil BDS C18 reverse-phase column (5 µm; 250 x 4 mm i.d.) was used for the analysis.

Derivatis~~z~~ation occurred before injection by mixing the sample (2 µl) with the precolumn derivatis~~z~~ation reagent (2.2 µl), which comprised 260 mM isobutyryl-L-cysteine (chiral thiol) and 170 mM o- phtaldialdehyde dissolved in 1.0 M potassium borate buffer solution at pH 10.4. Eluent A consisted of 23 mM sodium acetate with 1.5 mM sodium azide and 1.3 µM EDTA, adjusted to pH 6.00 with 10 M sodium hydroxide and 10% acetic acid. Eluent B was HPLC-grade methanol, and eluent C consisted of HPLC-grade acetonitrile. A linear gradient was performed at 1.0 ml/min and 25 °C, from 95% eluent A and 5% eluent B upon injection to 76.6% eluent A, 23% eluent B, and 0.4% eluent C at 31 min.

Some analytical subsamples seemed to have suffered some contamination and were rejected for the age calculation. Following Kaufman (2006), we used the cut-off value of 0.8 in the concentration of L-Ser to that of L-aspartic acid to determine anomalous samples as Ser decomposes rapidly, and excessive amounts indicate contamination by modern amino acids.

For *Glycymeris* sp., the mean D/L values of three amino acids (isoleucine, aspartic acid, and glutamic acid) were obtained, because they are the most appropriate amino acids for dating most marine molluscs because of their abundance and steady rates of racemis~~z~~ation/epimeris~~z~~ation (Torres et al., 2000; Ortiz et al., 2015). For *Glycymeris* sp., an age calculation algorithm based on D/L values does not exist, but the extensive use of AAR has allowed the establishment of a general aminostratigraphical framework of Pleistocene palaeoshorelines in the Mediterranean basin based on aminozones (Hearty et al., 1986; Hearty, 1987; Hearty and Dai Pra, 1992; Torres et al., 2000). For *Glycymeris* sp. shells, we referred to the aminozones based on values of isoleucine/alloisoleucine epimerisation (D/L = D-aIle/L-Ile), as they are commonly used for chronological purposes in the Mediterranean realm. In this regard, isoleucine/alloisoleucine epimerisation values obtained by RP-HPLC required transformation to be compared with D-aIle/L-Ile values measured by Gas Chromatography (GC) (Wehmiller, 1984; Torres et al., 1997; Ortiz et al., 2004; Wehmiller et al., 2010). Thus, the isoleucine/alloisoleucine epimerisation (D-aIle/L-Ile) values ranging between 0.35 and 1.1 by RP-HPLC were approximately 0.10 lower than those obtained by GC, i.e., D-aIle/L-Ile$_{GC}$ = D-aIle/L-Ile$_{HPLC-IE-LC}$ + 0.10.

In this regard, according to Powell et al. (2013) for RP-HPLC, D-aIle/L-Ile values were, on average, 30% (range: 15-40%) higher compared to those by GC, in coincidence with the results provided by Ortiz et al. (2004). In addition, Torres et al. (2013) provide a comparison of D/L values obtained with RP-HPLC and GC in *Glycymeris* shells from the same localities in the Mediterranean realm. For comparison, according to Witeacre et al. (2017), paired Ion Exchange Liquid Chromatography (IE-LC) and RP-HPLC analyses show that D-aIle/L-Ile values can be confidently converted to their equivalent D/L values for isoleucine, with 2s uncertainties of ±35%, although this value is markedly lower for the range of values observed in this study.

For ostracods, the aminochronology was obtained using D/L values of aspartic acid and glutamic acid because they account for an important percentage of the amino acid content of most ostracod valves and are the ones that racemize faster (Kaufman, 2000; Bright and Kaufman, 2011; Ortiz et al., 2013). With ostracods, it has been possible to obtain numerical ages using age calculation algorithms that convert aspartic acid and glutamic acid D/L ratios into numerical ages. These algorithms are those established by Ortiz et al. (2004) for the central and southern parts of the Iberian Peninsula and have already been applied extensively in southern Italy (De Santis et al., 2010, 2013, 2014b, 2018, 2020c; Caldara et al., 2013).

For Helicidae, the mean D/L values of five amino acids (isoleucine, aspartic acid, glutamic acid, leucine, and phenylalanine) have been obtained because, according to Torres et al. (1997), they are reliable for dating terrestrial gastropods. The numerical age was calculated by introducing the Asp,

Formatted: Subscript

Formatted: Subscript

Formatted: Subscript

Formatted: Font: Italic

Glu, Leu, Ile, and Phe D/L values into the age-calculation algorithms established by Torres et al. (1997) for gastropods in the central and southern parts of the Iberian Peninsula.

In this work, we also report previous AAR analyses carried out in the sector from Montagna Spaccata northwards (MS1-2, MS2-1, and MS6-1 samples in Table 2A) (De Santis et al., 2021a) based on isoleucine/alloisoleucine epimerisation. These analyses were carried out on shells of *Patella aspera* (Röding), *Patella caerulea* Linneo, *Patella* sp., and *Thetystrombus latus* (Gmelin). The reliability and results of these chronological analyses have already been published and discussed in De Santis et al. (2021a).

3.2.2 U–Th series dating

The following fragments of corals were prepared for U-series dating (see Table 2, Section 4.3):

1) two fragments of *Cladocora caespitosa* Linneo from sample G17-2b (Punta Pizzo locality; Figs. 2A, 2C, 3);

2) one fragment of *Hoplangia durotrix* Gosse from sample MS1-1 (Montagna Spaccata locality; Figs. 2A, 2C, 5);

3) one fragment of *Hoplangia durotrix* Gosse from sample G20-1 (Torre Sabea locality; Figs. 2A, 2C, 3; and

4) two fragments of *Cladocora caespitosa* Linneo from sample MS11-1 (Uluzzo locality Fig. 2A).

In particular, for all samples, we selected only a portion of the thecal wall and removed the septa and extraneous detrital material using a dental drill with a diamond-encrusted blade operated under a stereomicroscope. Any further contamination was removed by hand picking. Subsamples were crushed into coarse chips (ca. 1-2 mm in size) using an agate mortar and pestle, ultrasonicated in Milli-Q water, and dried in an oven at 50 °C overnight. Each sample (~50 mg) was dissolved in dilute HCl in a beaker in which a known amount of ^{229}Th, ^{233}U, and ^{236}U spikes were previously added. This tracer was calibrated against a Harwell Uraninite solution (HU-1) assumed to be at secular equilibrium. After FeOH precipitation, uranium and thorium fractions were separated and purified using Eichrom UTEVA ion exchange chromatography resin in nitric media following the procedure described in Pons-Branchu et al. (2014). The U and Th measurements were carried out on a ThermoScientific Neptune Plus MC-ICPMS installed at the Laboratoire des Sciences du Climat et de l'Environnement (LSCE, Gif-sur-Yvette, France), fitted with an Aridus II Desolvating Nebulizer system, and a jet pump interface, following the procedure described in Pons-Branchu et al. (2014). After blank and fractionation corrections, the activity ratios for $^{230}Th/^{238}U$, and $^{234}U/^{238}U$ were determined using the decay constants and reference values given in Cheng et al. (2013) and Jaffey et al. (1971).

The $^{230}Th/U$ ages were calculated through iterative age estimation (Ludwig and Titterington, 1994). The samples have $\delta^{234}U$ (0) values between 150.54 ± 2.65 and 206.6 ± 3.67‰, which are higher than those of modern seawater (146.8‰; Andersen et al., 2010), indicating that they might have experienced open-systems U-series behaviour, likely caused by alpha recoil mobilisation of ^{234}Th and ^{230}Th (Thompson et al., 2003). We tentatively corrected U-series ages for open system using the open-system age equations of Thompson et al. (2003), even though our limited dataset does not allow us to confirm the expected mixing slopes predicted by the Thompson model. Overall, both conventional and open-system U-series ages (data not shown) fall within the same time interval.

The ^{232}Th concentrations range between 8.26 and 63.81 ppb, with $^{230}Th/^{232}Th$ ratios varying between 158.71 and 1544,11, suggesting much less detrital contamination. We corrected for detrital Th assuming an initial $^{230}Th/^{232}Th$ activity ratio of 7 ± 50% (Table 2C).

3.3 Synchronous correlation method for model multiple sea-level highstands and multiple palaeoshorelines

Glacio-eustatic sea-level highstands combined with tectonic uplift produce geomorphic features named marine terraces and/or palaeoshorelines (Lajoe, 1986). Yet, the synchronous correlation method is derived from the idea that glacio-eustatic sea-level highstands are not equally spaced in time (Rohling et al. 2014); this suggests that preserved raised marine terraces and their inner edges (or palaeoshorelines) are not equally spaced in elevation, assuming the simplest tectonic scenario of constant uplift rates through time (Roberts et al., 2009, 2013). Furthermore, the synchronous correlation method is not sensitive if rates of uplift are constant or fluctuating th~~e~~rough time (Meschis et al. 2020, 2022). More importantly, this method has also been applied when fault-controlled uplift rates change over time, as shown by previous investigations in Greece and southern Italy (Roberts et al., 2009; Meschis et al., 2020). Indeed, the reoccupation of older marine terraces by younger terraces within relatively slow uplifting regions may occur for both constant and fluctuating uplift scenarios (Roberts et al., 2009, 2013). Furthermore, absolute dated marine terrace deposits, which act as age controls, drive the uplift rate iteration; this permits us to first test the simplest hypothesis of a constant uplift rate over time and assess if the iteratively calculated sea-level highstand elevations match the mapped palaeoshoreline elevations (Roberts et al., 2013). If a robust correlation is not claimed for the simplest scenario, then a changing uplift rate over time is tested, with iterations of uplift rates driven by age controls aiming to find the best match between expected and field-mapped palaeoshoreline elevations (Roberts et al., 2013).

To apply this method, we use a “terrace calculator” built in Excel, which uses sea-level highstands (Roberts et al., 2013; Robertson et al., 2019) and the uplift rate (UR) as inputs; the method allows us to calculate the present expected~~predicted~~ elevation (PE) of each sea-level highstand (that is, the present elevations of palaeoshorelines) using the age of the highstand (T) and the sea-level elevation of the highstand relative to the sea level of today (SLT) following this formula: PE = (UR x T) + SLT. Indeed, this approach forces the user to maximise the coefficient of determination (R^2 value) for linear regression analysis through data, including the “observed” elevations and the “expected” elevations of all palaeoshorelines (Roberts et al., 2013; Meschis et al., 2018; Robertson et al. 2019; Meschis et al., 2020).

The output of the terrace calculator is a set of expected elevations~~-~~for sea-level highstands (that is, a set of ~~expected palaeoshoreline elevations~~PE); we consider acceptable a difference up to 10 m between expected and observed palaeoshoreline elevations, based on the uncertainties of the sea-level curve that are used regarding both the sea-level highstands and their ages. If this is the case, we assign our observed palaeoshorelines to expected highstands.

In this paper, we have used well-known sea-level curves for this method, such as (i) Waelbroeck et al. (2002) from present to 410 ky BP and (ii) Rohling et al. (2014) from 410 to 590 ky BP, which have already proven suitable for correlating marine terraces and/or palaeoshorelines to sea-level highstands (Roberts et al., 2009, 2013; De Giosa et al., 2019; Robertson et al., 2019; Meschis et al., 2020; Ferranti et al., 2021).

Concerning the sea-level curve of Waelbroeck et al. (2002), the reported uncertainty about the sea level is ±13 m, while the uncertainty in the age of sea-level highstands is reported to be 800 yr during the last 30 kyr and1000 yr before.

Concerning the sea-level curve of Rohling et al. ~~il~~ (2014), the reported uncertainty in sea level is 6 m, while the uncertainty in the age of sea-level highstands is reported to be 4 kyr.

Formatted: Font: Not Italic

4 RESULTS

4.1 Palaeoshorelines recognised in the field and associated units

A detailed field survey of the study area reveals palaeoshoreline evidence, such as bands of lithophagid borings, ~~(~~especially *Gastrochaenolites torpedo* Kelly and Bromley due to *Lithophaga lithophaga* (Linneo~~)~~), relict littoral ridges, fossil tidal notches, sea caves, wave-cut platforms, and syn- wave- cut platform deposits. With the term littoral ridge, we mean an elongated landform higher than the surrounding area and linked to the presence of a palaeoshoreline. Therefore, this term indicates only a morphological element, without going into the specifics of the formation processes, according to Ricchetti and Ciaranfi (2013). Below, we describe, from the lowest to highest, palaeoshorelines identified in the field (Fig. 3) and sedimentary units (where present), which, from field observations, can be associated with them (Table 1).

Table 1

Fig. 3

*4.1.1 Palaeoshoreline PS1 (***elevation***: ∼+6) and PS1marine unit (PS1mu)*.

This palaeoshoreline has been mostly identified in the sector from Montagna Spaccata northwards, where it crops out with consistent lateral continuity. It is represented by a band of lithophagid borings in Mesozoic limestones (Fig. 4A, B) and is characterised by progressive growth in the density of borings up to an upper band with the highest density in the entire study area. The upper limit of this band of maximum density of borings varies between +4 and +6 m above the present sea level (a.p.s.l.). This band of lithophagid borings has been considered to be indicative of a palaeoshoreline at +6 m, since from the upper limit of the lithophagid band, a subhorizontal line is defined, which is considered a reliable marker of a past mean sea-level position (Stiros et al., 1992; Ferranti et al., 2006~~; Stiros et al., 1992~~).

PS1 is associated with the PS1marine unit (PS1mu), which consists of greyish to reddish, well-cemented calciruditic deposit that is rich in bioclasts forming a transgressive unit upon the Mesozoic limestone basement; the centimetric-sized clasts are mainly made of fragments of Mesozoic limestone, rhodoliths, and heavily reworked and smoothed mollusc shells. The PS1mu has its highest point of outcrop exactly coinciding with the upper limit of the band of maximum density of borings. The PS1mu contains the following marine fauna:

-gastropods: *Patella* sp., *P. caerulea* Linneo, *Bolma rugosa* (Linneo), *Cerithium lividulum* Risso, *Melarhaphe neritoides* (Linneo), *Gibbula* sp., *Murex* sp., *Columbella rustica* (Linneo), *Hexaplex trunculus* (Linneo), *Thetystrombus latus* (Gmelin);

-bivalves: *Barbatia barbata* (Linneo), *Spondylus gaederopus* Linneo, *Clanculus corallinus* (Gmelin), *Striarca lactea* (Linneo), *Chlamys* sp., *Mytilus* sp., *Arca* sp.;

-coral: *C. caespitosa* Linneo.

The depositional environment of this unit was a high-energy marine infralittoral environment.

In the sector south of Montagna Spaccata, PS1 is visible only at Punta Pizzo (site G17, Fig. 4B; see Fig. 2A for its location) within the following stratigraphic succession from bottom up:

1) Reddish sands (RS); this unit consists of reddish cemented sands and calcarenites, with bioturbations (*Thalassinoides* type) concentrated especially in the lower part of the unit; the upper part of this unit is characterised by a considerable concentration of marine bivalve *Loripes orbiculatus* Poli in life positions.

The depositional environment, as suggested by the bioturbations and fossil content (Bromley and D'Alessandro, 1987), varies from a deeper marine environment to a more superficial, low-energy environment (Muddy Sand in Sheltered Areas; SVMC *sensu* Pérès, 1967).

Formatted: Font: Italic

2) Discontinuous Marine Clastic Unit (DMCU); this unit outcrops in the form of small patches that appear in abrupt contact on the RS. These patches are composed of calcirudite whose centimetre-sized clasts are mainly made up of fragments of Mesozoic limestone, rhodoliths, and the following marine fauna:

- bivalves: *Glycymeris* sp., *Callista chione* (Linneo), *Tellina planata* Linneo, and *Loripes orbiculatus* Poli.
- coral: *C. caespitosa* Linneo.

3) Lower Palaeosol (LPA). This unit consists of brick red to brown silty palaeosol, which reaches a maximum thickness of ca. 60 cm; cemented traces of roots are internally visible. The observed fossil fauna includes terrestrial gastropods, such as Helicidae, *Rumina decollata* (Linneo), *Pomatia elegans* (Müller), fragments of indeterminable pulmonate gastropods, and rare fragments of reworked marine molluscs.

The depositional environment of this unit is continental.

3) PS1marine unit (PS1mu); this unit contains similar sedimentary and fossiliferous evidence already described for the sector from Montagna Spaccata northwards. Indeed, at site G17, this unit is transgressive on all lower and older units (Mesozoic limestones, RS, DMCU, LPA), with clasts that

are immersed in a matrix of reddish sand/silt and/or calcarenite/calcisiltite due to the erosion of the underlying LPA. Towards the top, the matrix becomes yellowish to greyish, and the clasts appear less abraded. Throughout all the units, in addition to the reworked clasts, a synsedimentary marine fauna is present, consisting mainly of bivalves *Glycymeris* spp. and *Pecten* spp., and coral *C. caespitosa* Linneo. At site G17, as already observed in the sector from Montagna Spaccata northwards, the upper limit of the PS1mu outcrop roughly coincides with the lower part of the band of lithophagid borings of PS1. The unit was deposited following a marine transgression that allowed it to incorporate elements reworked by all the underlying units.

Figure 4

4.1.2 Palaeoshoreline PS2 (elevation: ∼+7.5) and PS2 marine unit (PS2mu).

This palaeoshoreline has been mostly identified in the sector from Montagna Spaccata northwards. In the sector south of Montagna Spaccata, PS2 can be mapped at Punta Pizzo only (Fig. 4B). In both sectors, PS2 is represented by a band of lithophagid borings grouped in discontinuous clusters within Mesozoic limestones whose upper limit is ca. +7.5 m. a.p.s.l. (Figs. 4B, 5).

Sometimes, this palaeoshoreline appears well separated from the previous palaeoshoreline, yet in places, we can also map scattered lithophagid borings in the Mesozoic limestone interposed between palaeoshorelines PS1 and PS2 (Fig. 4B).

PS2 is discontinuously associated with a strongly cemented coarse calciruditic deposit, with a reddish matrix composed of calcarenite/calcisiltite, which we call PS2marine unit (PS2mu). This deposit is transgressive on the Mesozoic limestone basement and has its topographically highest outcrop just below the discontinuous band of lithophagid borings, which represents PS2. The stratigraphic relationship between the PS2mu and PS1mu is not easily recognisable in the field; the PS2mu probably underlies the PS1mu, but we do not rule out a partial lateral transition between the two units.

The macrofauna of the PS2mu is not widespread throughout the unit but is localised in clusters where the following marine fauna has been recognised:

-gastropods: *Bolma rugosa* (Linneo), Hexaplex *trunculus* (Linneo), *Cerithium* sp., *Clanculus corallinus* (Gmelin);

-bivalves: *Striarca lactea* (Linneo), *Spondylus gaederopus* Linneo, *Mytilus* sp., and *Arca* sp.

Figure 5

4.1.3 Palaeoshoreline PS3 (elevation: ∼+15) and PS3 Mixed Deposit (PS3-MD)

This palaeoshoreline, along with PS1, is the most continuous and well recognised in the study area. On the other hand, the associated PS3 Mixed Deposit (PS3-MD) is certainly the most complex of all the recognised deposits associated with all palaeoshorelines recognised in this study, as it is constituted by several units. In fact, with the informal term "mixed deposit", we mean a deposit correlated to a palaeoshoreline and settled in different environments (es: marine +continental).

In the sector from Montagna Spaccata northwards, PS3 is represented by a band of lithophagid borings grouped (Fig. 6A) in discontinuous clusters within Mesozoic limestones whose upper limit is ca. +15 m. a.p.s.l. In some places, PS3 is represented by residual tidal notches or inner edges cut into the Mesozoic limestones. At the Montagna Spaccata locality (MS1 site; see Fig. 2A for the location), at the walls of the coastal road trench (Fig. 6B), PS3 is represented by (i) a well-preserved inner edge (probably an altered tidal notch) with lithophagid borings and (ii) an associated wave-cut platform some metres wide (both carved into the Mesozoic limestones), where fossil specimens of *Hoplangia durotrix* Gosse are preserved within some small depressions carved on the platform.

PS3-MD lies above the wave-cut platform, and in this sector, it is represented by a marine deposit that we named the PS3marine unit (PS3mu; Fig. 6B). It consists of calcareous pebbles and rhodoliths in a coarse sandy matrix with algal calcarenite and mudstone and also contains the following marine fossils:

-gastropods: *Fissurella* sp., *Patella aspera* (Röding), *P. caerulea* Linneo, *Tritia neritea* (Linneo), *Jujubinus* sp., *Gibbula* sp., *Clanculus cruciatus* Linneo, *C. corallinus* (Gmelin), *Bolma rugosa* (Linneo), *Tricolia pullus* (Risso), *Littorina* sp. *Mitrella* sp., *Cerithium lividulum* Risso, *Vermetus* sp.;

Formatted: Italian (Italy)

-bivalves: *Cardita calyculata* Linneo;

- polychaeta: Spirorbidae spp.

Formatted: English (United Kingdom)

Continental reddish clinostratified coarse breccias (br in Fig. 6B) that are approximately 1.5 m thick and are interbedded with reddish silty-sandy deposits cover all marine deposits.

Figure 6

In the sector south of Montagna Spaccata, PS3 can be identified by the presence of two palaeo-littoral ridges north and south of the Gallipoli-Alezio ridge; they are arched in shape and have their concavities facing west, towards the sea (Fig. 2A, B, C). These littoral ridges extend parallel to PS3 towards the sea. We call the littoral ridge north of Gallipoli *Monte-Crocefisso* palaeo-littoral ridge (hereinafter MClr) and that south of Gallipoli *Carmine-Li Foggi* palaeo-littoral ridge (hereinafter CLlr). Both ridges are the local expression of the PS3 Mixed Deposit (PS3-MD; Figs. 3 and 7A, B), which ~~it~~ is constituted, from bottom to top, by the PS3marine unit (PS3mu), Aeolian Unit 1 (AU1), and Aeolian Unit 2 (AU2) and lies on three older units wich represent the local substrate: Yellowish Sand (YS), Upper Palaeosol (UPA), and lacustrine silts (LS).

PS3 extends approximately 200 metres landward of the inner margin of CLlr, where the palaeovalleys of ancient ephemeral streams (locally called *lame*) abruptly end along an alignment at ca. +15 m (Fig. 7e).

The stratigraphy and chronology of the PS3-MD and the older underlying units in the sector south of Montagna Spaccata (where the PS3-MD forms the MClr and CLlr) are shown in Fig. 7; it is important to note that these older units on which the PS3-MD lies (YS, UPA, and LS) are not described in detail because they refer to a phase prior to the formation of PS3 and are not directly correlatable with palaeoshorelines recognised in the field; therefore, they are beyond the scope of this work.

The PS3-MD starts with thePS3mu, which lies in abrupt, erosional contact on the underlying UPA and LS (Fig. 7A, b, B). The base of the PS3muis in places constituted by a pebbly lag that is ca. 30 cm thick (Fig. 7b, c), where specimens of marine bivalve *Ostrea* sp. can be found sporadically. Above the pebbly lag, the unit passes to irregularly cemented calcarenites that have high- and low-angle cross-bedding, and contains rare specimens of *Ostrea* sp. In some cases, the calcarenites appear organised in westwards-dipping foresets (towards the current coastline). In section G4 (Fig. 7B), the pebbly lag is not present, and the basis of the PS3muis made up of irregularly cemented, coarse subhorizontal-bedded calcarenite, which forms load casts over the underlying UPA. This basal calcarenite passes upwards to irregularly cemented coarse calcarenite, alternating with gravel and calcirudite levels that are rich in mollusc shells and that have a low-angle, hummocky-like cross-lamination or they appear organised in westwards-dipping foresets (towards the current coastline). Between the basal, coarse subhorizontal-bedded calcarenite and the overlying hummocky/clinostratified calcarenites/calcirudites, there is a thin interval of light grey clays (cll) (Fig. 7B, f) showing wavy deformation structures at their interfaces with the overlying calcarenites.

The macrofaunal content of the PS3mu in this sector includes (apart from the already mentioned *Ostrea* sp.) only marine bivalves: *Barbatia barbata* (Linneo), *Chama gryphoides* (Linneo), *Acanthocardia tuberculata* (Linneo), *Glycymeris nummaria* (Linneo), *Chamelea gallina* (Linneo), *Loripes lucinalis* (Lamarck), *Donax trunculus* Linneo, *D. venustus* Poli, and *Lentidium mediterraneum* (Costa).

Above the PS3mu, we mapped the AU1, which outcrops only in the northern and southern parts of the CLlr and consists of fine, whitish/reddish calcarenite organised in wavy to cross-bedded cosets dipping in various directions. Within the unit, there are thin layers or lenses characterised by the presence of numerous voids crossed by cemented fossil root traces.

The observed fossil macrofauna is made up exclusively of rare specimens of terrestrial gastropods Helicidae.

Above the AU1, we mapped the AU2. South-eastwards-dipping foresets dominate the internal structure of this unit, which consists of fine, whitish–reddish calcarenite with thin layers or lenses characterised by the presence of numerous voids crossed by cemented fossil root traces. The observed fossil macrofauna consists exclusively of rare specimens of terrestrial gastropods Helicidae, while the microfauna is mainly made up of reworked or fragmented benthic foraminifers.

The depositional environment of AU1 and AU2 is coastal dunes.

Figure 7

4.1.4 Palaeoshoreline PS4 (elevation: ∼+22) and PS4 Mixed Deposit (PS4-MD)

In the sector from Montagna Spaccata northwards, this palaeoshoreline is mainly represented by a band of lithophagid borings within Mesozoic limestones, grouped into discontinuous clusters whose upper limit is ca. +22 m. a.p.s.l. At the Uluzzo locality, and specifically at the MS5 site (Figs. 8, 9), this palaeoshoreline is represented by a small residual wave-cut platform, a residual tidal notch, sea caves, lithophagid borings, the trace *Gastrochaenolites cor* Bromley and D'Alessandro with the original borer marine bivalve *Petricola lithophaga* (Retzius), and small patches of a syn- wave- cut platform deposit (Figs. 8, 9) composed of well-cemented calcirudite, which is the local expression of PS4-MD.

Figure 8

In the sector south of Montagna Spaccata, PS4 can be identified by the presence of two small and discontinuous relict littoral ridges north and south of Gallipoli, which are situated landwards with respect to the MClr and CLlr (Fig. 2B, C). The small remnants of these ridges seem to depict arched shapes with the concavity facing west, that is, towards the sea; they ~~. These ridges~~ represent the PS4-MD in this sector; the few sections observable show aeolian whitish/reddish calcarenite, organised in wavy to cross-bedded cosets dipping in various directions but mostly landward-dipping. The observed macrofauna is exclusively made of very rare specimens of terrestrial gastropods Helicidae.

4.1.5 Palaeoshorelines PS5 (elevation: ∼+41), PS6 (elevation: ∼+62), and PS7 (elevation: ∼+67)

These three palaeoshorelines are described together because of the common characteristics that they share in the sector from Montagna Spaccata northwards. In addition, PS6 and PS7 were observed in the field only at the Montagna Spaccata locality (Fig. 10), likely because the rocky slope reaches a higher elevation above present sea level and is poorly vegetated. All these palaeoshorelines are represented by bands of lithophagid borings grouped in discontinuous clusters; note that the elevations represent, as always, the points of maximum elevation of these bands above the present sea level.

In the sector south of Montagna Spaccata, the presence of these three palaeoshorelines may likely be derived from geomorphological evidence, such as slope breaks and the likely remains of the inner edges of marine terraces. The only exception is PS5, which, in this sector of the study area, is still visible to the north of San Mauro Abbey (Figs. 2A, 3) in the form of a band of lithophagid borings within Mesozoic limestones grouped into discontinuous clusters. In addition, a well-identified marine terrace deposit less than 1 km^2 wide that crops out between ca. +40 and +30 m~~.,~~ may likely be correlated with PS5. This deposit, which we defined as the PS5 Marine Deposit (PS5-MaD), consists of yellowish-brownish fine calcareous-siliciclastic sands containing a few specimens of bivalves *Chlamys* sp., *Pecten* sp., and *Pseudamussium peslutrae* (Linneo). The microfauna is constituted of ostracods and foraminifers. Towards the top, the PS5-MaD becomes more silty/clayey and appears altered by the deposition of whitish caliche nodules, due to ~~post-deposition~~ diagenetic processes.

Figure 9

Figure 10

4.2 Chronological analyses results and consequent chronological attributions

Our chronological analyses allow us to directly date some units associated with some of the recognised palaeoshorelines.

4.2.1 PS1 and PS1mu

The chronological analysis obtained via the isoleucine/alloisoleucine epimerisation method on shells of *Patella* sp. and *T. latus* (Gmelin) contained, respectively, in two samples taken from PS1mu at sites MS6 (Fig. 4A) and MS2 (Fig. 10; see also Fig. 2A for their locations) indicated aminozone E (Table 2A). This aminozone is associated with MIS 5.5 (Hearty et al., 1986; Hearty, 1987; Hearty and Dai Pra, 1992; Torres et al., 2013). At site G17 (Fig. 4B, see Fig. 2A for its location), the numerical age obtained from a sample of the LPA of 122.1±33.6 ky BP (Table 2A) allows us to assign the PS1mu more precisely to the late MIS 5.5, as the PS1mu overlies the LPA.

4.2.2 PS3 and PS3 Mixed Deposit (PS3-MD).

Regarding the PS3-MD, it has been possible to perform chronological analyses on the PS3mu, which constitutes the basal unit of the PS3-MD. At the Montagna Spaccata locality (MS1 site; Figs. 5 and 9; see Fig. 2A for its location) along the road cut (Fig. 6B), two chronological constraints have been obtained: (i) the isoleucine/alloisoleucine epimerisation on shells of *Patella* sp. contained in a sample taken from the PS3mu (Table 2A) indicated aminozone E (MIS 5.5); (ii) U-series dating applied to two specimens of *H. durotrix* Gosse anchored on the wave-cut platform on which the PS3mu lies (Fig. 6B) provided ages of 213.39±3.0 and 211.17±4.8ky BP (Table 2A), revealing MIS 7.3 (Waelbroeck et al., 2002; Grant et al., 2014).

In the sector south of Montagna Spaccata, the chronological analysis obtained with the isoleucine/alloisoleucine epimerisation method on shells of *Glycymeris* sp. contained in two samples taken from the PS3mu at site G4 (Fig. 7B; see Fig. 2A for its location) indicate aminozone E (MIS 5.5) (Table 2A).

4.2.3 Other units not associable with the recognised palaeoshorelines

The chronological analyses allow us to also assign ages to some other units that are not associable with the recognised palaeoshorelines, except for the already mentioned LPA.

In the sector south of Montagna Spaccata, specifically at site G17 near Punta Pizzo (Fig. 4B; see Fig. 2 for its location), the DMCU has been dated using the isoleucine/alloisoleucine epimerisation method on shells of *Glycymeris* sp. contained in a sample taken from this unit (Fig. 4B; Table 2A); this method indicates aminozone F, corresponding to MIS 7 (Hearty et al., 1986; Hearty, 1987; Hearty and Dai Pra, 1992; Torres et al., 2013). The U-series dating applied to *C. caespitosa* Linneo contained in the same sample provided an age ranging from a minimum of 211.97±3.6 ky BP to a maximum of 232.02±5.3 ky BP (Fig. 4B; Table 2A), which allows us to assign it to MIS 7.3 (Waelbroeck et al., 2002; Grant et al., 2014). This chronological analysis, with two different methods applied to the same sample (G17-2b; Table 2A), mutually reinforces the reliability of the dates obtained. As a consequence, the unit RS, underlying DMCU, dates back to MIS7.5 or to an older stage.

The DMCU was also dated at Torre Sabea (G20 site; see Fig. 2A for the location), where sample G20-1 (Table 2A) gave an age of 208.44±5.3 ky BP (MIS 7.3).

In the sector south of Montagna Spaccata, it has also been possible to perform chronological analyses on the YS and LS, which represent the substrate on which the PS3-MD (which, in this sector, forms the CLlr) was deposited.

For the YS, the chronological analysis with the amino acid racemisation method applied to ostracods contained in a sample taken from this unit (Fig. 7B; Table 2A) provided the age of 137.2±29.3 ky BP, which allows us to attribute it to MIS 6-MIS 5.5.

For the LS, the date obtained with the amino acid racemis~~z~~ation method applied to ostracods contained in a sample taken from this unit (Fig. 7B; Table 2A) provided the ages of 138.4±17.9 and 118.1±17.9 ky BP, which allows us to attribute it to MIS 6-MIS 5.5.

Table 2

5 DISCUSSION

5.1 Focus on *Palaeoshoreline PS3 (elevation: ~+15) and PS3 Mixed Deposit (PS3-MD)*

5.1.1 Sector south of Montagna Spaccata

The *Carmine-Li Foggi* palaeo-littoral ridge (CLlr) and *Monte-Crocefisso* palaeo-littoral ridge (MClr) constitute the geomorphological expression (Fig. 2A, B, C) of the PS3 Mixed Deposit (PS3-MD) in the sector south of Montagna Spaccata.

Our field observations and chronological analyses allow us to establish that CLlr and MClr are two sedimentary bodies made up of the PS3mu, AU1, and AU2. The CLlr and MClr lie on previous units dating back to MIS 6-5.5 and not associable with the recognised palaeoshorelines: YS, UPA, and LS. The scheme of the stratigraphic relationships between all units recognised within the PS3-MD (Fig. 7B) allows us to identify the correlations ~~that~~ we have reconstructed between them.

The dates obtained from the PS3mu (MIS 5.5; Table 2A), the cll layer within the PS3mu (Fig. 7B, f), and the presence of a palaeoshoreline at ca. +15 m (PS3) elongated approximately 200 landward of the inner margin of CLlr (Fig. 7e) allow us to correlate PS3 and the PS3-MD (the latter morphologically represented by the CLlr and MClr) with each other and to reconstruct their parallel formation and evolution in the sector south of Montagna Spaccata.

The cll layer contributes to the reconstruction of the current elevation a.p.s.l. of the palaeoshoreline associated with the formation of the CLlr and MClr. The wavy deformation structures at the interface between the cll and the overlying calcarenites (Fig. 7B, f) typically form in the offshore transition due to storm waves (Henkel, 1970; Molina et al., 1998; Alfaro et al., 2002~~1~~). This evidence indicates that the sea level was likely 6-10 m over the top of cll during its deposition (De Santis et al., 2022). Our field interpretation is that the cll indicates the maximum water depth and, therefore, the maximum marine transgression, while calcarenites/calcirudites above the cll represent the prograding beach deposits following the maximum marine transgression.

Therefore, the contact between the cll and the overlying calcarenites/calcirudites can be interpreted as indicative of the offshore transition of the palaeo-beach at the time of the maximum marine transgression. Today, after the tectonic uplift, this contact is ca. 8.5 m a.p.s.l. and we can assume a palaeo-depth, at the time of formation of this contact, of ca. 6-10 metres (Henkel, 1970; Molina et al., 1998; Alfaro et al., 2002~~1~~). Adding the 8.5 metre-current elevation of the contact with the 6-10 metre-palaeo-depth, we obtain that the paleo-~~-~~sea level today is uplifted within the range of 16.5 ± 2 m. The palaeoshoreline PS3, extending landward of the inner margin of CLlr at ca. +15 m, is the only one within this range, so we interpret 15 m as the current height a.p.s.l. reached, after the ~~tectonic~~ uplift, by the palaeoshoreline due to the sea level at the time of the maximum marine transgression, which started the formation of the CLlr and MClr.

Therefore, we conclude that the CLlr and MClr were formed immediately after the first MIS 5.5 highstand, which brought the sea on a palaeoshoreline (PS3) that today is ca. +15 m: soon after this first highstand was attained, the CLlr and MClr began to form as a barrier just offshore from the palaeoshoreline (Fig. 11 A-E), following the pattern of barrier formation reported in Roy et al. (1994) and Otvos (2012).

Fig. 11

5.1.2 Sector from Montagna Spaccata northwards; evidence of the reoccupation of the MIS 7.3 highstand by the MIS 5.5 highstand

In this sector, PS3 and the associated PS3-MD are more visible just at Montagna Spaccata (MS1 site; Fig. 6B). Here, the PS3-MD is represented only by the PS3mu, which dates back to MIS 5.5 (Table 2A). Nevertheless, on the wave-cut platform of Mesozoic limestones, two specimens of *H. durotrix* Gosse indicate MIS 7.3 (Table 2A). We interpret this apparent discrepancy as a case of the reoccupation of an older palaeoshoreline by a younger palaeoshoreline. The phases of palaeoshoreline formation and reoccupation can be summarised as follows (Fig. 12):

First, during the MIS 7.3 highstand, an inner edge with a syn-wave cut platform forms; in this phase, specimens of *H. durotrix* Gosse grow on the platform; note that this coral lives between 0 and 5 m below sea level (Picton and Morrow, 2016). As the current position of the fossils of *H. durotrix* Gosse is ca. +13 m, the near palaeoshoreline PS3 at +15 m (Fig. 6B) is the only one associable with fossils of this coral, as this situation indicates that the corals lived at ca. 2 m depth. The subsequent higher palaeoshoreline (PS4 at +22 m) cannot be associated with the fossils of *H. durotrix* Gosse because this would involve the corals living at a water depth of 9 m.

Second, the subsequent MIS 5.5 highstand settled more or less at the same position, reoccupying the palaeoshoreline of MIS 7.3. In this phase, the PS3muwas deposited on the previously formed wave cut platform, covering the fossil specimens of *H. durotrix* Gosse.

The reoccupation of PS3 dating back to MIS 7.3 by a subsequent highstand that reached PS3 again is well mapped only at Montagna Spaccata (MS1 site; Fig. 6B) because the Mesozoic limestone where palaeoshorelines are cut is prone to preserving better palaeo-landforms.

Fig. 12

However, more generally, evidence of the transgression of MIS 5.5 deposits on MIS 7.3 deposits in this study area is widely present. For example, at Torre Sabea (G20 site; see Fig. 2A for the location), the contact between the underlying DMCU and the overlying PS1mu can be observed in the field. At this site, the dating carried out on the DMCU (sample G20-1; Table 2A) gave an age of 208.44±5.3

ky BP (MIS 7.3), while the overlying PS1mu is attributable to MIS 5.5, which is also confirmed by the presence at this site of numerous specimens of *T. latus* (Gmelin), which, in Italy, is exclusive to MIS 5.5 (Hearty and Dai Pra, 1992; Antonioli et al., 2018). The same evidence is also found in the Uluzzo locality (MS11 site; see Fig. 2A for the location), where dating carried out on a marine deposit not attributable to any of the recognised units (sample MS11-1; Table 2A) gave ages of 223.84±7.2ky BP and 225.17±5.4 ky BP (MIS 7.3 onset). Our evidence and new absolute age controls from the Torre Sabea locality, in particular, confirm the stratigraphy, ages, and interpretation of that site reported in Hearty and Dai Pra (1992; see Fig. 9 of that work).

5.2 Uplift scenario; comparison between observed and expected palaeoshorelines

New chronological analyses, combined with the synchronous correlation method, have been used to test different sea level curves and uplift rate scenarios to produce the best match between observed and expected palaeoshorelines.

The best fitting scenario has been obtained using, as input into the terrace calculator, the sea-level curves of Waelbroeck et al. (2002) from present to 410 ky BP and Rohling et al. (2014) from 410 to 590 ky (Table 2, 1st and 2nd columns for sea level and age, respectively).

The scenario we reconstructed implies an uplift rate of 0.09 mm/yr from 590 to 130 ky BP (middle Pleistocene or MIS 15 - MIS 6 interval) and of 0.07 mm/yr from 130 ky BP onwards (late Pleistocene or MIS 5 - onwards).

The uplift rate of 0.07 mm/yr is derived from chronological analyses carried out on the PS3-MD (more specifically, on the PS3mu). Using the IE results from sites MS1 and G4 (Table 2A) and taking into account the link of origin between PS3 and the PS3-MD (see par. 5.1), we concluded that PS3 dates back to a first and higher peak of MIS 5.5, attained at ca. 127 ky BP (Waelbroeck et al., 2002), when the sea level reached an elevation of +6 m a.p.s.l (Waelbroeck et al., 2002).

The sea-level elevation attained during the first peak of MIS 5.5 is an object of debate. Some global compilations of RSL data combined with Glacial Isostatic Adjustment (GIA) modeling indicate that peak of global mean sea level during MIS 5.5 was higher than the previous long-standing estimate (4 to 6 m), in the range of ~6 to 9 m above present (Kopp et al., 2009; Dutton and Lambeck, 2012~~; Kopp et al., 2009~~). This is in agreement with site-specific, GIA-corrected coastal records in ~~the~~ Seychelles at 7.6 ± 1.7 m (Dutton et al., 2015b). The Red Sea planktic $\delta^{18}O$ record places peak RSL values during MIS 5.5 at 6.7 ± 3.4 m (maximum probability with 95% probability envelope; Grant et al., 2012). Differences in RSL reconstructions obtained from several locations (Rovere et al., 2016) yield a range of interpretations about the evolution of global mean sea level during the MIS 5.5 highstand (Siddal et al., 2007; Stocchi et al,~~;~~ 2018), also comparing field data with numerical modelling (Stocchi et al,~~;~~ 2018). Differences in RSL reconstructions from site to site yield a range of interpretations about the evolution of global mean sea level during the MIS 5.5 highstand, going from a stable sea level (Stirling et al., 1998) to four peaks in sea level reflecting repeated sea-level oscillations (Thompson et al., 2011; Rohling et al., 2019). As yet, no consensus exists regarding this suite of scenarios.

In this work, for the application of the synchronous method, highstands from a sea-level curve have to be introduced as one of the inputs. Since the best fitting scenario between observed and expected palaeoshorelines has been obtained using as input the sea-level curve from Waelbroeck et al. (2002) from present to 410 ky BP, we used for MIS 5.5 the mean sea level reported in that curve, that is, +6 m a.p.s.l. In any case, this value is within the value range indicated in several literature works for the peak of global mean sea level during MIS 5.5 (Hearty et al., 2007; O'Leary et al., 2013; Dutton et al., 2015a and references therein; Rohling et al., 2019).

Based on the chronological analyses (IE) at sites MS2 and MS6 (Table 2A) and the presence of *T. latus* (Gmelin) at the MS2 site (Fig. 10), we concluded that PS1 and the associated PS1mu also belong to aminozone E (MIS 5.5). Nevertheless, given its minor elevation a.p.s.l. and, above all, the chronological constraint given by the age (122.1±33.6 ky BP) of the LPA, which at the G17 site underlies the PS1mu, we assign PS1 and the PS1mu to the second peak of MIS 5.5 (Hearty et al., 2007; O'Leary et al., 2013; Dutton et al., 2015a and references therein; Stocchi et al., 2018; Rohling et al., 2019), that is, ca. 120 ky BP, which has been recognised in other regions within the

Mediterranean realm (Cinque and Romano, 1990; Meschis et al., 2020). As a consequence, LPA indicates a sea-level fluctuation between the two sea-level highstands recognised in the study area within MIS 5.5. We interpret LPA as one of the palaeosols interbedded within marine deposits dating back to MIS 5.5 which had already been reported from~~in~~ the area of Gallipoli by Hearty and Dai Pra (1992) even if, at the site G17 (Fig. 4B), the LPA lies between the MIS 7 and 5.5. This is because here the deposits referable to the first highstand of MIS 5.5 are missing due to erosion and/or non-deposition.

Ultimately, the uplift rate of 0.07 mm/y is derived by assigning an age of 127 ky (MIS 5.5) and a palaeo-sea-~~-~~level at +6 m (2nd column in Table 3) to PS3, which is currently at +15 m a.p.s.l; thus, the vertical displacement is ca. 9 m within 127 ky.

The uplift rate of 0.09 mm/y is derived from the evidence that PS3 is also the palaeoshoreline of MIS 7.3, as explained in paragraph 5.1.2. During MIS 7.3, the sea level reached an elevation of -4 m b.p.s.l. (Waelbroeck et al., 2002). Thus, the uplift rate of 0.09 mm/yr is derived by assigning a mean age of 212 ky (MIS 7.3) and a palaeo-sea-~~-~~level at -4 m (2nd column in Table 3) to PS3, which is currently at +15 m a.p.s.l., thus yielding a vertical displacement of ca. 19 m within 212 ky.

It is important to emphasise that the two uplift rates are so similar to each other that, even assuming a constant average rate of 0.08 mm/y for the entire period (middle Pleistocene-onwards, or interval MIS 15-onwards; that is, 590 ky BP-onwards), the results of the synchronous method do not change.

Table 3

The expected palaeoshoreline elevations generated by our synchronous correlation method are listed in the 3rd column of Table 3.

We ~~have~~ associated the expected palaeoshorelines generated by our synchronous correlation method (3rd column of Table 3 and Fig. 13) with the observed palaeoshorelines ~~, as indicated in the (~~4th column of Table 3 and ~~in~~ Fig. 13)~~. We make the association between expected and observed~~

palaeoshorelies being guided by seeking the best match between them. This match is mathematically expressed by the coefficient of determination (R^2 value) for linear regression analysis of the "observed" and the "expected" elevations of all palaeoshorelines (see Fig. 13).

Given the maximum uncertainty of ± 13 m. in the sea--level curves we used (Waelbroeck et al., 2002; Rohling et al., 2014), we prudentially consider acceptable a gap of up to 10 m between an expected and the observed palaeoshoreline that we associate with it (compare the 3rd and 4th columns in Table 3).

Ultimately, the palaeoshorelines recognised in the field in this study are associated with sea-level highstands (Table 3 and Fig. 13), such as 120 ky BP (MIS 5.5, second peak; Hearty et al., 2007; Rohling et al., 2008; Kopp et al., 2009, 2013; O'Leary et al., 2013; Dutton et al., 2015a and references therein; Düusterhus et al., 2016), 127 ky BP (MIS 5.5, first peak), 212 ky BP (MIS 7.3), 330 ky BP (MIS 9.3), 410 ky BP (MIS 11), 525 ky BP (MS 13.3), and 590 ky BP (MIS 15).

Some expected palaeoshoreline elevations are lower or (nearly) equal to the next younger expected palaeoshorelines, suggesting that they may be overprinted or reoccupied, that is, partly or completely removed by erosion during the rising sea level of a subsequent highstand. Thus, except for other than PS3, none of the observed palaeoshorelines hasve been correlated with overprinted or reoccupied palaeoshorelines. The exception of PS3 -results from a MIS 7.3 highstand, reoccupied by the first peak of the MIS 5.5 highstand, and documented by our new absolute age controls. In addition, the synchronous correlation method predicts the presence of several currently submerged palaeoshorelines, which are probably completely overprinted.

Figure 132 shows, for two of the seven topographic profiles extracted from the DTM, the elevations of observed (coloured arrows) versus expected (horizontal lines) palaeoshoreline elevations. In this figure, the association between expected (and not overprinted) and observed palaeoshorelines is represented using the same colour for continuous horizontal lines and arrows, where the first represents the elevations of expected (and not overprinted) palaeoshorelines, and the second represents the corresponding observed palaeoshorelines.

Figure 13

Field measurements versus expected palaeoshoreline elevations show an R^2 value of ca. 0.99 (Fig. 14). This value confirms that the fits between the expected and observed palaeoshorelines are good, giving confidence to the uplift rates.

Figure 14

5.3 Terrace phases and vertical movements of the Apulian foreland in the middle-late Pleistocene; considerations of the MIS 7.3 highstand

The Apulian foreland represents an uncommon case of a foreland shared by two opposite- verging chains: the SW-verging Albanides- Hellenides and NE-verging southern Apennines. The deformation occurring within this type of foreland is uncommon and poorly understood.

To date, the Apulian foreland has been characterised by a scarcity of reliable chronological data concerning the marine terraces older than the last interglacial and, as a consequence, uplift rates have been estimated only for the late Pleistocene by using the elevation of the marine terrace related to the last interglacial period (MIS 5.5) (Hearty and Dai Pra, 1992; Belluomini et al., 2002).

The new chronological constraints and results of the synchronous correlation presented in this work allow us to update the results recently published in De Santis et al. (2021a).

The two uplift rates of 0.09 mm/yr from 590 to 130 ky and of 0.07 mm/yr from 130 ky BP onwards are more similar and have been obtained from precise chronological constraints. Although these data show a slight slowdown in the regional uplift, also an average constant uplift rate over time of 0.08 mm/yr may be claimed to explain the regional uplift for the last 590 ka for an almost tectonically stable region such as the Apulian foreland.

PS1 and PS2 (+6 and +7.5 m, respectively) both refer to the highstand at ca. 120 ky BP; the presence, in the study area, of sites where scattered lithophagid borings in the Mesozoic limestone are interposed between PS1 and PS2 seems to confirm this reconstruction, along with the stratigraphic relationship between the PS1mu and PS2mu. In addition, as PS3 (+15 m) is referred to 127 ky BP, we can confirm that, in the area of Gallipoli, there is evidence of at least two highstands during MIS 5.5.

Nevertheless, the chronological attribution and current elevation of PS3 (127 ky BP and +15 m a.p.s.l., respectively) suggest that they could represent the palaeoshoreline and deposit of MIS 5.5 found at an elevation that is one of the highest among those reported in previous studies between Taranto and Santa Maria di Leuca (Hearty and Dai Pra, 1992; Belluomini et al., 2002; Ferranti et al., 2006). One of the possible explanations could be that previous studies always considered MIS 5.5 deposits in a restricted coastal belt~~,~~ without recognising the real MIS 5.5 palaeoshoreline.

Our study highlights an important aspect of the MIS 7.3 highstand. Given the chronological constraint provided by the dating of *H. durotrix* Gosse for PS3, the latter can also be attributed to the MIS 7.3 highstand. Due to the almost -stability of the Apulia foreland, the only way to place the current position of the MIS 7.3 palaeoshoreline at +15 m is to postulate an elevation of the MIS 7.3 highstand close to the present sea level, as in Waelbroeck et al. (2002).

Indeed, entering into the synchronous method a MIS 7.3 highstand reconstructed many metres below the current sea level (i.e., ~ -29 metres in Grant e~~a~~t al., 2014) would imply a vertical displacement of the MIS 7.3 palaeoshoreline of ca. 40-45 m, with a mean uplift rate (between MIS 7.3 and today) of approximately 0.2 mm/yr. This value is very far from all uplift rates obtained for the coastal stretch where ~~in~~ our study area is located (Ferranti et al., 2006; Cerrone et al., 2021b). In addition, the uplift rate of 0.2 mm/yr implies that the synchronous method assigns the ~~palaeoshoreline at~~ +15 m palaeoshoreline to MIS 7.5, which does not match the chronological constraints of ~~obtained by~~ U-series dating applied to *H. durotrix* Gosse. This mismatch is due to the subsequent lowering of the uplift rate to 0.07 mm/y, which is also constrained by chronological analyses. However, more investigations are needed within the Apulian foreland to test whether MIS 7.3 is as high as we mapped it in this study.

In conclusion, the data arising for the Apulian foreland suggest a MIS 7.3 highstand near that reported in Waelbroeck et al. (2002), that is, near the present sea level.

A remarkable characteristic of the palaeoshorelines that we recognised is that they can be observed at the same elevation a.p.s.l. for the entire study area, which, from a structural point of view, spans horsts and grabens (Fig. 1) limited by normal faults (Ambrosetti et al., 1987); this feature indicates that these faults did not displace the coastal sector of the study area into blocks with differential uplift and suggests that, at least in the middle and late Pleistocene, this sector of the Salento Peninsula uplifted uniformly.

Palaeoshorelines dating back to the middle-late Pleistocene have been recognised in other peri-Mediterranean areas, and they are all characterised by geodynamic contexts different from the Apulian foreland. Table 4 summaris~~z~~es some examples of emerged palaeoshorelines, with the ages to which they have been attributed.

Table 4

All areas listed in Table 4 are characterised by uplift rates higher than those of the Apulian foreland. The main result of the difference in the uplift rates between the sites listed in Table 4 and the Apulia region is that, in the latter, a smaller number of highstands left a trace in the form of a palaeoshoreline. Due to the slow uplift rates, the palaeoshorelines have undergone overprinting or reoccupation or are now submerged: the synchronous correlation method highlights this situation. Extensive overprinting and reoccupation are symptomatic of slow uplift rates (Pedoja et al., 2018; Cerrone et al., 2021a,b).

CONCLUSIONS

The synchronous correlation method, applied for the first time extensively to the Apulian foreland, modifies the previously applied technique, known as "sequential correlation" (e.g., Roberts et al., 2013; Robertson et al., 2019), where it is assumed that starting from a single dated palaeoshoreline, the next higher and older palaeoshoreline belongs to the next older sea-level highstand. It is therefore probable that this classic methodological approach, if accompanied by the absence of reliable datings, does not highlight cases of overprinting or reoccupation, which instead are highly probable in geodynamic contexts characterised by fairly stable territories or with weak and constant vertical movements, such as that in the Apulian foreland.

Acknowledgements

We wish to thank all the staff at the Polo Scientifico e Tecnologico Magna Grecia (Taranto) for the topographic instruments. We also are very grateful to the three anonymous reviewers for their comments and suggestions that have allowed us to improve the quality of the paper.

Figure and table caption

Figure 1 - Study area. A: Regional context showing the main geological–structural domains in southern Italy. B: Simplified geological map of the Salento Peninsula (from Boenzi et al., 2010), showing the structural tectonic setup defined as "Serre Salentine": a series of horsts and grabens elongated in the NW–SE direction. C: Detailed geological map from Ciaranfi et al. (1992).

Figure 2 – A: 2-m +8-m digital terrain models (DTMs). B: 3D scene of the study area with sites and main localities cited in the text; the colours represent the elevation above the present sea level, as in the right up box in A.

Table 1- list of palaeoshorelines recognised with associated deposits and units (these latter are only if it has been possible to define them) and landforms in which palaeoshorelines and associated deposits/units appear. With the informal term "mixed deposit" we mean a deposit correlated to a palaeoshoreline settled in different environments (es: marine +continental).

Fig. 3 - Reconstructed palaeoshorelines and associated units and the topographic profiles reported in Fig. 13. The panel on the top right shows the abbreviations of the recognised paleoshorelines and colors of representation and abbreviations of the associated units, described in detail in Section 4.1 and reported also in Tab. 1. Each palaeoshoreline is indicated with a continuous line where it is well recognis~~z~~able in the field, with a dotted line where its position is detectable by geomorphological and/or geological indicators. See the text and Tab. 1 for the descriptions of the units associated with the recognised palaeoshorelines. Note that the units reported in this map are only those genetically associated with the recognised palaeoshorelines~~; the areas of outcropping units reported in this map are only those recognised and/or surveyed in the present study~~.

Figure 4- Field photographs of PS1 and PS1mu. A: sector from Montagna Spaccata northwards, specifically sites MS6 (left) and MS5 (right) at the Uluzzo locality (see Fig. 2A for the location). The upper limit of the band of lithophagid borings is indicated by black arrows; note the upper boundary of greyish PS1mu deposits, which follows the course of the band of lithophagid borings. Black horizontal lines with elevations in metres above the present sea level are indicated. B: Sector south of Montagna Spaccata: schematic stratigraphy of the Punta Pizzo locality, specifically site G17 (see Fig. 2A for the location); a: detail of the contact between two older Quaternary units: Reddish Sands (RS) and Discontinuous Marine Clastic Unit (DMCU). b: detail of the contact between the underlying LPA and the overlying PS1mu. c: detail of the basal part of the PS1mu, made up of centimetric clasts represented by fragments of Mesozoic limestone, rhodoliths, and heavily reworked and smoothed mollusc shells. These clasts are immersed in a matrix of reddish sand/silt and/or calcarenite/calcisiltite, evidently coming from the erosion of the underlying LPA. d: detail of the contact between the PS1mu and Mesozoic limestones (black arrows), with lithophagid borings. e: band of lithophagid borings at ca. +6 m. The legend of this figure is also used for Figures 6, 8, 9, and 11.

Figure 5- Field photographs of PS2, all taken in the sector from Montagna Spaccata northwards, specifically sites MS6 (upper photos) and MS5 (lower photo), both at the Uluzzo locality (see Fig. 2A for the location). The black arrows indicate

the main clusters of lithophagid borings. Black horizontal lines with elevations in metres above the present sea level are indicated.

Figure 6 - Field photographs of PS3. A: sector from Montagna Spaccata northwards, specifically site MS5 at the Uluzzo locality (see Fig. 2A for the location). B: Montagna Spaccata; cut along the landward side of the coastal road, that is, the MS1 site (see Fig. 2A for the location). The red arrow indicates a probable residual tidal notch; the black arrows indicate lithophagid borings; dashed line follows the palaeo tidal notch and shore platform. c: cut along the seaward side of the coastal road, with the position of sample MS1-1 (*Hoplangia durotrix* Gosse; see Table 2A) reported in d, where lithophagid borings on the Mesozoic limestones are also visible. Black horizontal lines with elevations in metres above the present sea level are indicated. ML: Mesozoic limestones; PS3mu: PS3marine unit; br: continental breccias.

Figure 7 – A: Field photographs of sections at the G2-2 site (see Fig. 2A for the location) within the *Carmine-Li Foggi* palaeolittoral ridge (CLlr), formed by the following units grouped within the PS3 Mixed Deposit (PS3-MD): PS3marine unit (PS3mu), Aeolian Unit 1 (AU1), and Aeolian Unit 2 (AU2). The PS3-MD lies on older units: Yellowish sand (YS) and Upper Palaeosol (UPA). b: Detail of the succession, from bottom to top, of the units cropping out at site G2-2: Yellow Sands (YS), Upper Palaeosol (UPA), PS3marine Unit (PS3mu), Aeolian Unit 1 (AU1). c: Detail of the abrupt, erosional contact of the PS3mu on the underlying UPA, with the pebbly lag at the base of the PS3mu, which often forms a protruding shelf. B: Scheme of stratigraphic relationships between all units of the PS3 Mixed Deposit (PS3-MD) and older units cropping out at sites G2-2, G2-3 and G4 within the *Carmine-Li Foggi* palaeolittoral ridge (CLlr) (see Fig. 2A for the locations of sites G2-2, G2-3 and G4). e: Google Earth image of the trace of PS3 still visible approximately 200 metres landward of the inner margin of the southern sector of the CLlr, where the inactive valleys of ancient ephemeral streams (locally called *lame*) abruptly interrupt along an alignment at ca. +15 m. f: Field photographs of the G4 site (see Fig. 2A for the location) showing the cll layer within the PS3mu; the cll layer is very important to establishing a genetic link between the PS3 Mixed Deposit (PS3-MD) in this sector.

Figure 8 – A: Field photographs of PS4 at the Uluzzo locality in the sector from Montagna Spaccata northwards, specifically at the MS5 site (see Fig. 2A for the location and Fig. 9 for an overview of the MS5 site); the black squares labelled B and C contain details reported in photographs B and C. B: Sea cave. C: Small residual syn- wave- cut platform deposit (PS4-MD) characterised by the tace *Gastrochaenolites cor* (black arrow) with the original borer marine bivalve *Petricola lithophaga* (Retzius). Black horizontal lines with elevations in metres above the present sea level are indicated.

Figure 9 - Field photographs (up) and a sketch (down) of a cliff at the Uluzzo locality (MS5 site of Fig. 2A) in the sector from Montagna Spaccata northwards, showing the recognised palaeoshorelines and units (represented by the legend of Fig. 4). The legend on the left is also used for Figure 10.

Figure 10 – Google Earth image (top) of the Montagna Spaccata locality (MS1 and MS2 sites of Fig. 2A), showing the recognised palaeoshorelines and units (represented by the legend of Fig. 4). MS1 site is represented in detail in Fig. 6B. For the legend, see Fig. 9.

Table 2 – A: Samples on which chronological analyses were carried out with amino acid racemisation, isoleucine/alloisoleucine epimerisation, U-series dating, and relative results. The first part of the sample ID indicates the site from which the sample comes (reported in Fig. 2A). Amino acid racemisation was applied to ostracods, and due to the conversion algorithm of Ortiz et al. (2004), it gives numerical data. The isoleucine/alloisoleucine epimerisation allows us to attribute the samples to aminozones corresponding to specific MISs (Hearty et al., 1986; Hearty, 1987; Hearty and Dai Pra, 1992; Torres et al., 2000). The reported U-series ages are those corrected for detrital ^{230}Th using an initial ^{230}Th/^{232}Th activity ratio of 7 ± 50%. Samples MS1-2, MS2-1, and MS6-1 are from De Santis et al. (2021a)

B: D/L and D-allo/L-Ile ratios of all amino acids analysed for each sample reported in Table 1A; these ratios are the basis for calculating the numerical ages (if a conversion algorithm exists) or for aminozone determination; N: number of subsamples prepared for the analysis. C: U-series dating parameters obtained for the samples reported in Table 1A; N: numbers of subsamples prepared for the analysis. The ^{238}U and ^{232}Th concentrations were determined using the enriched ^{236}U and ^{229}Th isotopes, respectively.

$\delta^{234}U_m = \{[(^{234}U/^{238}U)_{sample}/(^{234}U/^{238}U)_{eq}]-1\}x1000$, where $(^{234}U/^{238}U)_{sample}$ is the measured atomic ratio and $(^{234}U/^{238}U)_{eq}$ is the atomic ratio at secular equilibrium

$\delta^{234}U_{(0)}$ is the initial value and is calculated by the equation $\delta^{234}U_{(0)} = \delta^{234}U_m \exp(\lambda_{234}t)$, where t is the age in years. and λ_{234} is the decay constant for ^{234}U

Ages (ky)$_{corr}$ are the ages corrected for detrital ^{230}Th using an initial ^{230}Th/^{232}Th activity ratio of 7 ± 50%

*denotes reanalysed sample solution

Fig. 11 – The formation phases of CLlr and MClr. A: Situation preceding the transgression. B: First highstand of MIS 5.5 (ca. 127 ky BP) and formation of palaeoshoreline PS3; formation of the cll level and overlying beach calcarenites

visible in the G4 section (Fig. 7B); C-D: formation of a barrier immediately after the maximum landward shift of the sea; E: uplift and present situation with palaeoshoreline PS3, as modelled by the first highstand of MIS 5.5, at ca. +15 m.

Fig. 12 – Reconstruction of the reoccupation of the MIS 7.3 palaeoshoreline by the MIS 5.5 palaeoshoreline at Montagna Spaccata (MS1 site, Fig. 6B; see Fig. 2A for the location). A: Pre-MIS 7.3; B: MIS 7.3 highstand; C: creation of an abrasion platform and tidal notch during the MIS 7.3 highstand; *H. durotrix* Gosse coral grew on the platform; D: phase of emersion; E: MIS 5.5 reoccupation by the sea of the MIS 7.3 palaeoshoreline (PS3) and deposition of the PS3marine unit (PS3mu); the underlying fossil specimens of *H. durotrix* Gosse are preserved only within holes in the platform. Compare this figure with Fig. 6.

Table 3 – Sea-level highstands (that is, expected palaeoshoreline elevations) and observed palaeoshorelines for the uplift scenario reconstructed in this work. The expected palaeoshoreline elevations are derived from synchronous correlation using sea-level highstands from Waelbroeck et al. (2002) from present to 410 ky BP and Rohling et al. (2014) from 410 to 590 ky (1st and 2nd columns for sea level and age, respectively) and an uplift rate of 0.09 mm/y from 590 to 130 ky BP (middle Pleistocene, interval MIS 15 - MIS 6) and of 0.07 mm/y from 130 ky BP onwards (late Pleistocene or MIS 5 - onwards). Note that some expected palaeoshoreline elevations are lower than or equal to the next younger expected palaeoshoreline, suggesting that they may well be overprinted or reoccupied; that is, removed by erosion during rising sea level by the subsequent highstand. Thus, none of the observed palaeoshorelines were correlated with overprinted/reoccupied palaeoshorelines, with the exception of PS3. Note also that, given the maximum uncertainty of ± 13 in sea-level curves that were used, we consider an acceptable gap of up to 10 m between an expected palaeoshoreline (3rd column) and the observed palaeoshoreline that we associate with it (4th column).

Figure 13 – Elevations of observed palaeoshorelines (coloured arrows) versus expected emerged palaeoshorelines (horizontal, coloured lines) using the synchronous method for topographic profiles of Figure 3. The scenario of expected palaeoshorelines was obtained using sea-level highstands from Waelbroeck et al. (2002) from present to 410 ky BP and Rohling et al. (2014) from 410 to 590 ky BP, and an uplift rate of 0.09 mm/y from 590 to 130 ky BP (middle Pleistocene or interval MIS 15 - MIS 6) and of 0.07 mm/y from 130 ky BP onwards (late Pleistocene or MIS 5 - onwards). Each horizontal line marked with a certain colour represents an expected palaeoshoreline elevation; the arrow of the same colour represents the corresponding observed palaeoshoreline. Note that some expected palaeoshoreline elevations are lower than or equal to the next younger expected palaeoshoreline, suggesting that they may well be overprinted or

reoccupied (dashed horizontal lines). Thus, none of the observed palaeoshorelines have been correlated with overprinted or reoccupied palaeoshorelines. The only exception is PS3, where reoccupation is well documented. The elevations in m. a.p.s.l. of the horizontal lines and arrows are the same as those in the 3^{rd} and 4^{th} columns in Table 3, respectively. Since both the expected and observed palaeoshorelines are at the same heights for the entire study area, they have been reported for only two topographic profiles.

Figure 14~~3~~ – A: Graph showing linear regressions between observed and expected palaeoshoreline elevations. Good fits are quantified by R^2 values that are ≥ 0.99. B: Expected palaeoshoreline elevations; the graph also shows the submerged and overprinted palaeoshorelines. Both graphs are valid for all topographic profiles, as the palaeoshorelines observed in several profiles are always at the same elevation (m.a.p.s.l.).

Table 4- Some examples of emerged palaeoshorelines, with the ages to which they have been attributed, reconstructed uplift rates, and relative references.

References

Alfaro, P., Delgado, J., Estévez, A., Molina, J.M., Moretti, M., Soria, J.M., 2002. Liquefaction and fluidization structures in Messinian storm deposits of the Lower Segura Basin (Betic Cordillera, Southern Spain). International Journal of Earth Sciences 91, 505-513.

Ambrosetti, P., Bosi, C., Carraro, F., Ciaranfi, N., Panizza, M., Papani, G., Vezzani, L., Zanferrari, A., 1987. Neotectonic Map of Italy: Scale 1:500,000. Consiglio Nazionale delle Ricerche, Progetto Finalizzato Geodinamica, Sottoprogetto Neotettonica. Litografia Artistica Cartografica, Florence (Italy).

Amorosi, A., Antonioli, F., Bertini, A., Marabini, S., Mastronuzzi, G., Montagna, P.,Negri, A., Rossi, V., Scarponi, D., Taviani, M., Angeletti, L., Piva, A., Vai, G.B., 2014. The Middle-Upper Pleistocene Fronte Section (Taranto, Italy): An exceptionally preserved marine record of the Last Interglacial. Global and Planetary Change 119, 23-38.

Andersen, M.B., Stirling, C.H., Zimmermann, B., Halliday, A.N. 2010. Precise determination of the open ocean 234U/238U composition. Geochemistry, Geophysics, Geosystems 11, Q12003.

Antonioli, F., Ferranti, L., Stocchi, P., Deiana, G., Lo Presti, V., Furlani, S., Marino, C., Orru, P., Scicchitano, G., Trainito, E., 2018. Morphometry and elevation of the last interglacial tidal notches in tectonically stable coasts of the Mediterranean Sea. Earth-Science Reviews 185, 600–623.

Antonioli, F., Lo Presti, V., Rovere, A., Ferranti, L., Anzidei, M., Furlani, S., Mastronuzzi, G., Orru P., Scicchitano, G., Sannino, G., Spampinato, C.R., Pagliarulo, R., Deiana, G., de Sabata, E., Sansò, P., Vacchi, M., Vecchio, A., 2015. Tidal notches in Mediterranean Sea: a comprehensive analysis. Quaternary Science Reviews 119, 66-84.

Armijo, R., Meyer, B., King, G. C. P., Rigo, A., Papanastassiou, D. 1996. Quaternary evolution of the Corinth Rif and its implications for the Late Cenozoic evolution of the Aegean. Geophys. Journal International 126, 11–53.

Ascione, A., Romano, P., 1999. Vertical movements on the eastern margin of the Tyrrhenian extensional basin. New data from Mt. Bulgheria (Southern Apennines, Italy). Tectonophysics 315, 337–356. https://doi.org/10.1016/S0040-1951(99) 00279-6.

Azzaroli, A.,1968. Calcarenite di Gravina. Studi illustrativi della Carta Geologica d'Italia - Servizio Geologico d'Italia, Formazioni Geologiche, Fasc. 1, 183-187.

~~Azzaroli, A., Perno, U., Radina, B., 1968. Note illustrative del Foglio 188 "Gravina di Puglia" della Carta Geologica d'Italia alla scala 1:100.000. Servizio Geologico d'Italia, Roma.~~

Belluomini, G., Caldara, M., Casini, C., Cerasoli, M., Manfra, L., Mastronuzzi, G., Palmentola, G., Sansò, P., Tuccimei, P., Vesica, P.L., 2002. The age of Late Pleistocene shorelines and tectonic activity of Taranto area, Southern Italy. Quaternary Science Reviews 21, 525-547.

Benjamin, J., Rovere, A., Fontana, A., Furlani, S., Vacchi, M., Inglis, R.H., Galili E., Antonioli, F., Sivan D., Miko, S., Mourtzas, N., Felja, I., Meredith-Williams, M., Goodman-Tchernov, B., Kolaiti, E., Anzidei, M., Gehrels, R., 2017. Late Quaternary sea-level changes and early human societies in the central and eastern Mediterranean Basin: An interdisciplinary review. Quaternary International 449, 29–57

Bianca, M., Catalano S., De Guidi, G., Gueli, A.M., Monaco, C., Ristuccia, G.M, Stella, G., Tortorici, G., Tortorici, L., Troja, S. O., 2011. Luminescence chronology of Pleistocene marine terraces of Capo Vaticano peninsula (Calabria, southern Italy). Quaternary International 232(1-2), 114-121.

Boenzi, F., Caldara, M., Pennetta, L., 1986. La trasgressione tirreniana nei dintorni di Castellaneta (Taranto). Geologia Applicata ed Idrogeologia 20(1) 1985, 163-175.

Boenzi, F., Caldara, M., Pennetta, L., 2010. L'ambiente fisico e la distribuzione dei vini nella regione pugliese. In: Storia regionale della vite e del vino in Italia: le Puglie. La Daunia, la Terra di Bari, la Terra d'Otranto, in: Calò, A., Bertoldi Le Noci, L (Eds.), Edizioni Pugliesi s.r.l. Martina Franca, pp. 17-31, ISBN 9788883481642.

Bright, J., Kaufman, D.S., 2011. Amino acid racemization in lacustrine ostracodes, part I: effect of oxidizing pre-treatments on amino acid composition. Quaternary Geochronology, 6, 154-173.

Bromley R.G., D'Alessandro A., 1987. Bioerosion of the Plio-Pleistocene transgression of Southern Italy. Riv. It. Paleont. Strat., 93(3), 379-442.

Brückner, H., 1980. Marine Terrassen in Süditalien. Eine quartärmorphologische Studie über das Küstentiefland von Metapont. Düsseldorfer Geographische Schriften, 14, 235 pp., Düsseldorf (PhD thesis).

Caldara, M., D'Alessandro, A., Di Geronimo, I., 1981. Paleocomunità circalitorali del Pleistocene di Gallipoli (Lecce). Bollettino Malacologico 17(7-8), 25-164.

Caldara, M., Iannone, A., Lopez, R., Simone, O., De Santis, V., Torres, T., Ortiz, J.E., 2013. New data on the Pleistocene of Trani (Adriatic coast, southern Italy). Italian Journal of Geosciences 132(2), 239-253.

Caldara, M., Mastronuzzi, G., Palmentola, G., Sansò, P., Tuccimei, P., Vesica, P.L., 2003. Reply to the comment by. Hearty, P.J and Dai Pra, G. Quaternary Science Reviews 22(4-6), 2369-2371.

Caputo, R., Bianca, M., D'Onofrio, R., 2010. Ionian marine terraces of southern Italy: Insights into the Quaternary tectonic evolution of the area. Tectonics 29(4), TC4005.

.

Cerrone, C., Ascione, A., Robustelli G., Soligo, M., Balassone, G., Tuccimei, P., 2021a. Late Quaternary uplift and sea level fluctuations along the Tyrrhenian margin of Basilicata-northern Calabria (southern Italy): new constraints from raised paleoshorelines. Geomorphology 395, 107978. https://doi.org/10.1016/j.geomorph.2021.107978

Cerrone, C., Vacchi, M., Fontana, A., Rovere, A., 2021b. Last Interglacial sea-level proxies in the Western Mediterranean. Earth System Science Data 13(9), 4485-4527.

Cheng, H., Lawrence Edwards, R., Shen, C.-C., Polyak, V. J., Asmerom, Y., Woodhead, J., Hellstrom, J., Wang, Y., Kong, X., Spötl, C., Wang, X., and Calvin Alexander, E., 2013. Improvements in ^{230}Th dating, ^{230}Th and ^{234}U half-life values, and U–Th isotopic measurements by multi-collector inductively coupled plasma mass spectrometry. Earth and Planetary Science Letters 371-372, 82-91.

Ciaranfi, N., Pieri, P., Ricchetti, G., 1992. Note alla carta geologica delle Murge e del Salento (Puglia centro-meridionale). Memorie della Società Geologica Italiana 41(1988), 449-460.

Cinque, A., Romano, P., 1990. Segnalazioni di nuove evidenze di antiche linee di riva in Penisola Sorrentina (Campania). Geografia Fisica e Dinamica Quaternaria 13,23-26.

~~Cowie, P. A., Roberts, G. P., Bull, J. M., Visini, F., 2012. Relationships between fault geometry, slip rate variability and earthquake recurrence in extensional settings. Geophysical Journal International 189(1), 143-160.~~

Cowie, P.A., Roberts, G.P., 2001. Constraining slip rates and spacings for active normal faults. Journal of Structural Geology 23(12), 1901-1915.

Cowie, P. A., Roberts, G. P., Bull, J. M., Visini, F., 2012. Relationships between fault geometry, slip rate variability and earthquake recurrence in extensional settings. Geophysical Journal International 189(1), 143-160.

Formatted: Italian (Italy)

Formatted: English (United Kingdom)

Formatted: English (United Kingdom)

De Giosa, F., Scardino, G., Vacchi, M., Piscitelli, A., Milella, M., Ciccolella, A., Mastronuzzi, G., 2019. Geomorphological signature of late Pleistocene sea level oscillations in Torre Guaceto marine protected area (Adriatic Sea, SE Italy). Water 11(11), 2409.

De Santis, V., Caldara, M., 2016. Evolution of an incised valley system in the southern Adriatic Sea (Apulian margin): an onshore–offshore correlation. Geological Journal 51 (2), 263-284.

De Santis, V., Caldara, M., Pennetta, L., 2014a. The marine and alluvial terraces of Tavoliere di Puglia plain (southern Italy). Journal of Maps 10(1), 114-125.

De Santis, V., Caldara, M., Pennetta, L., 2020a. Continuous backstepping of Holocene coastal barrier systems into incised valleys: Insights from the Ofanto and Carapelle-Cervaro valleys. Water 12(6), 1799.

De Santis, V., Caldara, M., Pennetta, L., 2020b. Transgressive architecture of coastal barrier systems in the Ofanto incised valley and its surrounding shelf in response to stepped sea-level rise. Geosciences 10(12), 497.

De Santis, V., Caldara, M., Pennetta, L., Torres, T., Ortiz, J.E., 2013. Unconformity Bounded Stratigraphic Units in an Italian alluvial plain area: recognising and dating. Journal of Sedimentary Research 83, 96-114.

De Santis, V., Caldara, M., Torres, T., Ortiz, J.E., 2010. - Stratigraphic units of the Apulian Tavoliere Plain: chronology, correlation with marine isotope stages and implication regarding vertical movements. Sedimentary Geology 228, 255-270.

De Santis, V., Caldara, M., Torres, T., Ortiz, J.E., 2014b - Two middle Pleistocene warm stages in the Terraced Deposits of the Apulia Region (southern Italy). Quaternary international 332, 2-18.

De Santis, V., Caldara, M., Torres, T., Ortiz, J.E., Sánchez-Palencia, Y., 2018. A review of MIS 7 and MIS 5 terrace deposits along the gulf of Taranto based on new stratigraphic and chronological data. Italian Journal of Geosciences 137, 349-368.

De Santis, V., Caldara, M., Torres T., Ortiz J.E., Sánchez-Palencia Y., 2020c. The role of beach ridges, spits, or barriers in understanding marine terraces processes on loose or semiconsolidated substrates: Insights from the givoni of the Gulf of Taranto (southern Italy). Geological Journal 55(4), 2951-2975.

De Santis, V., Scardino, G., Meschis, M., Ortiz J.E., Sánchez-Palencia Y., Caldara M., 2021a. Refining the middle-late Pleistocene chronology of marine terraces and uplift history in a sector of the Apulian foreland (southern Italy) by applying a synchronous correlation technique and amino acid racemization to Patella spp. and Thetystrombus latus. Italian Journal of Geosciences 140 (3), 438-463

De Santis, V., Scardino, G., Ortiz, J.E., Sánchez-Palencia, Y., Caldara, M., 2021b. Pleistocene terracing phases in the metropolitan area of Bari - AAR dating and deduced uplift rates of the Apulian foreland. Rendiconti online della Società Geologica Italiana 54, 49-61.

De Santis, V., Scardino, G., Scicchitano, G., Montagna, P., Pons-Branchu, E., Ortiz J.E., Sánchez-Palencia Y, Lisco S, Moretti M., Caldara M., 2022. Last interglacial pressure pattern over the Mediterranean from aeolian sediments: A case study from Apulia. Palaeogeography, Palaeoclimatology, Palaeoecology 605, https://doi.org/10.1016/j.palaeo.2022.111228 .

Doglioni, C., Mongelli, F., Pieri, P., 1994. The Puglia uplift (SE Italy): an anomaly in the foreland of the Apenninic subduction due to buckling of a thick continental lithosphere. Tectonics 13(5), 1309-1321.

Doglioni, C., Tropeano, M., Mongelli, F., Pieri, P., 1996. Middle-late Pleistocene uplift of Puglia: an anomaly in the Apenninic foreland. Memorie della Società Geologica Italiana 51, 101-117.

Düsterhus, A., Tamisiea, M. E., Jevrejeva, S., 2016. Estimating the sea level highstand during the Last Interglacial: a probabilistic massive ensemble approach. Geophysical Journal International 206, 900–920.

Dutton, A., Carlson, A.E., Long, A.J., Milne, G.A., Clark, P.U., De Conto, R., Horton, B.P., Rahmstorf, S., Raymo, M.E., 2015a. Sea- level rise due to polar ice- sheet mass loss during past warm periods. Science 349(6244), aaa4019.

Dutton, A., Webster, J. M., Zwartz, D., Lambeck, K., Wohlfarth, B., 2015b. Tropical tales of polar ice: Evidence of last interglacial polar ice sheet retreat recorded by fossil reefs of the granitic Seychelles islands. Quaternary Science Review 107, 182–196.

Dutton A., Lambeck, K., 2012. Ice volume and sea level during the last interglacial. Science 337, 216–219

Evelpidou, N., Vassilopoulos, A., Pirazzoli, P.A., 2012. Holocene emergence in Euboea Island (Greece). Marine Geology 295–298, 14–19

Ferranti, L., Antonioli, F., Mauz, B., Amorosi, A., Dai Pra, G., Mastronuzzi, G., Monaco, C., Orru P., Pappalardo, M., Radtke, U., Renda, P., Romano, P., Sansò, P., Verrubbi, V., 2006. Markers of the last interglacial sea-level high stand along the coast of Italy: tectonic implications. Quaternary International 145-146, 30-54.

Ferranti, L., Burrato, P., Sechi, D., Andreucci, S., Pepe, F., Pascucci, V., 2021. Late Quaternary coastal uplift of southwestern Sicily, central Mediterranean Sea. Quaternary Science Reviews 255, 106812.

Ferranti, L., Oldow, J.S., 2006. Rates of late Neogene deformation along the southwestern margin of Adria, southern Apennines orogen, Italy, in: Pinter, N., Gyula, G., Weber J., Stein S., Medak D. (Eds.), The Adria Microplate: GPS Geodesy, Tectonics and Hazards. Nato Science Series: IV: Earth and Environmental Sciences 61. Springer, Dordrecht.

Gallen, S.F., Wegmann, KW, Bohnenstiehl, D.R., Pazzaglia, F.J., Brandon, M.T, Fassoulas, C., 2014. Active simultaneous uplift and margin-normal extension in a forearc high, Crete, Greece. Earth and Planetary Science Letters 398, 11-24.

Gignoux, M., 1913. Les formations marines: Pliocènes et Quaternaires de l’Italie du sud et de la Sicile. A. Rey; J.-B. Baillière, Lyon; Paris

Grant, K.M., Rohling, E.J., Bar-Matthews, M., Ayalon, A., Medina-Elizalde, M., Ramsey, C.B., Satow, C., Roberts, A.P., 2012. Rapid coupling between ice volume and polar temperature over the past 150,000 years. Nature. 2012 Nov 29; 491(7426).

Grant, K.M., Rohling, E.J, Ramsey, C.B., Cheng, H., Edwards, R.L., Florindo, F., Heslop, D., Marra F., Roberts, A.P., Tamisiea, M.E., Williams, F., 2014. Sea-level variability over five glacial cycles. Nature Communications 5, 5076.

Hearty, P.J., 1987. New data on the Pleistocene of Mallorca. Quaternary Science Reviews 6, 245-257.

Hearty, P.J., Dai Pra, G., 1987. Paleogeographic reconstruction of Quaternary environments in Toscana and north Lazio, central Italy. Bollettino del Servizio Geologico d'Italia 106, 189-224.

Hearty P.J., Dai Pra G., 1992. The age and stratigraphy of Middle Pleistocene and younger deposits along the Gulf of Taranto (Southeast Italy). Journal of Coastal Research 8(4), 82-105.

Hearty P.J., Hollin, J.T., Dumas, B., 1987. Geochronology of Pleistocene littoral deposits on the AIicante and Almeria coasts of Spain, in: Zazo, C. (Eds.), Late Quaternary Sea Level Changes in Spain. Trab. Neogeno-Cuaternario 10, 95-105.

Hearty, P.J., Hollin, J.T., Neumann, A.C., O'Leary, M.J., Mcculloch, M., 2007. Global sea-level fluctuations during the Last Interglaciation (MIS 5e). Quaternary Science Reviews 26, 2090-2112.

Hearty, P.J., Miller, G., Stearns, C., Szabo, B.J., 1986. Aminostratigraphy of Quaternary shorelines in the Mediterranean basin. Geological Society of America Bulletin 97, 850-858.

Henkel, D.J., 1970. The Role of Waves in Causing Submarine Landslides. Géotechnique 20(1), 75-80.

Iannone, A., Pieri, P., 1979. Considerazioni critiche sui tufi calcarei delle Murge. Nuovi dati litostratigrafici e paleoambientali. Geografia Fisica e Dinamica Quaternaria 2, 173-186.

Formatted: Italian (Italy)

Formatted: Italian (Italy)

Jaffey, A.H., Flynn, K.F., Glendenin, L.E., Bentley, W.C., Essling, A.M., 1971. Precision measurement of half-lives and specific activities of ^{235}U and ^{238}U. Physical Review C 4 (5), 1889–1906.

Kaufman, D.S., 2000. Amino acid racemization in ostracodes, in: Goodfriend, G., Collins, M., Fogel, M., Macko, S., Wehmiller, J., (Eds.), Perspectives in Amino Acid and Protein Geochemistry: New York, Oxford University Press, 145–160.

Kaufman, D.S., 2006. Temperature sensitivity of aspartic and glutamic acid racemization in the foraminifera Pulleniatina. Quaternary Geochronology 1, 188–207.

Kaufman, D.S., Manley, W.F., 1998. A new procedure for determining DL amino acid ratios in fossils using reverse phase liquid chromatography. Quaternary Science Reviews, 17, 987-1000.

Kershaw, S., 2000. Quaternary reefs of northeastern Sicily: structure and growth controls in an unstable tectonic setting. Journal of Coastal Research, 1037-1062.

Kidwell, S.M., 1998. Time-averaging in the marine fossils record: overview of strategies and uncertainties. Geobios 30 (7), 977-995.

Kopp, R.E., Simons, F.J., Mitrovica, J.X., Maloof, A.C., Oppenheimer, M., 2009. Probabilistic assessment of sea level during the last interglacial stage. Nature 462, 863–867.

Kopp, R.E., Simons, F.J., Mitrovica, J.X., Maloof, A.C., Oppenheimer M., 2013. A probabilistic assessment of sea level variations within the last interglacial stage. Geophysical Journal International 193, 711–716.

Iannone, A., Pieri, P., 1979. Considerazioni critiche sui tufi calcarei delle Murge. Nuovi dati litostratigrafici e paleoambientali. Geografia Fisica e Dinamica Quaternaria 2, 173-186.

Kershaw, S., 2000. Quaternary reefs of northeastern Sicily: structure and growth controls in an unstable tectonic setting. Journal of Coastal Research, 1037-1062.

Lajoie, K.R., 1986. Coastal tectonics. Active tectonics, pp.95-124.

Formatted: Italian (Italy)

Largaiolli, T., Martinis, B., Mozzi, G., Nardin, M., Rossi, D., Ungaro, S., 1969. Note illustrative del della Carta Geologica d'Italia alla scala 1:100.000, F. 214 "Gallipoli". Servizio Geologico d'Italia, Roma.

Lorscheid, T., Stocchi, P., Casella, E., Gómez-Pujol, L., Vacchi, M., Mann, T., Rovere, A., 2017. Paleo sea-level changes and relative sea-level indicators: Precise measurements, indicative meaning and glacial isostatic adjustment perspectives from Mallorca (Western Mediterranean). Palaeogeography, Palaeoclimatology, Palaeoecology 473, 94–107.

Ludwig, K.R., Titterington, D.M., 1994. Calculation of ^{230}Th/U Isochrons, Ages, and Errors. Geochimica et Cosmochimica Acta 58, 5031-5042.

Marra, F., Florindo, F., Anzidei, M., Sepe, V., 2016. Paleo-surfaces of glacio-eustatically forced aggradational successions in the coastal area of Rome: assessing interplay between tectonics and sea-level during the last ten interglacials. Quaternary Science Review 148, 85-100.

Marra, F., Bahain, J.J., Jicha, B.R., Nomade, S., Palladino, D.M., Pereira, A., Tolomei, C., Pierre Voinchet, P., Anzidei, M., Aureli, D., Ceruleo, P., Falgueres, C., Florindo, F., Gatta, M., Ghaleb, B., La Rosa, M., Peretto, C., Petronio, C., Rocca, R., Rolfo, M.F., Salari, L., Smedile, A., Tombret, O., 2019. Reconstruction of the MIS 5.5, 5.3 and 5.1 coastal terraces in Latium (central Italy): A re-evaluation of the sea-level history in the Mediterranean Sea during the last interglacial. Quaternary International 525, 54-77.

Marra, F., Rolfo, F.M., Gaeta, M., Florindo, F., 2020. Anomalous Last Interglacial Tyrrhenian sea levels and Neanderthal settling at Guattari and Moscerini caves (central Italy). Scientific Reports 10:11929.

Meschis, M., Roberts, G. P., Robertson, J., Briant, R. M., 2018. The relationships between regional Quaternary uplift, deformation across active normal faults, and historical seismicity in the upper plate of subduction zones: the Capo D'Orlando fault. NE Sicily. Tectonics 37(5), 1231-1255.

Meschis, M., Scicchitano, G., Roberts, GP., Robertson, J., Barreca, G., Monaco, C., Spampinato, C., Sahy D., Antonioli F., Mildon Z.K., Scardino, G., 2020 Regional deformation and offshore crustal local faulting as combined processes to explain uplift through time constrained by investigating differentially uplifted late quaternary paleoshorelines: the Foreland Hyblean Plateau, SE Sicily. Tectonics 39, e2020TC006187.

Meschis, M., Roberts, G.P., Robertson, J., Mildon, Z.K., Sahy, D., Goswami, R., Sgambato, C., Faure Walker, J., Michetti, A.M., Iezzi, F., 2022. Out of phase Quaternary uplift-rate changes reveal normal fault interaction, implied by deformed marine palaeoshorelines. Geomorphology 108432, https://doi.org/10.1016/j.geomorph.2022.108432Molina, J. M., Alfaro, P., Moretti, M., Soria J. M., 1998. Soft-sediment deformation structures induced by cyclic stress of storm-waves in tempestites (Miocene, Guadalquivir Basin, Spain). Terra Nova 10(3), 145-150.

Murray-Wallace, C.V., Woodroffe, C.D., 2014. Quaternary Sea-Level Changes: A Global Perspective. Cambridge University Press.

Negri, A., Amorosi, A., Antonioli, F., Bertini, A., Florindo, F., Lurcock, P.C., Marabini, S., Mastronuzzi, G., Regattieri, E., Rossi V., Scarponi, D., Taviani, M., Zanchetta, G., Vai, G.B., 2015. A potential global boundary stratotype section and point (GSSP) for the Tarentian Stage, Upper Pleistocene, from the Taranto area (Italy): Results and future perspectives. Quaternary International 383, 145-157.

O'Leary, M., Hearty, P., Thompson, W., Raymo M.E, Mitrovica, J.X., Webster, J.M., 2013. Ice sheet collapse following a prolonged period of stable sea level during the last interglacial. Nature Geosciences 6, 796-800.

Ortiz, J.E., Gutiérrez-Zugasti, I., Torres, T., González-Morales, M., Sánchez-Palencia, Y., 2015. Protein diagenesis in Patella shells: implications for amino acid racemisation dating. Quaternary Geochronology 27, 105-118.

Ortiz, J.E., Torres, T., Pérez-González, A., 2013. Amino acid racemization in four species of ostracodes: taxonomic, environmental, and microstructural controls. Quaternary Geochronology 16, 129-143.

Ortiz, J.E., Torres, T., Julià, R., Delgado, A., Llamas, F.J., Soler, V., Delgado, J., 2004. Numerical dating algorithms of amino acid racemization ratios from continental ostracodes. Application to Guadix-Baza basin (southern Spain). Quaternary Science Reviews 23(5-6), 717-730.

Otvos, E.G., 2021. Coastal barriers-nomenclature, processes, and classification issues. Geomorphology 139–140, 39–52.

Pedoja, K., Jara-Muñoz, J., De Gelder, G., Robertson, J., Meschis, M., Fernandez-Blanco, D., Nexer, M., Poprawski, Y., Dugué, O., Delcaillau, B., Bessin, P., Benabdelouahed, M., Authemayou, C., Husson, L., Regard, V., Menier, D., Pinel, B., 2018. Neogene-Quaternary slow coastal uplift of western Europe through the perspective of sequences of strandlines from the Cotentin Peninsula (Normandy, France). Geomorphology 303, 338-356.

Pérès, J.M., 1967. The Mediterranean benthos. Oceanography Marine Biology Annual Review 5, 449–533.

Picton, B.E., Morrow, C.C., 2016. Hoplangia durotrix Gosse, 1860. In: Encyclopedia of Marine Life of Britain and Ireland. http://www.habitas.org.uk/marinelife/species.asp?item=D13860 Accessed on 2022-05-20.

Pons-Branchu E., Douville E., Roy-Barman M., Dumont E., Branchu P., Thil F., Frank N., Bordier L., Borst W., 2014. A geochemical perspective on Parisian urban history based on U-Th dating, laminae counting and yttrium and REE concentrations of recent carbonates in underground aqueducts. Quaternary Geochronology 24, 43-54.

Powell, J., Collins, M.J., Cussens, J., McLeod, N., Penkman, K.E.H., 2013. Results from an amino acid racemization inter-laboratory proficiency study; design and performance evaluation. Quaternary Geochronology 16, 183-197.

Progetto PST - Dati Lidar [WWW Document], 2021. Geoportale Nazionale. URL http://www.pcn.minambiente.it/mattm/progetto-pst-dati-lidar/

Ricchetti, G., Ciaranfi N., 2013. Note Illustrative della Carta Geologica d'Italia alla scala 1:50.000, F. 536 Ugento. 120 pp., LAC, Firenze.

Ricchetti, G., Ciaranfi, N., Luperto Sinni, E., Mongelli, F., Pieri, P., 1992. Geodinamica ed evoluzione sedimentaria e tettonica dell'avampaese apulo. Memorie Società Geologica Italiana, 41(1988), 57-82.

Roberts, G. P., Houghton, S. L., Underwood, C., Papanikolaou, I., Cowie, P. A., Van Calsteren, P., Wigley, T., Cooper, F.J., McArthur, J.M.,~~et al.,~~ 2009. Localization of quaternary slip rates in an active rift in 105 years: An example from central Greece constrained by ^{234}U- ^{230}Th coral dates from uplifted paleoshorelines. Journal of Geophysical Research 114, B10406.

Roberts, G. P., Meschis, M., Houghton, S., Underwood, C., Briant, R. M., 2013. The implications of revised Quaternary palaeoshoreline chronologies for the rates of active extension and uplift in the upper plate of subduction zones. Quaternary Science Reviews 78, 169-187.

Robertson, J., Meschis, M., Roberts, G. P., Ganas, A., Gheorghiu, D.M., 2019. Temporally constant quaternary uplift rates and their relationship with extensional upper- plate faults in south Crete (Greece), constrained with ^{36}Cl~~L~~ cosmogenic exposure dating. Tectonics 38(4), 1189-1222.

Robertson, J.,~~;~~ Roberts, G. P.,~~;~~ Iezzi, F.,~~;~~ Meschis, M.,~~;~~ Gheorghiu, D. M.,~~;~~ Sahy, D.,~~;~~ Bristow, C.,~~;~~ Sgambato, C., 2020. Distributed normal faulting in the tip zone of the South Alkyonides Fault System, Gulf of Corinth, constrained using 36Cl exposure dating of late-Quaternary wave-cut platforms 36: 104063.

Rohling, E., Grant, K., Hemleben, C., Siddal, M., Hoogakker, B.A.A., Bolshaw, M., Kucera M., 2008. High rates of sea-level rise during the last interglacial period. Nature Geosciences, 1, 38–42.

Rohling, E.J., Foster, G.L., Grant, K.M., Marino, G., Roberts, A.P., Tamisiea, M.E., Williams, F., 2014. Sea- level and deep- sea- temperature variability over the past 5.3 million years. Nature 508(7497), 477-482.

Rohling, E.J., Hibbert, F.D., Gran,t K.M., Galaasen, E.V., Irval, N., Kleiven, H.F., Marino G., Ninnemann, U., Roberts, A.P., Rosenthal, Y., Schulz, H., Williams, F.H., Yu, J., 2019. Asynchronous Antarctic and Greenland ice- volume contributions to the last interglacial sea-level highstand. Nature Communications 10(1), 5040.

Roy, P. S., Cowell, P. J., Ferland, M. A., Thom, B. G., 1994. Wave dominated coast, in: Carter, R.W.G., Woodroffe, C.D. (Eds.), Coastal evolution, Late Quaternary shoreline morphodynamics, Cambridge University Press, Cambridge, pp. 121–186.

Rovere, A., Antonioli, F., Bianchi, C. N., Shennan, I., Long, A. J., & Horton, B. P., 2015. Fixed biological indicators. Handbook of sea-level research, 268-280.

Rovere, A., Raymo, M.E., Vacchi, M., Lorscheid, T., Stocchi, P., Gómez-Pujol, L., Harris, D.L., Casella, E., O'Leary, M.J., Hearty, P.J., 2016. The analysis of Last Interglacial (MIS 5e) relative sea-level indicators: Reconstructing sea-level in a warmer world. Earth-Science Reviews 159, 404–427.

Roy, P. S., Cowell, P. J., Ferland, M. A., Thom, B. G., 1994. Wave dominated coast, in: Carter, R.W.G., Woodroffe, C.D. (Eds.), Coastal evolution, Late Quaternary shoreline morphodynamics, Cambridge University Press, Cambridge, pp. 121–186.

Scicchitano, G., C. R. Spampinato, L. Ferranti, F. Antonioli, C. Monaco, M. Capano, and C. Lubritto. "Uplifted Holocene shorelines at Capo Milazzo (NE Sicily, Italy): evidence of co-seismic and steady-state deformation." Quaternary International 232(1-2), 201-213.

M. Siddall, J. Chappell, E.-K. Potter. 2007. Eustatic sea level during past interglacials, in: Frank Sirocko, Martin Claussen, María Fernanda Sánchez Goñi, Thomas Litt. (Eds.), Developments in Quaternary Sciences (7), Elsevier, pp.75-92.

Stirling, C.H., Esat, T.M., Lambeck, K., McCulloch, M.T., 1998. Timing and duration of the Last Interglacial: Evidence for a restricted interval of widespread coral reef growth. Earth Planetary Science Letters 160, 745–762.

Formatted: English (United Kingdom)

Formatted: English (United Kingdom)

Stiros, S.C., Arnold, M., Pirazzoli, P.A., Laborel, J., Laborel, F., Papageorgiou, S., 1992. Historical coseismic uplift on Euboea Island, Greece. Earth and Planetary Science Letters, 108, 109-117.

Stocchi, P., Vacchi, M., Lorscheid, T., de Boer, B., Simms, A. R., van de Wal, R.S.W., Vermeersen, B.L.A., Pappalardo, M., Rovere, A., 2018. MIS 5e relative sea-level changes in the Mediterranean Sea: Contribution of isostatic disequilibrium. Quaternary Science Reviews, 185, 122-134.

Taviani, M., 2014. Unpersisting Persististrombus: a Mediterranean story. Vieraea 42, 9–18.

Thompson, W.G., Curran, H.A., Wilson, M.A., White, B. 2011. Sea-level and ice-sheet instability during the Last Interglacial: New Bahamas evidence. Nature Geosciences 4, 684.

Thompson, W.G., Spiegelman, M.W., Goldstein, S.L., Speed, R.C., 2003. An open-system model for U-series age determinations of fossil corals. Earth and Planetary Science Letters, 210, 365-381.

~~Torres T., Llamas J., Canoira L., García-Alonso P., García-Cortés A., Mansilla H., 1997. Amino acid chronology of the Lower Pleistocene deposits of Venta Micena (Orce, Granada, Andalusia, Spain). Organic Geochemistry 26, 85-97.~~

Torres, T., Llamas, J.F., Canoira, L., Coello, J., García-Alonso, P., Ortiz J.E., 2000. Aminostratigraphy of two marine sequences from the Mediterranean coast of Spain. Cabo de Huertas (Alicante) and Garrucha (Almería), in: Goodfriend, G.A., Collins, M.J., Fogel, M.L., Macko S.A., Wemiller J.F. (Eds.), Perspectives in Amino Acid and Protein Geochemistry. Oxford University Press, New York, pp. 263-278.

Torres T., Llamas J., Canoira L., García-Alonso P., García-Cortés A., Mansilla H., 1997. Amino acid chronology of the Lower Pleistocene deposits of Venta Micena (Orce, Granada, Andalusia, Spain). Organic Geochemistry 26, 85-97.

Torres, T., Ortiz, J.E., Arribas, I., 2013. Variations in racemization/epimerization ratios and amino acid content of Glycymeris shells in raised marine deposits in the Mediterranean. Quaternary Geochronology 16, 35-49.

~~Tropeano, M., Sabato, L., Pieri P, 2002. Filling and cannibalization of a foredeep: the Bradanic Trough, Southern Italy. Geological Society, London, Special Publications 191, 55-79.~~

Formatted: Italian (Italy)

Vacchi, M., Marriner, N., Morhange, C., Spada, G., Fontana, A., Rovere, A., 2016. Multiproxy assessment of Holocene relative sea-level changes in the western Mediterranean: Sea-level variability and improvements in the definition of the isostatic signal. Earth Science Reviews 155, 172–197.

Valenzano, E., Scardino, G., Cipriano, G., Fago, P., Capolongo, D., De Giosa, F., Lisco, S., Mele, D., Moretti, M., Mastronuzzi, G., 2018. Holocene morpho-sedimentary evolution of the Mar Piccolo basin (Taranto, Southern Italy). Geografia Fisica e Dinamica Quaternaria 41, 119-135

Waelbroeck, C., Labeyrie, L., Michel, E., Duplessy, J.C., McManus, J.F., Lambeck, K., Balbon, E., Labracherie, M., 2002. Sea-level and deep water temperature changes derived from benthic foraminifera isotopic records. Quaternary Science Reviews 21, 295-305.

Wehmiller, J. F., 1984. Interlaboratory comparison of amino acid enantiomeric ratios in fossil mollusks. Quaternary Research 22, 109-120.

Wehmiller, J.F., Miller, G., De Vogel, S., Kaufman, D.S., Brigth, J., Murray-Wallace, C.V., Ortiz, J.E., Penkman, K., 2010. Interlaboratory comparison of amino acid D/L values. Geological Society of America Annual Meeting, Denver, Abstracts with Programs 42(5), 86.

Westaway, R., 1993. Quaternary uplift of southern Italy. Journal of Geophysical Research: Solid Earth 98(B12), 21741-21772.

Whitacre, K.E., Kaufman, D.S., Kosnik, M.A., Hearty, P.J., 2017. Converting A/I values (ion exchange) to D/L values (reverse phase) for amino acid geochronology. Quaternary Geochronology 37, 1-6.

Zander, A., Fülling, A., Brückner, H., Mastronuzzi, G., 2006. OSL dating of Upper Pleistocene littoral sediments: a contribution to the chronostratigraphy of raised marine terraces bordering the Gulf of Taranto, South Italy. Geografia Fisica e Dinamica Quaternaria 29(1), 33-50.

Zazo, C., Goy, J.L., Dabrio, C.J., Bardajì, T., Hillaire-Marcel, C., Ghaleb, B., Gonza¤lez-Delgado, J.A., Soler, V., 2003. Pleistocene raised marine terraces of the Spanish Mediterranean and Atlantic coasts: records of coastal uplift, sea-level highstands and climate changes. Marine Geology 194, 103–133.

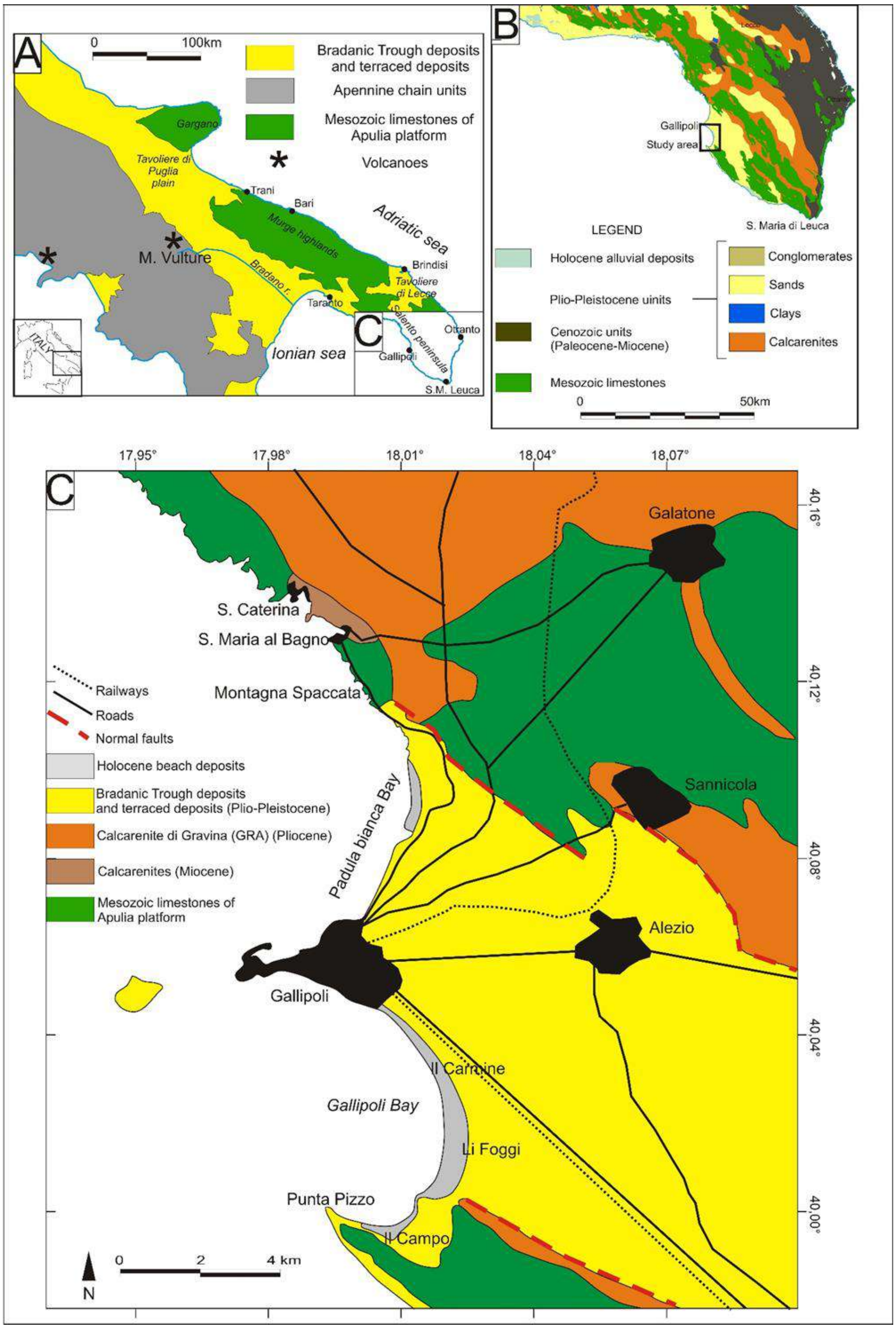
A
0
100km
Bradanic Trough deposits and terraced deposits
Apennine chain units
Mesozoic limestones of Apulia platform
Volcanoes
Gargano
Tavoliere di Puglia plain
Trani
Bari
Murge highlands
Adriatic sea
M. Vulture
Bradano r.
Brindisi
Tavoliere di Lecce
Taranto
Ionian sea
ITALY
C
Salento peninsula
Otranto
Gallipoli
S.M. Leuca
B
Gallipoli
Study area
S. Maria di Leuca
LEGEND
Holocene alluvial deposits
Plio-Pleistocene uinits
Cenozoic units (Paleocene-Miocene)
Mesozoic limestones
Conglomerates
Sands
Clays
Calcarenites
0
50km
17,95°
17,98°
18,01°
18,04°
18,07°
40,16°
40,12°
40,08°
40,04°
40,00°
C
Galatone
S. Caterina
S. Maria al Bagno
Montagna Spaccata
Railways
Roads
Normal faults
Holocene beach deposits
Bradanic Trough deposits and terraced deposits (Plio-Pleistocene)
Calcarenite di Gravina (GRA) (Pliocene)
Calcarenites (Miocene)
Mesozoic limestones of Apulia platform
Padula bianca Bay
Sannicola
Alezio
Gallipoli
Il Carmine
Gallipoli Bay
Li Foggi
Punta Pizzo
Il Campo
0
2
4 km
N

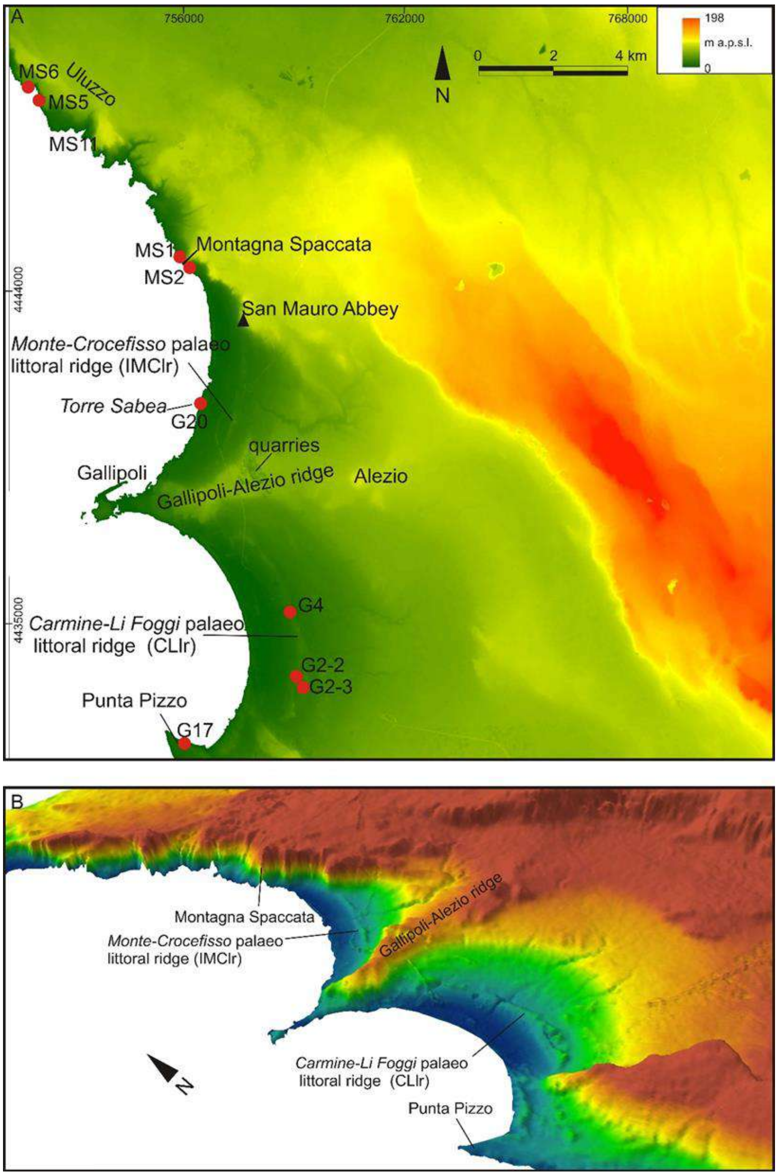
A
756000
762000
768000
198
m a.p.s.l.
0
0
2
4 km
N
MS6
Uluzzo
MS5
MS11
MS1
Montagna Spaccata
MS2
4444000
San Mauro Abbey
Monte-Crocefisso palaeo
littoral ridge (lMClr)
Torre Sabea
G20
quarries
Gallipoli
Gallipoli-Alezio ridge
Alezio
G4
4435000
Carmine-Li Foggi palaeo
littoral ridge (CLlr)
G2-2
G2-3
Punta Pizzo
G17
B
Montagna Spaccata
Monte-Crocefisso palaeo
littoral ridge (lMClr)
Gallipoli-Alezio ridge
N
Carmine-Li Foggi palaeo
littoral ridge (CLlr)
Punta Pizzo

PALAEOSHORELINE	ASSOCIATED DEPOSITS	UNITS OF MIXED DEPOSITS (if has been possible to define them)	LANDFORMS IN THE SECTOR FROM BROKEN MOUNTAIN NORTHWARDS	LANDFORMS IN THE SECTOR SOUTH OF BROKEN MOUNTAIN
PS1 (+6 m)	PS1 marine unit (PS1mu)		Band of lithophagid borings	Band of lithophagid borings
PS2 (+7 m)	PS2 marine unit (PS2mu)		Band of lithophagid borings	Band of lithophagid borings
PS3 (+15 m)	PS3 Mixed Deposit (PS3-MD)	PS3 marine unit (PS3mu), Aeolian Unit 1 (AU1), Aeolian Unit 2 (AU2)	Band of lithophagid borings, tidal notches, wave-cut platform	*Monte-Crocefisso* palaeo littoral ridge (IMClr); *Carmine-Li Foggi* palaeo littoral ridge
PS4 (+22 m)	PS4 Mixed Deposit (PS4-MD)		Band of lithophagid borings, sea caves; patches of marine syn-wave cut platform deposits	Small and discontinuous relict littoral ridges with aeolian deposits
PS5 (+41 m)	PS5 Marine Deposit (PS5-MaD)		Band of lithophagid borings,	Band of lithophagid borings (near San Mauro abbey); marine terraced deposit less than 1 km^2 wide
PS6 (+62 m), PS7 (+67 m)			Band of lithophagid borings	Morphological inner edges

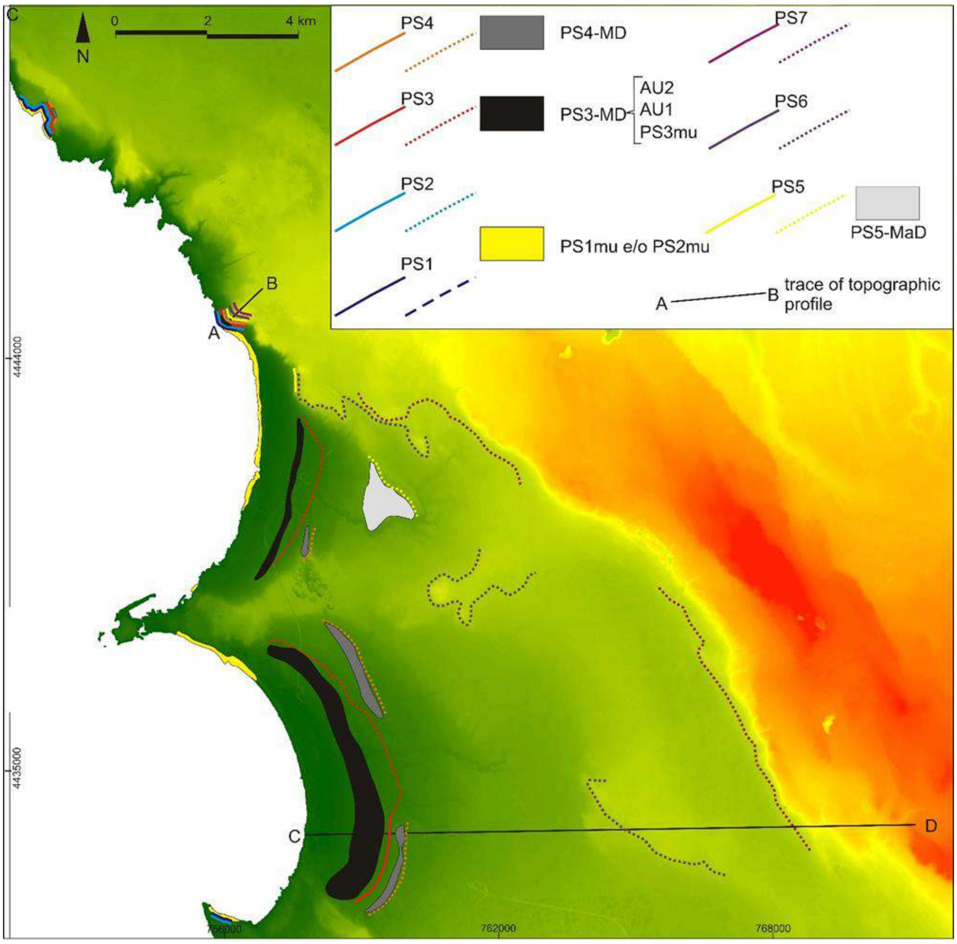
C
N
0
2
4 km
PS4
PS4-MD
PS7
PS3
PS3-MD
AU2
AU1
PS3mu
PS6
PS2
PS5
PS5-MaD
PS1mu e/o PS2mu
PS1
A
B
trace of topographic profile
4444000
4435000
C
D
762000
768000

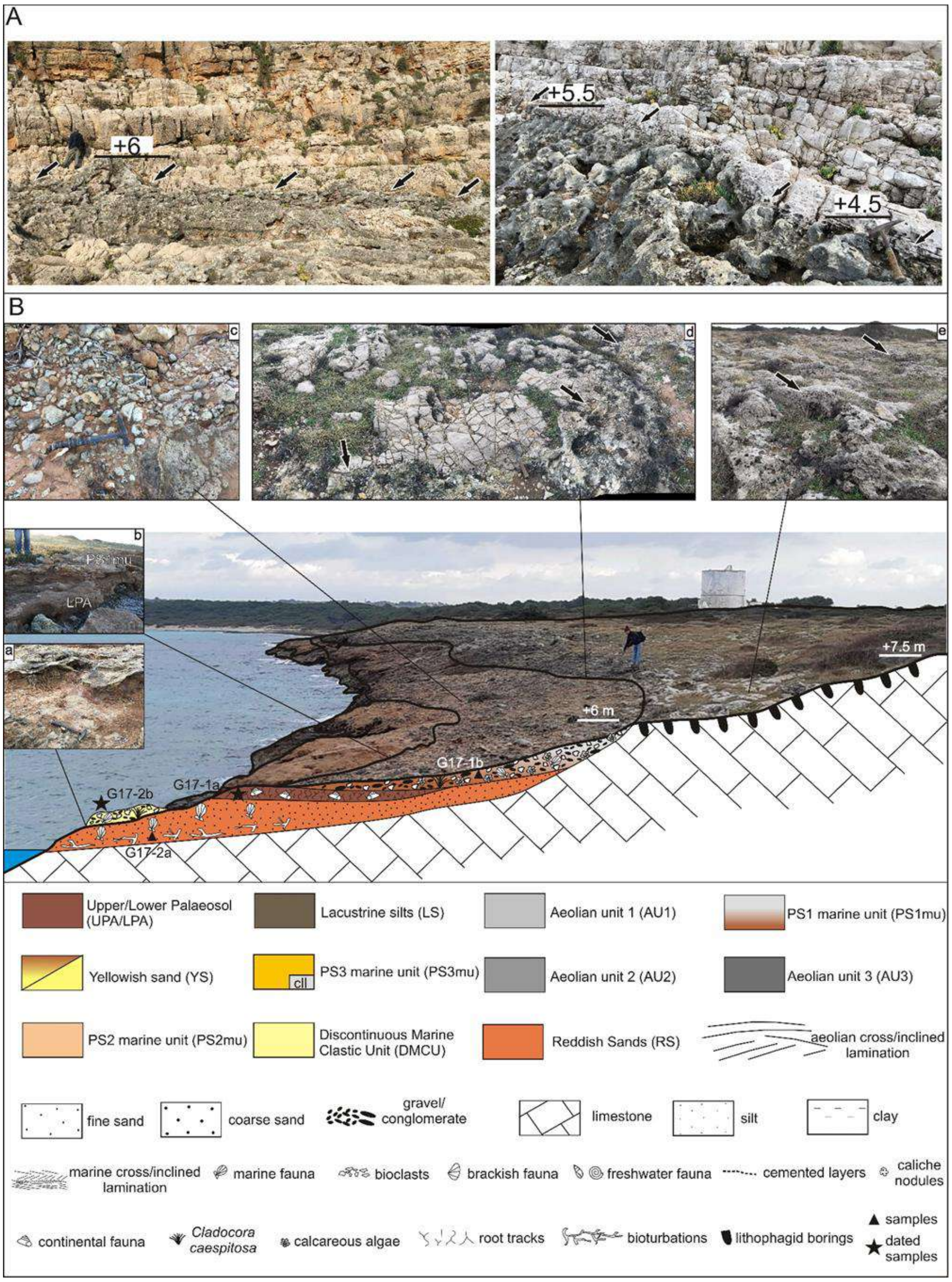

A
+6
+5.5
+4.5
B
c
d
e
b
LPA
a
+7.5 m
+6 m
G17-1b
G17-1a
G17-2b
G17-2a
Upper/Lower Palaeosol (UPA/LPA)
Lacustrine silts (LS)
Aeolian unit 1 (AU1)
PS1 marine unit (PS1mu)
Yellowish sand (YS)
PS3 marine unit (PS3mu)
cll
Aeolian unit 2 (AU2)
Aeolian unit 3 (AU3)
PS2 marine unit (PS2mu)
Discontinuous Marine Clastic Unit (DMCU)
Reddish Sands (RS)
aeolian cross/inclined lamination
fine sand
coarse sand
gravel/ conglomerate
limestone
silt
clay
marine cross/inclined lamination
marine fauna
bioclasts
brackish fauna
freshwater fauna
cemented layers
caliche nodules
continental fauna
Cladocora caespitosa
calcareous algae
root tracks
bioturbations
lithophagid borings
samples
dated samples


+7.6
+7.3
+7.5


A
+15
B
ML
br
br
br
+15
br
PS3mu
MS1-2
ML
ML
d
c
PS3mu
MS1-1
ML

1572

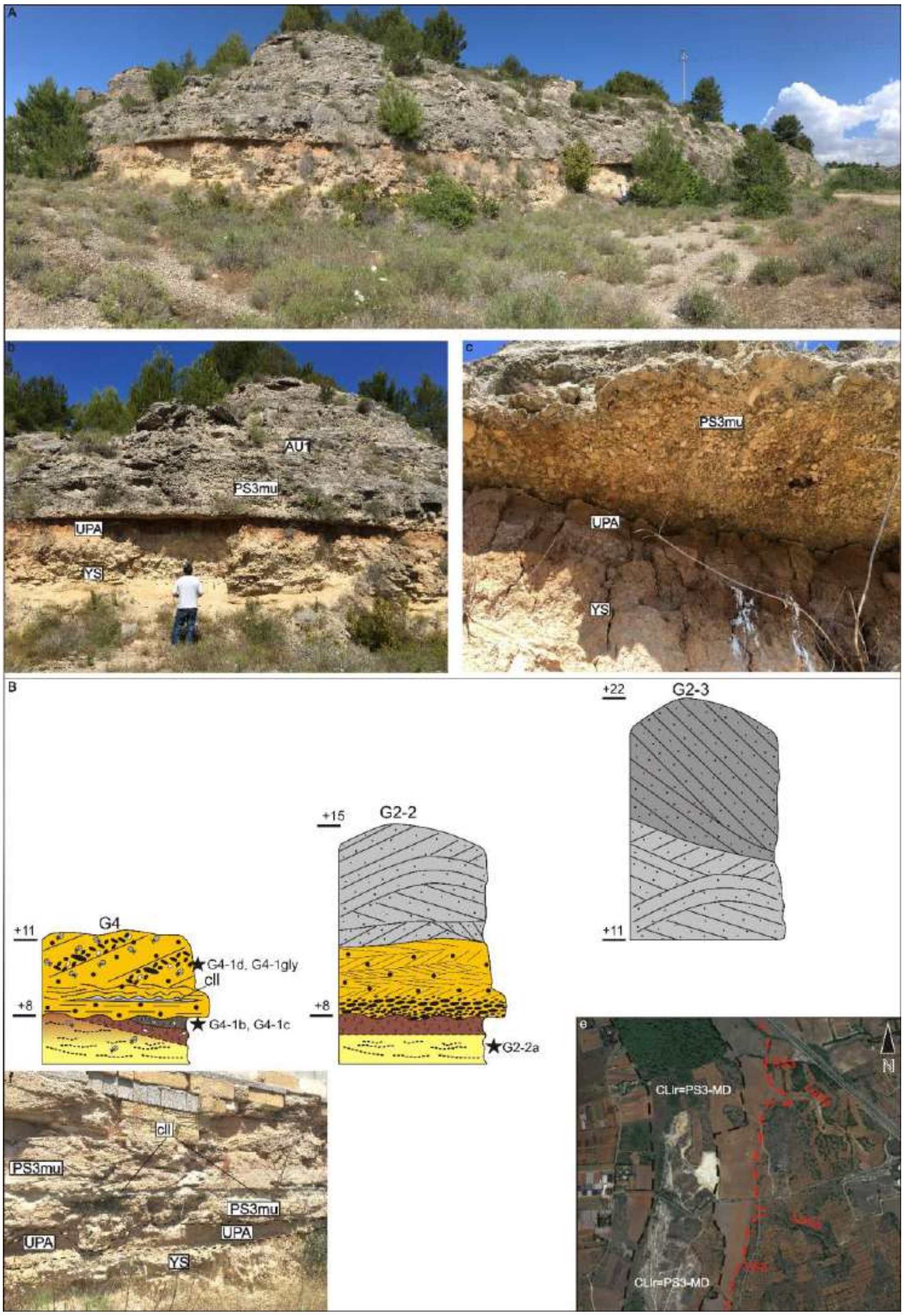
A
AU1
PS3mu
UPA
YS
C
PS3mu
UPA
YS
B
+22
G2-3
+11
+15
G2-2
+8
G2-2a
+11
G4
G4-1d, G4-1gly
cII
+8
G4-1b, G4-1c
cII
PS3mu
PS3mu
UPA
UPA
YS
e
N
CLIr=PS3-MD
CLIr=PS3-MD


A
B
+22
C
B
C

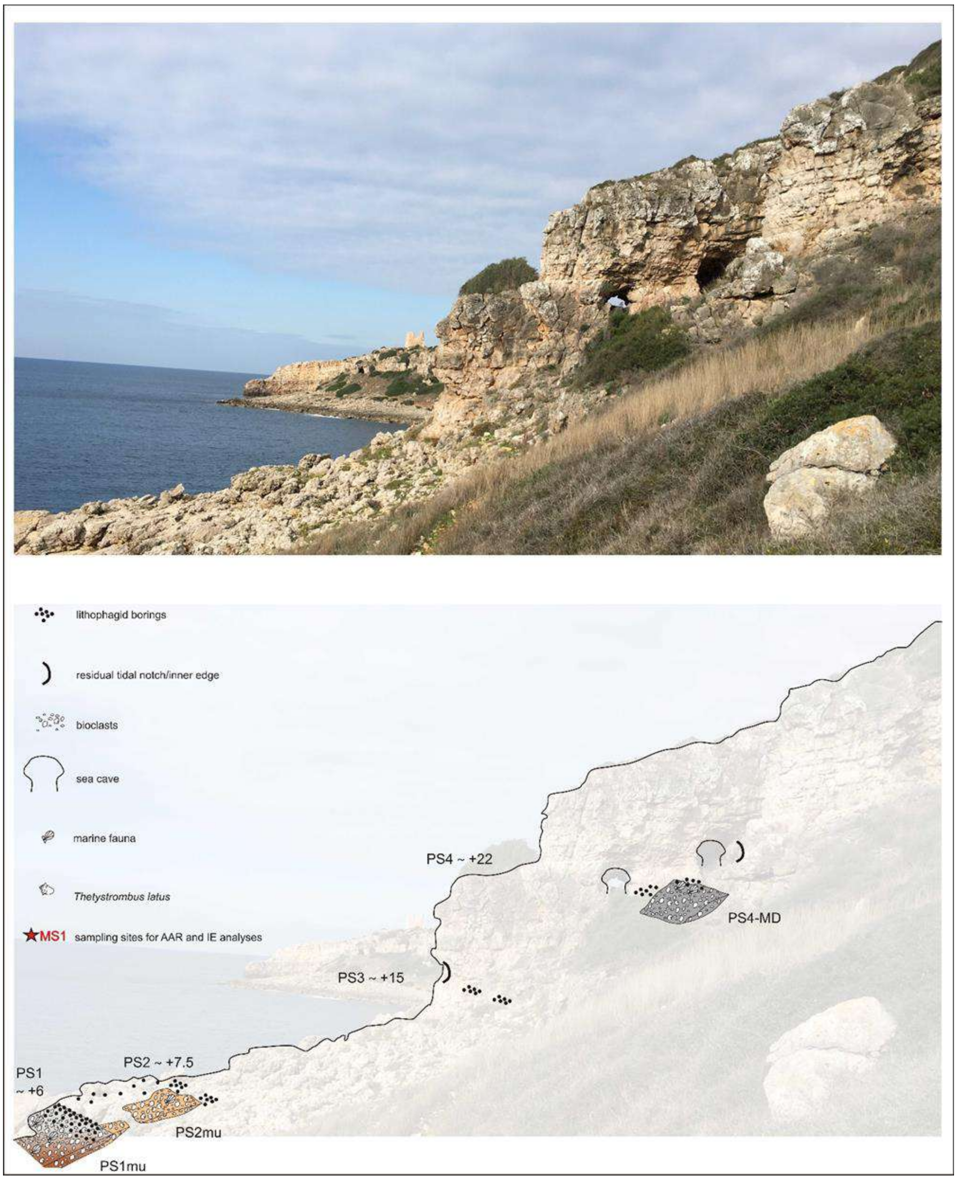

lithophagid borings
residual tidal notch/inner edge
bioclasts
sea cave
marine fauna
Thetystrombus latus
MS1 sampling sites for AAR and IE analyses
PS4 ~ +22
PS4-MD
PS3 ~ +15
PS2 ~ +7.5
PS1
~ +6
PS2mu
PS1mu


PS7 ~ +67
PS6 ~ +62
PS4 ~ +22
PS3 ~ +15
PS5 ~ +41
PS2 ~ +7.5
PS1 ~ +6
MS2 (+2 m)

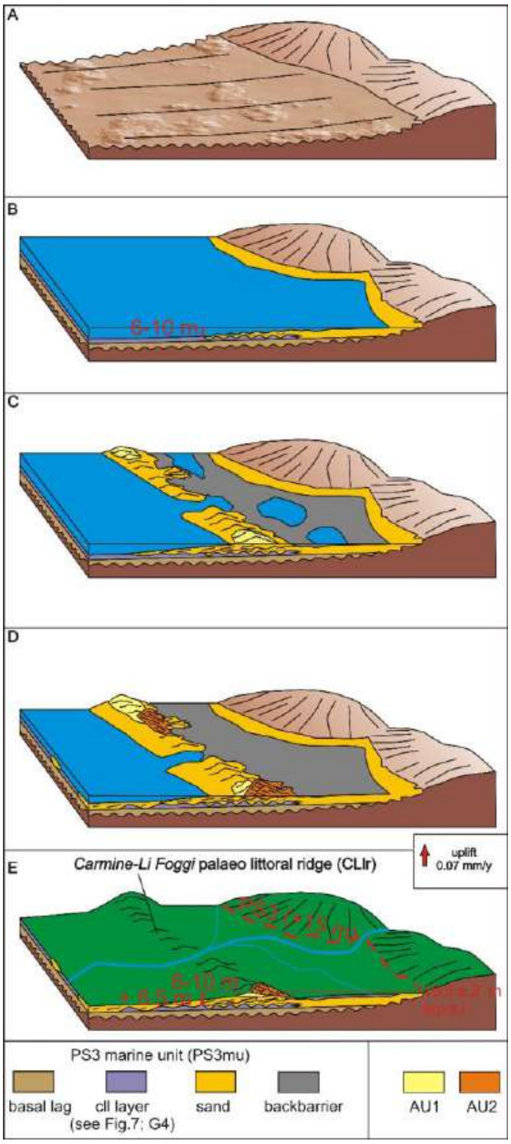
A
B
6-10 m
C
D
E
Carmine-Li Foggi palaeo littoral ridge (CLlr)
uplift
0.07 mm/y
6-10 m
PS3 marine unit (PS3mu)
basal lag
cll layer
(see Fig.7; G4)
sand
backbarrier
AU1
AU2

TAB. 2A							
	Sample ID/site	**Unit**	**Palaeoshore line**	**Material for chronological analyses**	**Type of analysis**	**Age/Aminozone**	**Stage**
South of Montagna Spaccata	G2-2a	YS		ostracod	AAR	137.2±29.3 ky BP	MIS 6-5.5
	G4-1c	LS		ostracod	AAR	138.4±17.9 ky BP	MIS 6-5.5
	G4-1b	LS		ostracod	AAR	118.1±17.9 ky BP	
	G4-1d	PS3mu	+15 m (PS3)	*Glycymeris* spp.	IE	E	MIS 5.5
	G4-1gly	PS3mu	+15 m (PS3)	*Glycymeris* spp.	IE	E	
	G17-1a	LPA		Helicidae	IE/AAR	122.1±33.6 ky BP	MIS 5.5
	G17-2b	DMCU		*Glycymeris* sp.	IE	F	MIS 7
	G17-2b	DMCU		*Cladocora caespitosa*	U-Th	232.02±5.3 ky BP 211.97±3.6 ky BP	MIS 7.3
	G20-1	DMCU		*Hoplangia durotrix*	U-Th	208.44±5.3 ky BP	MIS 7.3
From Montagna Spaccata northwards	MS1-2	PS3mu	+15 m (PS3)	*Patella* spp.	IE	E	MIS 5.5
	MS1-1	PS3 wave-cut platform	+15 m (PS3)	*Hoplangia durotrix*	U-Th	213.39±3.0 ky BP 211.07±4.8 ky BP	MIS 7.3
	MS2-1	PS1mu	+6 m (PS1)	*T. latus*	IE	E	MIS 5.5
	MS6-1	PS1mu	+6 m (PS1)	*Patella* spp.	IE	E	MIS 5.5
	MS11-1	Undefined		*Cladocora caespitosa*	U-Th	223.84±7.2 ky BP 225.17±5.4 ky BP	MIS 7.3

TAB. 2B							
Sample ID	**Taxa**	**N**	**D-allo/L-Ile**	**D/L Asp**	**D/L Glu**	**D/L Leu**	**D/L Phe**
G2-2a	*Candona neglecta*	5		0.357±0.031	0.144±0.025		
G4-1c	*Cyprideis torosa*	6		0.386±0.009	0.120±0.003		
G4-1d	*Glycymeris* sp.	5	0.389±0.082	0.567±0.105	0.437±0.055		
G4-1gly	*Glycymeris* sp.	6	0.359±0.047	0.581±0.010	0.438±0.016		
G17-1a	Helicidae-Pulmonata	6	0.387±0.058	0.484±0.064	0.344±0.043	0.353±0.026	0.517±0.080
G17-2b	*Glycymeris* sp.	6	0.486±0.062	0.729±0.038	0.553±0.059		
MS1-2	*Patella* spp	8	0.242±0.094	0.561±0.060	0.307±0.073		
MS6-1	*Patella* spp	3	0.224±0.005	0.543±0.011	0.341±0.023		
MS2-1	*T. latus*	2	0.496±0.129	0.619±0.049	0.483±0.093		

TAB. 2C

Sample ID	Taxa	N	[^{238}U] μg/g	[^{232}Th] ng/g	$\delta^{234}U_m$	(^{230}Th/^{238}U)	(^{230}Th/^{232}Th)	$\delta^{234}U_{(0)}$	Age (ky)	Age (ky)$_{corr}$
G17-2b	*Cladocora caespitosa*	1	2.591±0.021	39.240±0.320	107.24±1.02	1.00723±0.0021	202.90±0.43	206.60±3.67	237.71±2.6	232.02±5.3
		2	2.854±0.025	46.363±0.373	103.29±1.71	0.97192±0.0013	182.11±0.24	188.04±3.67	215.30±2.0	211.97±3.6
G20-1	*Hoplangia durotrix*	1	4.403±0.036	8.260±0.068	83.52±0.78	0.95114±0.0019	1544.11±3.05	150.54±2.65	215.64±1.9	208.44±5.3
MS1-1	*Hoplangia durotrix*	1	4.758±0.038	63.815±0.514	87.37±1.12	0.95613±0.0011	218.43±0.26	159.69±2.44	216.21±1.6	213.39±3.0
		1*	4.768±0.038	63.806±0.518	88.05±2.17	0.95331±0.0028	218.10±0.66	159.89±4.50	213.86±3.5	211.07±4.8
MS11-1	*Cladocora caespitosa*	1	3.146±0.029	58.340±0.476	95.67±3.66	0.98447±0.0016	161.68±0.26	180.11±7.80	230.14±4.3	223.84±7.2
		1*	3.150±0.025	59.480±0.481	91.65±0.96	0.98231±0.0018	158.71±0.30	173.19±3.21	231.83±2.3	225.17±5.4

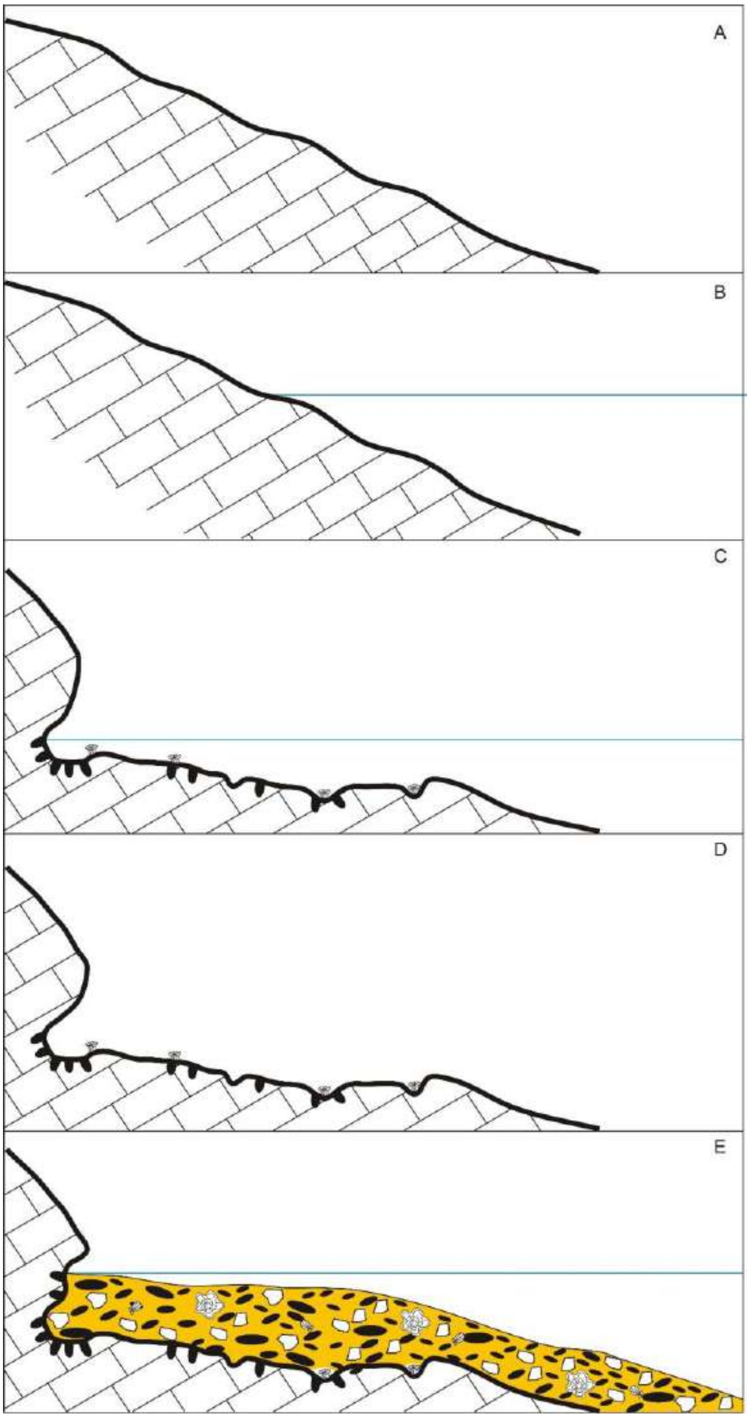

1695

Ages of highstands (yrs); from Waelbroeck et al., 2002	Sea level relative to present sea level (m); from Waelbroeck et al., 2002	Expected highstand-palaeoshoreline elevations (m relative to present sea level)	DTM/field observed palaeoshoreline elevations (m) and our association with expected palaeoshorelines	Comments on our association between expected and observed palaeoshorelines	MIS
0	0	0	0		
30000	-80	-78		currently submerged	
50000	-60	-56		currently submerged	
76500	-30	-24		currently submerged	
100000	-25	-18		currently submerged	
115000	-21	-13		currently submerged	
120000	0	9	6/7.5	PS1 +PS2	5.5
127000	6	15	15	PS3	5.5
166000	-50	-37		currently submerged	6.5
196500	-10	5		overprinted	7.1
215000	-4	13	15	PS3 re-occupied by 127 ky BP highstand	7.3
235000	-12	7		overprinted	7.5
287000	-15	8		overprinted	8.5
303000	-15	4		overprinted	9.1
330000	5	32	22	PS4	9.3
410000	6	41	41	PS5	11
478000	0	41		re-occupied by 410 ky BP highstand	13.1
525000	20	65	62	PS6	13.3
550000	10	57		overprinted	15.1 (?)
560000	3	51		overprinted	15.1 (?)
590000	20	71	67	PS7	15.3 (?)

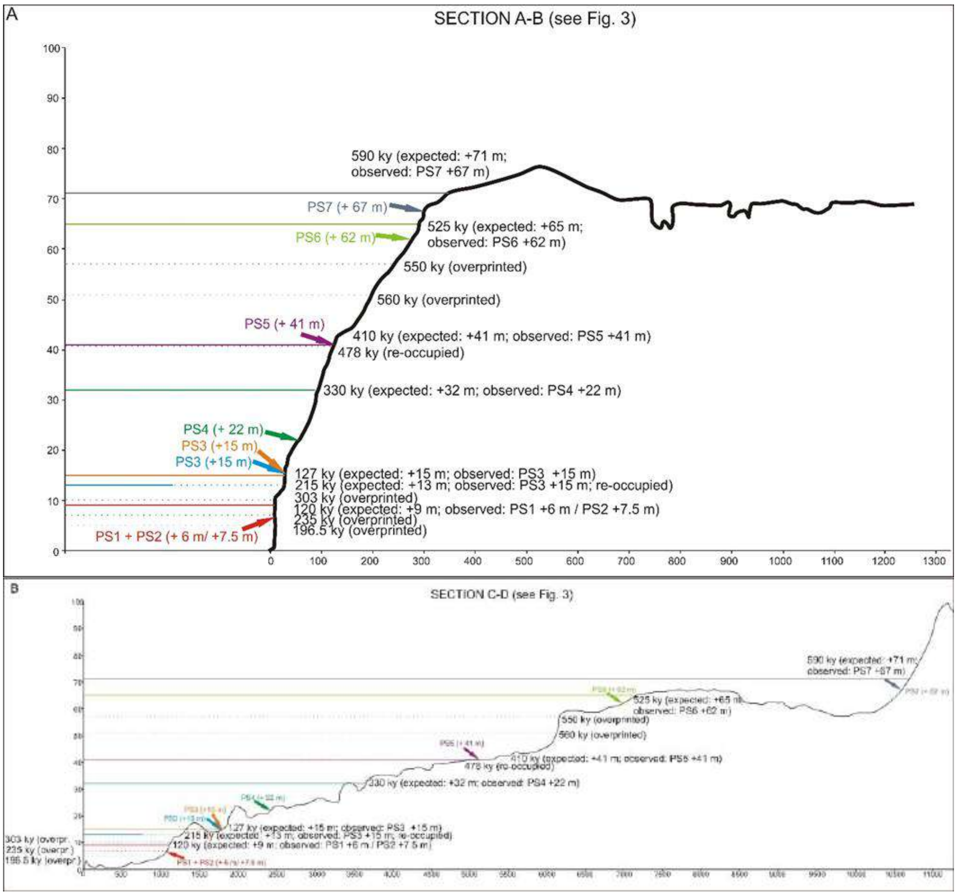
A
SECTION A-B (see Fig. 3)
590 ky (expected: +71 m;
observed: PS7 +67 m)
PS7 (+ 67 m)
525 ky (expected: +65 m;
observed: PS6 +62 m)
PS6 (+ 62 m)
550 ky (overprinted)
560 ky (overprinted)
PS5 (+ 41 m)
410 ky (expected: +41 m; observed: PS5 +41 m)
478 ky (re-occupied)
330 ky (expected: +32 m; observed: PS4 +22 m)
PS4 (+ 22 m)
PS3 (+15 m)
PS3 (+15 m)
127 ky (expected: +15 m; observed: PS3 +15 m)
215 ky (expected: +13 m; observed: PS3 +15 m; re-occupied)
303 ky (overprinted)
120 ky (expected: +9 m; observed: PS1 +6 m / PS2 +7.5 m)
235 ky (overprinted)
196.5 ky (overprinted)
PS1 + PS2 (+ 6 m/ +7.5 m)
B
SECTION C-D (see Fig. 3)

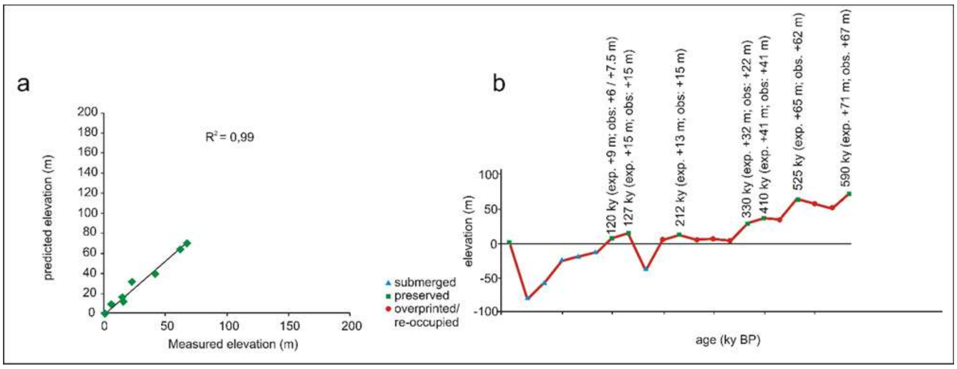
a
b
predicted elevation (m)
Measured elevation (m)
R^2 = 0,99
elevation (m)
age (ky BP)
submerged
preserved
overprinted/
re-occupied
120 ky (exp. +9 m; obs: +6 / +7.5 m)
127 ky (exp. +15 m; obs: +15 m)
212 ky (exp. +13 m; obs: +15 m)
330 ky (exp. +32 m; obs: +22 m)
410 ky (exp. +41 m; obs: +41 m)
525 ky (exp. +65 m; obs. +62 m)
590 ky (exp. +71 m; obs. +67 m)

AREA	NUMBER OF PALAEOSHORELINE RECOGNISED	AGES (ky BP)	UPLIFT RATES (mm/y)	REFERENCES
Vibo Valentia (Tyrrhenian coast of the Calabria region, southern Italy)	11	50, 76.5, 100, 125, 178, 200, 217, 240, 285, 310, 340	between 0.4 and 1.75	Roberts et al., 2013
Capo D'Orlando (Tyrrhenian coast of the Sicilia region, southern Italy)	10	76.5, 100, 125, 178, 200, 217, 240, 285, 310, 340	between 0.4 and 0.89	Meschis et al., 2018
SE Sicily, along the Ionian coastal sector	9	119, 125, 200, 240, 310, 340, 410, 478, 525	between 0.16 and 0.41	Meschis et al., 2020
SW Sicily	11	82, 103, 124, 167, 197, 215, 236, 287, 313, 331, 406	between 0.46 and 0.82	Ferranti et al., 2021
Ionian coast of southern Italy	18	5-10, 30-35, 45-50, 55-65, 70-80, 80-85, 85-95, 10-105, 115-125, 165-180, 185-200, 225-240, 280-295, 305-315, 320-335, 390-410, 480-500, 570-590	between 0.2 and 2	Caputo et al., 2010
South Crete (Greece)	9	76.5, 100, 125, 175, 200, 240, 310, 340, 410	between 0.24 and 0.89	Robertson et al., 2019
Gulf of Corinth (Greece)	8	76, (possibly) 100, 125, 175, 200, 216, 240, 340	between 0.15 and 0.51	Roberts et al., 2009

Middle-late Pleistocene chronology of palaeoshorelines and uplift history in the low-rising to stable Apulian foreland: overprinting and reoccupation

Vincenzo De Santis [a*], Giovanni Scardino [a], Giovanni Scicchitano [a] Marco Meschis [b], Paolo Montagna [c], Edwige Pons-Branchu [d]

José E. Ortiz [e], Yolanda Sánchez-Palencia [e], Massimo Caldara [a]

[a] Dipartimento di Scienze della Terra e Geoambientali, Università degli Studi di Bari "Aldo Moro", Via Orabona 4, 70125 Bari, Italy;

[b] Istituto Nazionale di Geofisica e Vulcanologia, Sezione di Palermo, via Ugo La Malfa, 153, 90146 Palermo, Italy;

[c] Istituto di Scienze Polari (ISP), Consiglio Nazionale delle Ricerche (CNR) Via Gobetti 101, 40129 Bologna, Italia

[d] LSCE/IPSL, UMR 8212, CEA-CNRS-UVSQ, Université Paris-Saclay, Chemin de Saint Aubin - RD 128, F-91191 Gif sur Yvette Cedex, France

[e] Biomolecular Stratigraphy Laboratory, Madrid School of Mines, C/Rios Rosas 21, E-28003 Madrid, Spain.

*Corresponding author. Tel.: 0039 080 5442471; Fax: 0039 080 5442625
E mail address: vincenzo.desantis@uniba.it

Abstract

To refine knowledge about terrace phases and uplift history for a tectonically poor deformed region, we apply the synchronous correlation method to reconstruct the chronology of a poorly constrained sequence of raised palaeoshorelines on the Apulian foreland, southern Italy. This work uses new chronological constraints obtained by amino acid racemisation (AAR) and isoleucine/alloisoleucine epimerisation (IE) on Patella spp., *Thetystrombus latus* (Gmelin), *Glycymeris* sp., and ostracods and U-series dating on corals *Hoplangia durotrix* Gosse and *Cladocora caespitosa* Linneo. This procedure provides a quantitative estimate of the vertical movements and associated rates within a region of the Apulian foreland. The synchronous correlation method uses sea-level highstands and uplift rate(s) as inputs; in particular, for sea-level highstands, the inputs are the age of the highstands and the sea-level elevation of the highstands relative to the present-day sea level. The output is a set of currently expected elevations of each sea-level highstand (the present elevations of palaeoshorelines). We then used regression analysis to assess the robustness between our observed palaeoshorelines and expected elevations of sea-level highstands. Our results show that the best fitting scenario is obtained using the sea-level curves of (i) Waelbroeck et al. (2002) from present to 410 ky BP and (ii) Rohling et al. (2014) from 410 to 590 ky BP as inputs for our synchronous correlation method, with uplift rates ranging from 0.09 mm/y to 0.07 mm/y with a mean value of 0.08 mm/y from 590 ky BP onwards.

We recognised palaeoshorelines in the field belonging to the following highstands: 120 ky BP (MIS 5.5, second peak), 127 ky BP (MIS 5.5, first peak), 212 ky BP (MIS 7.3), 330 ky BP (MIS 9.3), 410 (MIS 11), 525 ky BP (MIS 13.3), and 590 ky BP (MIS 15). Our results show field observations of the reoccupation effect of younger palaeoshorelines over older ones due to the relatively slow uplift rates measured in the investigated area as predicted by our synchronous correlation method. In particular, we show a well-mapped and described reoccupation of the MIS 5.5 palaeoshoreline over the MIS 7.3 palaeoshoreline, constrained by new absolute dating.

In addition, the data from the Apulian foreland suggest an MIS 7.3 highstand close to the present sea level.

Keywords: synchronous correlation method, palaeoshorelines, MIS 5.5, MIS7.3, reoccupation, overprinting,

1 INTRODUCTION

Past interglacial periods have attracted the scientific community because they are used to study the climate system during warm intervals, and this is crucial for understanding the interaction mechanisms between natural climatic and anthropogenic forcings. Some of the most prominent evidences of past interglacial periods are raised marine terraces and palaeoshorelines, which result from the interactions between sea-level changes and tectonic processes (uplift) during the Quaternary (Lajoie, 1986). Among the assessments of past sea-level changes, the study of these geomorphic features is fundamental to understanding vertical land movements (Grant et al., 2014; Murray-Wallace and Woodroffe, 2014; Marra et al., 2016, 2019, 2020; Cerrone et al., 2021a) and the associated rates of crustal uplift or subsidence (Ferranti et al., 2006; Caputo et al., 2010; Meschis et al., 2020).

Our study area is located in the southern part of the Apulian foreland (southern Italy), the Salento Peninsula. Although the extensive presence of preserved marine terraces has been documented throughout the central-southern Apulian foreland, that is, in the Murge and Salento highlands (Ciaranfi et al., 1992), there is a lack of knowledge about their ages and the associated rates of crustal uplift over time. Indeed, the chronology of uplifted palaeoshorelines is still a matter of debate within the investigated area, where only a few works have associated preserved palaeoshorelines with specific highstands (Antonioli et al., 2018; De Santis et al., 2021a). This also supplements the ongoing debate on whether regional uplift rates affecting the Apulian foreland are constant or fluctuating over time (Ferranti and Oldow, 2006; De Santis et al., 2021a, b). The Apulian foreland shows slow uplift rates, suggesting that processes of reoccupation and overprinting of older palaeoshorelines by younger ones can be fairly common (Westaway, 1993; Ascione and Romano, 1999; Roberts et al., 2013). If this process is not taken into account, geoscientists may be likely to (i) assign erroneous ages to undated marine terraces and, consequently, (ii) estimate inaccurate uplift rates (e.g., Roberts et al., 2013). For instance, when a sequential correlation approach is applied to model sequences of preserved marine terraces (see Roberts et al., 2013 for a critical analysis of this approach) without considering the reoccupation problem, unrealistic uplift rate changes may be reconstructed (e.g., Roberts et al., 2013; Meschis et al., 2018). The sequential correlation method is based on the idea that, given a dated paleoshoreline, the next higher and older paleoshoreline is likely to belong to the next older sea-level highstand (e.g., Armijo et al., 1996; Bianca et al., 2011; Gallen et al., 2014). Unrealistic variations in uplift rates result from not taking into account the "reoccupation problem" (e.g., Roberts et al. 2013 and Robertson et al. 2019) and have not been reported in the vicinity of active seismogenic sources worldwide to date (Cowie and Roberts, 2001; Cowie et al., 2012; Meschis et al., 2020).

Therefore, applying a synchronous correlation method and overcoming the reoccupation problem, becomes crucial when raised palaeoshorelines are used for a better assessment of tectonic and geodynamic implications, as shown by previous studies (e.g., Roberts et al., 2013; Meschis et al., 2018; Robertson et al., 2019; Meschis et al., 2020). For this reason, we have undertaken an in-depth study of uplifted palaeoshorelines and their associated sedimentary deposits within a coastal sector of the Salento Peninsula (Fig. 1) to provide new insights into their morphology and chronology. Our study aims to (i) map the palaeoshoreline elevations, (ii) provide new chronological constraints for undated palaeoshorelines, and (iii) refine the uplift history of the region. We carried out intensive field surveys and detailed topographic analysis using Digital Terrain Models (DTMs) obtained from high-resolution Light Detection And Ranging (LiDAR) data. Thus, we mapped palaeoshorelines (e.g., Armijo et al., 1996; Roberts et al., 2013) and ground-truthed them in the field with the associated deposits, where present. We then applied a synchronous correlation method to correlate multiple uplifted palaeoshorelines unevenly spaced in elevations and multiple unevenly spaced in time sea-level highstands (Waelbroeck et al., 2002; Rohling et al., 2014) by iterating uplift rates driven by new chronological constraints, obtained using amino acid racemisation (AAR), isoleucine/alloisoleucine epimerisation (IE), and U-series dating. We then assessed the robustness of our correlations between multiple GIS and field-mapped palaeoshoreline elevations and multiple predicted sea-level highstand elevations iteratively calculated through linear regression analysis.

Finally, we discuss our results in terms of local and regional tectonic implications within the -almost tectonically undeformed Apulian foreland.

2 GEOLOGICAL SETTING AND PREVIOUS RESEARCH

The Apulian foreland, which is composed of Mesozoic limestone (Fig. 1A) overlain by Plio-Pleistocene coastal deposits, has experienced uplifting since the middle-late Pleistocene (Azzaroli, 1968; Iannone and Pieri, 1979; Ciaranfi et al., 1992; Ricchetti et al., 1992; Doglioni et al., 1994, 1996; De Santis and Caldara, 2016; Valenzano et al., 2018; De Santis et al., 2020 a, b)

To date, the Apulian foreland has been characterised by a scarcity of reliable documentation of palaeoshorelines and chronological data concerning their formation during the middle-late Pleistocene (Cerrone et al., 2021b). Indeed, for this period, the well constrained chronological data are those related to some areas with extensive presences of Quaternary terrace deposits (Brückner, 1980; Boenzi et al., 1986; Hearty and Dai Pra, 1992; Belluomini et al., 2002; Caldara et al., 2003; Zander et al., 2006; Caldara et al., 2013; Amorosi et al., 2014; De Santis et al., 2010, 2013, 2014a, b, 2018, 2020c, 2021b; Negri et al., 2015). In particular, close to the city of Gallipoli, several marine and aeolian geological units with interbedded palaeosols, all dating back to MIS 5.5, have been described (Hearty and Dai Pra, 1992). Similarly, stratigraphic deposits revealing sea-level oscillations during the Last Interglacial Maximum (LIM) have been described in other localities in Italy (Hearty and Dai Pra, 1987), Mallorca (Hearty, 1987), Spain (Hearty et al., 1987), and Tunisia (Hearty et al., 1986).

In any case, except for the investigations by De Santis et al. (2021a), all the above-mentioned studies describe and date preserved marine terrace deposits; yet their correlations with associated palaeoshoreline locations and elevations are poorly constrained and, therefore, a reliable possibility of reconstructing the current position of the past sea-level highstands lacks.

As a consequence of this lack of knowledge, most uplift rates of the Apulian foreland have been estimated only for the late Pleistocene and almost exclusively along the Ionian coast based on the elevations of the marine terrace deposits related to the LIM (MIS 5.5) (Hearty and Dai Pra, 1992; Belluomini et al., 2002; Ferranti et al., 2006). These data show a decreasing uplift rate from northwest to southeast, from a maximum uplift rate of 0.31 mm/yr northwest of Taranto (Ponte del Re locality) to a subsidence rate of 0.03 mm/yr at Torre Castiglione.

2.1 Geological and geomorphological setting of the study area

The study area is a ca. 30 km long coastal stretch (Figs. 1B, 2A), lying close to the city of Gallipoli and located along the Ionian coast of the Salento Peninsula, which forms the southern portion of the Apulian foreland. The morpho-structural setting of the Salento Peninsula is identified by the Serre Salentine domain, which consists of NW–SE-oriented horsts and grabens (Ricchetti and Ciaranfi, 2013; Fig. 1B); the horsts, whose top surfaces are flat and slightly tilted towards the SW, consist of Mesozoic or Palaeogene-Miocene carbonate units; the grabens contain Plio-Pleistocene deposits belonging to the Bradanic Trough cycle and marine terrace deposits, suggesting middle-late Pleistocene regional tectonic uplift.

From geological and geomorphological points of view, the study area can be divided into two main sectors: a sector from Montagna Spaccata (included) northwards and a sector to the south of the Montagna Spaccata locality (Fig. 2A, B). The sector from Montagna Spaccata northwards coincides with a flank of a horst that represents one of the few coastal stretches with high rocky coasts on the entire Apulian Ionian side. It is characterised almost exclusively by outcrops of Mesozoic limestone (Fig. 1C), with small patches of marine terrace deposits, which have never been mapped to date. Only in the coastal stretch between Santa Caterina and Santa Maria al Bagno, Miocene-aged calcarenites and sands crop out (Fig. 1C) (more inland, Plio-Pleistocene calcarenites crop out (Largaiolli et al., 1969; Ciaranfi et al., 1992; Boenzi et al., 2010).

The sector south of Montagna Spaccata coincides with the terminal part of a graben, characterised by very gentle slopes. Here, Quaternary marine terrace deposits crop out overlying regressive calcarenite deposits of the Bradanic Trough cycle (Caldara et al.,1981; Hearty and Dai Pra,1992). These regressive deposits are well documented in some quarries on the Gallipoli-Alezio ridge (Fig. 2A, B). They constitute the local substrate of the terrace deposits.

Figure 1

3 METHODS

3.1 Field survey and digital terrain model (DTM)

We mapped palaeoshorelines and their associated deposits (see Table 1, Section 4.1) by combining field mapping and GIS analysis using high-resolution Digital Terrain Models (2-m resolution along the coastline and 8-m resolution farther inland). DTMs were extracted by high-resolution Light Detection And Ranging (LiDAR) provided by the "Ministero dell'Ambiente e della Tutela del Territorio e del Mare" (Fig. 2A, B) and acquired during the years 2008-2009. The elevations of LiDAR data were reported on the geodetic reference datum ITALGEO2005 and showed a vertical accuracy of ±0.15 m (*Progetto PST - Dati Lidar*, 2021). The tidal datum is referred to the Mean Low Water Springs (MLWS) that, for the study area, presents an uncertainty of ±0.151 m. Considering the different resolutions of the cell width for the two different DTMs (on the coast and inland), the vertical uncertainty of the DTM with 2-m resolution resulted equal to ±0.30 m, while the vertical uncertainty of the DTM with 8-m resolution resulted equal to ±1.0 m.

Elevations of palaeoshorelines were obtained using a Global Position System Real-Time Kinematic (GPS-RTK) receiver, with an accuracy ranging between 0.05 and 0.1 m.

A survey with total stations was performed to assess the elevations of the palaeoshorelines located on the steep slopes, where it was difficult to use the GPS-RTK receiver. The accuracy of the total station ranged between 0.001 and 0.005 m, depending on atmospheric perturbations. Field geological/geomorphological indicators used to identify palaeoshorelines include inner margins, notches, sea caves, bands of lithophagid borings, marine deposits on wave- cut platforms (Ferranti et al., 2006; Vacchi et al., 2016; Robertson et al. 2020), and relict littoral ridges (*sensu* Ricchetti and Ciaranfi, 2013).

The margin of error related to the palaeoshoreline elevations mapped in the field is prominently linked to the uncertainty of associated markers. Lithophagids colonise calcareous rocky coasts down to deeper than 30 m below the sea level of and can be detected up to 2 m below sea level (Ferranti et al., 2006). However, if the upper limit of *Lithophaga* populations is clearly visible and well recognised, it can represent a reliable sea-level indicator (Evelpidou et al., 2012), and the margin of error associated with lithophagid borings was assumed to be ± 2 m at the upper limit (Kershaw, 2000; Ferranti et al., 2006; Scicchitano et al., 2011; Rovere et al., 2015)

The margin of error associated with the tidal notches, when used as palaeo-sea-level benchmarks in the Mediterranean depends on the local tidal range, which is ~0.4 m (Antonioli et al., 2015, 2018). Indeed, the base of a tidal notch is considered the best and most precise marker of the average palaeo-sea-level because its width is closely linked to the local tidal phase (Antonioli et al., 2015; Rovere et al., 2016; Lorscheid et al., 2017).

The elevation of beach facies with the presence of *Thetystrombus latus* (Gmelin) (previously known as *Strombus bubonius*) and senegalensis fauna (Gignoux, 1913; Zazo et al., 2003; Taviani, 2014; Benjamin et al., 2017) can indicate a palaeo-beach deposit (Benjamin et al., 2017), yet they do not always indicate a well-approximated palaeo-sea-level.

Figure 2

3.2 Chronological analyses

Chronological analyses were performed on deposits that, from field observations, seem to be associated with palaeoshorelines and, where present, on substrate deposits.

3.2.1 Amino acid racemisation (AAR) and isoleucine/alloisoleucine epimerisation (IE) analyses

We applied amino acid racemisation and isoleucine/alloisoleucine epimerisation to shells of (see Table 2, Section 4.3):

1) ostracods for lacustrine and marine deposits where no marine bivalve *Glycymeris* spp. were present;
2) marine bivalve *Glycymeris* spp. (where present) for marine deposits;
3) continental gastropod Helicidae for palaeosols.

For IE applied to *Glycymeris* sp., a hollow diamond drill was used to remove a discoid sample (8 mm in diameter) from the apexes of shells. Outer layers (approximately 20-30%) were removed after chemical etching with 2 N HCl. Afterward, 10-20 mg of sample was collected and divided into a certain number of subsamples (Tab.2A).

For AAR applied to ostracods, sediment samples were washed with running water and sieved. After drying, the sediment remnant (>0.062 mm) was analysed under a binocular microscope, and ostracod carapaces were picked with a needle. The ostracod shells were carefully sonicated and cleaned with water to remove sediment and left for 2-3 hours in hydrogen peroxide to remove organic matter. Only translucent individuals were selected for the analysis, giving a certain number of specimens (subsamples; Tab 2A) for each sample of sediment.

For both *Glycymeris* sp. and ostracods, amino acid concentrations were quantified using Reverse Phase-High Performance Liquid Chromatography (RP-HPLC) following the sample preparation protocol described in Kaufman and Manley (1998) and Kaufman (2000). This procedure involves hydrolysis, performed under an N_2 atmosphere in 20 μl/mg 7 N HCl. The hydrolysates were evaporated to dryness in vacuo and then rehydrated in 10 μl/mg 0.01 N HCl with 1.5 mM sodium azide and 0.03 mM L-homoarginine (internal standard).

Samples were injected into an Agilent HPLC-1100 equipped with a fluorescence detector. Excitation and emission wavelengths were programmed at 335 and 445 nm, respectively. A Hypersil BDS C18 reverse-phase column (5 µm; 250 x 4 mm i.d.) was used for the analysis.

Derivatisation occurred before injection by mixing the sample (2 µl) with the precolumn derivatisation reagent (2.2 µl), which comprised 260 mM isobutyryl-L-cysteine (chiral thiol) and 170 mM o- phtaldialdehyde dissolved in 1.0 M potassium borate buffer solution at pH 10.4. Eluent A consisted of 23 mM sodium acetate with 1.5 mM sodium azide and 1.3 µM EDTA, adjusted to pH 6.00 with 10 M sodium hydroxide and 10% acetic acid. Eluent B was HPLC-grade methanol, and eluent C consisted of HPLC-grade acetonitrile. A linear gradient was performed at 1.0 ml/min and 25 °C, from 95% eluent A and 5% eluent B upon injection to 76.6% eluent A, 23% eluent B, and 0.4% eluent C at 31 min.

Some analytical subsamples seemed to have suffered some contamination and were rejected for the age calculation. Following Kaufman (2006), we used the cut-off value of 0.8 in the concentration of L-Ser to that of L-aspartic acid to determine anomalous samples as Ser decomposes rapidly, and excessive amounts indicate contamination by modern amino acids.

For *Glycymeris* sp., the mean D/L values of three amino acids (isoleucine, aspartic acid, and glutamic acid) were obtained, because they are the most appropriate amino acids for dating most marine molluscs because of their abundance and steady rates of racemisation/epimerisation (Torres et al., 2000; Ortiz et al., 2015). For *Glycymeris* sp., an age calculation algorithm based on D/L values does not exist, but the extensive use of AAR has allowed the establishment of a general aminostratigraphical framework of Pleistocene palaeoshorelines in the Mediterranean basin based on aminozones (Hearty et al., 1986; Hearty, 1987; Hearty and Dai Pra, 1992; Torres et al., 2000). For *Glycymeris* sp. shells, we referred to the aminozones based on values of isoleucine/alloisoleucine epimerisation (D/L = D-aIle/L-Ile), as they are commonly used for chronological purposes in the Mediterranean realm. In this regard, isoleucine/alloisoleucine epimerisation values obtained by RP-HPLC required transformation to be compared with D-aIle/L-Ile values measured by Gas

Chromatography (GC) (Wehmiller, 1984; Torres et al., 1997; Ortiz et al., 2004; Wehmiller et al., 2010). Thus, the isoleucine/alloisoleucine epimerisation (D-aIle/L-Ile) values ranging between 0.35 and 1.1 by RP-HPLC were approximately 0.10 lower than those obtained by GC, i.e., D-aIle/L-Ile $_{GC}$ = D-aIle/L-Ile $_{HPLC\text{-}IE\text{-}LC}$ + 0.10.

In this regard, according to Powell et al. (2013) for RP-HPLC, D-aIle/L-Ile values were, on average, 30% (range: 15-40%) higher compared to those by GC, in coincidence with the results provided by Ortiz et al. (2004). In addition, Torres et al. (2013) provide a comparison of D/L values obtained with RP-HPLC and GC in *Glycymeris* shells from the same localities in the Mediterranean realm. For comparison, according to Witeacre et al. (2017), paired Ion Exchange Liquid Chromatography (IE-LC) and RP-HPLC analyses show that D-aIle/L-Ile values can be confidently converted to their equivalent D/L values for isoleucine, with 2s uncertainties of ±35%, although this value is markedly lower for the range of values observed in this study.

For ostracods, the aminochronology was obtained using D/L values of aspartic acid and glutamic acid because they account for an important percentage of the amino acid content of most ostracod valves and are the ones that racemize faster (Kaufman, 2000; Bright and Kaufman, 2011; Ortiz et al., 2013). With ostracods, it has been possible to obtain numerical ages using age calculation algorithms that convert aspartic acid and glutamic acid D/L ratios into numerical ages. These algorithms are those established by Ortiz et al. (2004) for the central and southern parts of the Iberian Peninsula and have already been applied extensively in southern Italy (De Santis et al., 2010, 2013, 2014b, 2018, 2020c; Caldara et al., 2013).

For Helicidae, the mean D/L values of five amino acids (isoleucine, aspartic acid, glutamic acid, leucine, and phenylalanine) have been obtained because, according to Torres et al. (1997), they are reliable for dating terrestrial gastropods. The numerical age was calculated by introducing the Asp, Glu, Leu, Ile, and Phe D/L values into the age-calculation algorithms established by Torres et al. (1997) for gastropods in the central and southern parts of the Iberian Peninsula.

In this work, we also report previous AAR analyses carried out in the sector from Montagna Spaccata northwards (MS1-2, MS2-1, and MS6-1 samples in Table 2A) (De Santis et al., 2021a) based on isoleucine/alloisoleucine epimerisation. These analyses were carried out on shells of *Patella aspera* (Röding), *Patella caerulea* Linneo, *Patella* sp., and *Thetystrombus latus* (Gmelin). The reliability and results of these chronological analyses have already been published and discussed in De Santis et al. (2021a).

3.2.2 U–Th series dating

The following fragments of corals were prepared for U-series dating (see Table 2, Section 4.3):

1) two fragments of *Cladocora caespitosa* Linneo from sample G17-2b (Punta Pizzo locality; Figs. 2A, 2C, 3);

2) one fragment of *Hoplangia durotrix* Gosse from sample MS1-1 (Montagna Spaccata locality; Figs. 2A, 2C, 5);

3) one fragment of *Hoplangia durotrix* Gosse from sample G20-1 (Torre Sabea locality; Figs. 2A, 2C, 3; and

4) two fragments of *Cladocora caespitosa* Linneo from sample MS11-1 (Uluzzo locality Fig. 2A).

In particular, for all samples, we selected only a portion of the thecal wall and removed the septa and extraneous detrital material using a dental drill with a diamond-encrusted blade operated under a stereomicroscope. Any further contamination was removed by hand picking. Subsamples were crushed into coarse chips (ca. 1-2 mm in size) using an agate mortar and pestle, ultrasonicated in Milli-Q water, and dried in an oven at 50 °C overnight. Each sample (~50 mg) was dissolved in dilute HCl in a beaker in which a known amount of ^{229}Th, ^{233}U, and ^{236}U spikes were previously added. This tracer was calibrated against a Harwell Uraninite solution (HU-1) assumed to be at secular equilibrium. After FeOH precipitation, uranium and thorium fractions were separated and purified using Eichrom UTEVA ion exchange chromatography resin in nitric media following the procedure described in Pons-Branchu et al. (2014). The U and Th measurements were carried out on a

ThermoScientific Neptune Plus MC-ICPMS installed at the Laboratoire des Sciences du Climat et de l'Environnement (LSCE, Gif-sur-Yvette, France), fitted with an Aridus II Desolvating Nebulizer system, and a jet pump interface, following the procedure described in Pons-Branchu et al. (2014). After blank and fractionation corrections, the activity ratios for ^{230}Th/^{238}U, and ^{234}U/^{238}U were determined using the decay constants and reference values given in Cheng et al. (2013) and Jaffey et al. (1971).

The ^{230}Th/U ages were calculated through iterative age estimation (Ludwig and Titterington, 1994). The samples have δ^{234}U (0) values between 150.54 ± 2.65 and 206.6 ± 3.67‰, which are higher than those of modern seawater (146.8‰; Andersen et al., 2010), indicating that they might have experienced open-systems U-series behaviour, likely caused by alpha recoil mobilisation of ^{234}Th and ^{230}Th (Thompson et al., 2003). We tentatively corrected U-series ages for open system using the open-system age equations of Thompson et al. (2003), even though our limited dataset does not allow us to confirm the expected mixing slopes predicted by the Thompson model. Overall, both conventional and open-system U-series ages (data not shown) fall within the same time interval.

The ^{232}Th concentrations range between 8.26 and 63.81 ppb, with ^{230}Th/^{232}Th ratios varying between 158.71 and 1544,11, suggesting much less detrital contamination. We corrected for detrital Th assuming an initial ^{230}Th/^{232}Th activity ratio of 7 ± 50% (Table 2C).

3.3 Synchronous correlation method for model multiple sea-level highstands and multiple palaeoshorelines

Glacio-eustatic sea-level highstands combined with tectonic uplift produce geomorphic features named marine terraces and/or palaeoshorelines (Lajoe, 1986). Yet, the synchronous correlation method is derived from the idea that glacio-eustatic sea-level highstands are not equally spaced in time (Rohling et al. 2014); this suggests that preserved raised marine terraces and their inner edges (or palaeoshorelines) are not equally spaced in elevation, assuming the simplest tectonic scenario of constant uplift rates through time (Roberts et al., 2009, 2013). Furthermore, the synchronous correlation method is not sensitive if rates of uplift are constant or fluctuating through time (Meschis et al. 2020, 2022). More importantly, this method has also been applied when fault-controlled uplift rates change over time, as shown by previous investigations in Greece and southern Italy (Roberts et al., 2009; Meschis et al., 2020). Indeed, the reoccupation of older marine terraces by younger terraces within relatively slow uplifting regions may occur for both constant and fluctuating uplift scenarios (Roberts et al., 2009, 2013). Furthermore, absolute dated marine terrace deposits, which act as age controls, drive the uplift rate iteration; this permits us to first test the simplest hypothesis of a constant uplift rate over time and assess if the iteratively calculated sea-level highstand elevations match the mapped palaeoshoreline elevations (Roberts et al., 2013). If a robust correlation is not claimed for the simplest scenario, then a changing uplift rate over time is tested, with iterations of uplift rates driven by age controls aiming to find the best match between expected and field-mapped palaeoshoreline elevations (Roberts et al., 2013).

To apply this method, we use a "terrace calculator" built in Excel, which uses sea-level highstands (Roberts et al., 2013; Robertson et al., 2019) and the uplift rate (UR) as inputs; the method allows us to calculate the present expected elevation (PE) of each sea-level highstand (that is, the present elevations of palaeoshorelines) using the age of the highstand (T) and the sea-level elevation of the highstand relative to the sea level of today (SLT) following this formula: PE = (UR x T) + SLT.

Indeed, this approach forces the user to maximise the coefficient of determination (R^2 value) for linear regression analysis through data, including the "observed" elevations and the "expected" elevations of all palaeoshorelines (Roberts et al., 2013; Meschis et al., 2018; Robertson et al. 2019; Meschis et al., 2020).

The output of the terrace calculator is a set of expected elevationsfor sea-level highstands (that is, a set of PE); we consider acceptable a difference up to 10 m between expected and observed palaeoshoreline elevations, based on the uncertainties of the sea-level curve that are used regarding both the sea-level highstands and their ages. If this is the case, we assign our observed palaeoshorelines to expected highstands.

In this paper, we have used well-known sea-level curves for this method, such as (i) Waelbroeck et al. (2002) from present to 410 ky BP and (ii) Rohling et al. (2014) from 410 to 590 ky BP, which have already proven suitable for correlating marine terraces and/or palaeoshorelines to sea-level highstands (Roberts et al., 2009, 2013; De Giosa et al., 2019; Robertson et al., 2019; Meschis et al., 2020; Ferranti et al., 2021).

Concerning the sea-level curve of Waelbroeck et al. (2002), the reported uncertainty about the sea level is ±13 m, while the uncertainty in the age of sea-level highstands is reported to be 800 yr during the last 30 kyr and1000 yr before.

Concerning the sea-level curve of Rohling et al. (2014), the reported uncertainty in sea level is 6 m, while the uncertainty in the age of sea-level highstands is reported to be 4 kyr.

4 RESULTS

4.1 Palaeoshorelines recognised in the field and associated units

A detailed field survey of the study area reveals palaeoshoreline evidence, such as bands of lithophagid borings, especially *Gastrochaenolites torpedo* Kelly and Bromley due to *Lithophaga lithophaga* (Linneo), relict littoral ridges, fossil tidal notches, sea caves, wave-cut platforms, and syn- wave- cut platform deposits. With the term littoral ridge, we mean an elongated landform higher than the surrounding area and linked to the presence of a palaeoshoreline. Therefore, this term indicates only a morphological element, without going into the specifics of the formation processes, according to Ricchetti and Ciaranfi (2013). Below, we describe, from the lowest to highest, palaeoshorelines identified in the field (Fig. 3) and sedimentary units (where present), which, from field observations, can be associated with them (Table 1).

Table 1

Fig. 3

4.1.1 Palaeoshoreline PS1 (*elevation*: ~+6) and PS1marine unit (PS1mu).

This palaeoshoreline has been mostly identified in the sector from Montagna Spaccata northwards, where it crops out with consistent lateral continuity. It is represented by a band of lithophagid borings in Mesozoic limestones (Fig. 4A, B) and is characterised by progressive growth in the density of borings up to an upper band with the highest density in the entire study area. The upper limit of this band of maximum density of borings varies between +4 and +6 m above the present sea level (a.p.s.l.). This band of lithophagid borings has been considered to be indicative of a palaeoshoreline at +6 m, since from the upper limit of the lithophagid band, a subhorizontal line is defined, which is considered a reliable marker of a past mean sea-level position (Stiros et al., 1992; Ferranti et al., 2006).

PS1 is associated with the PS1marine unit (PS1mu), which consists of greyish to reddish, well-cemented calciruditic deposit that is rich in bioclasts forming a transgressive unit upon the Mesozoic limestone basement; the centimetric-sized clasts are mainly made of fragments of Mesozoic limestone, rhodoliths, and heavily reworked and smoothed mollusc shells. The PS1mu has its highest point of outcrop exactly coinciding with the upper limit of the band of maximum density of borings.

The PS1mu contains the following marine fauna:

-gastropods: *Patella* sp., *P. caerulea* Linneo, *Bolma rugosa* (Linneo), *Cerithium lividulum* Risso, *Melarhaphe neritoides* (Linneo), *Gibbula* sp., *Murex* sp., *Columbella rustica* (Linneo), *Hexaplex trunculus* (Linneo), *Thetystrombus latus* (Gmelin);

-bivalves: *Barbatia barbata* (Linneo), *Spondylus gaederopus* Linneo, *Clanculus corallinus* (Gmelin), *Striarca lactea* (Linneo), *Chlamys* sp., *Mytilus* sp., *Arca* sp.;

-coral: *C. caespitosa* Linneo.

The depositional environment of this unit was a high-energy marine infralittoral environment.

In the sector south of Montagna Spaccata, PS1 is visible only at Punta Pizzo (site G17, Fig. 4B; see Fig. 2A for its location) within the following stratigraphic succession from bottom up:

1) Reddish sands (RS); this unit consists of reddish cemented sands and calcarenites, with bioturbations (*Thalassinoides* type) concentrated especially in the lower part of the unit; the upper part of this unit is characterised by a considerable concentration of marine bivalve *Loripes orbiculatus* Poli in life positions.

The depositional environment, as suggested by the bioturbations and fossil content (Bromley and D'Alessandro, 1987), varies from a deeper marine environment to a more superficial, low-energy environment (Muddy Sand in Sheltered Areas; SVMC *sensu* Pérès, 1967).

2) Discontinuous Marine Clastic Unit (DMCU); this unit outcrops in the form of small patches that appear in abrupt contact on the RS. These patches are composed of calcirudite whose centimetre-sized clasts are mainly made up of fragments of Mesozoic limestone, rhodoliths, and the following marine fauna:

- bivalves: *Glycymeris* sp., *Callista chione* (Linneo), *Tellina planata* Linneo, and *Loripes orbiculatus* Poli.
- coral: *C. caespitosa* Linneo.

3) Lower Palaeosol (LPA). This unit consists of brick red to brown silty palaeosol, which reaches a maximum thickness of ca. 60 cm; cemented traces of roots are internally visible. The observed fossil fauna includes terrestrial gastropods, such as Helicidae, *Rumina decollata* (Linneo), *Pomatia elegans* (Müller), fragments of indeterminable pulmonate gastropods, and rare fragments of reworked marine molluscs.

The depositional environment of this unit is continental.

3) PS1marine unit (PS1mu); this unit contains similar sedimentary and fossiliferous evidence already described for the sector from Montagna Spaccata northwards. Indeed, at site G17, this unit is transgressive on all lower and older units (Mesozoic limestones, RS, DMCU, LPA), with clasts that are immersed in a matrix of reddish sand/silt and/or calcarenite/calcisiltite due to the erosion of the

underlying LPA. Towards the top, the matrix becomes yellowish to greyish, and the clasts appear less abraded. Throughout all the units, in addition to the reworked clasts, a synsedimentary marine fauna is present, consisting mainly of bivalves *Glycymeris* spp. and *Pecten* spp., and coral *C. caespitosa* Linneo. At site G17, as already observed in the sector from Montagna Spaccata northwards, the upper limit of the PS1mu outcrop roughly coincides with the lower part of the band of lithophagid borings of PS1. The unit was deposited following a marine transgression that allowed it to incorporate elements reworked by all the underlying units.

Figure 4

4.1.2 Palaeoshoreline PS2 (elevation: ∼+7.5) and PS2 marine unit (PS2mu).

This palaeoshoreline has been mostly identified in the sector from Montagna Spaccata northwards. In the sector south of Montagna Spaccata, PS2 can be mapped at Punta Pizzo only (Fig. 4B). In both sectors, PS2 is represented by a band of lithophagid borings grouped in discontinuous clusters within Mesozoic limestones whose upper limit is ca. +7.5 m. a.p.s.l. (Figs. 4B, 5).

Sometimes, this palaeoshoreline appears well separated from the previous palaeoshoreline, yet in places, we can also map scattered lithophagid borings in the Mesozoic limestone interposed between palaeoshorelines PS1 and PS2 (Fig. 4B).

PS2 is discontinuously associated with a strongly cemented coarse calciruditic deposit, with a reddish matrix composed of calcarenite/calcisiltite, which we call PS2marine unit (PS2mu). This deposit is transgressive on the Mesozoic limestone basement and has its topographically highest outcrop just below the discontinuous band of lithophagid borings, which represents PS2. The stratigraphic relationship between the PS2mu and PS1mu is not easily recognisable in the field; the PS2mu probably underlies the PS1mu, but we do not rule out a partial lateral transition between the two units.

The macrofauna of the PS2mu is not widespread throughout the unit but is localised in clusters where the following marine fauna has been recognised:

-gastropods: *Bolma rugosa* (Linneo), Hexaplex *trunculus* (Linneo), *Cerithium* sp., *Clanculus corallinus* (Gmelin);

-bivalves: *Striarca lactea* (Linneo), *Spondylus gaederopus* Linneo, *Mytilus* sp., and *Arca* sp.

Figure 5

4.1.3 Palaeoshoreline PS3 (elevation: ~+15) and PS3 Mixed Deposit (PS3-MD)

This palaeoshoreline, along with PS1, is the most continuous and well recognised in the study area. On the other hand, the associated PS3 Mixed Deposit (PS3-MD) is certainly the most complex of all the recognised deposits associated with all palaeoshorelines recognised in this study, as it is constituted by several units. In fact, with the informal term "mixed deposit", we mean a deposit correlated to a palaeoshoreline and settled in different environments (es: marine +continental).

In the sector from Montagna Spaccata northwards, PS3 is represented by a band of lithophagid borings grouped (Fig. 6A) in discontinuous clusters within Mesozoic limestones whose upper limit is ca. +15 m. a.p.s.l. In some places, PS3 is represented by residual tidal notches or inner edges cut into the Mesozoic limestones. At the Montagna Spaccata locality (MS1 site; see Fig. 2A for the location), at the walls of the coastal road trench (Fig. 6B), PS3 is represented by (i) a well-preserved inner edge (probably an altered tidal notch) with lithophagid borings and (ii) an associated wave-cut platform some metres wide (both carved into the Mesozoic limestones), where fossil specimens of *Hoplangia durotrix* Gosse are preserved within some small depressions carved on the platform.

PS3-MD lies above the wave-cut platform, and in this sector, it is represented by a marine deposit that we named the PS3marine unit (PS3mu; Fig. 6B). It consists of calcareous pebbles and rhodoliths in a coarse sandy matrix with algal calcarenite and mudstone and also contains the following marine fossils:

-gastropods: *Fissurella* sp., *Patella aspera* (Röding), *P. caerulea* Linneo, *Tritia neritea* (Linneo), *Jujubinus* sp., *Gibbula* sp., *Clanculus cruciatus* Linneo, *C. corallinus* (Gmelin), *Bolma rugosa* (Linneo), *Tricolia pullus* (Risso), *Littorina* sp. *Mitrella* sp., *Cerithium lividulum* Risso, *Vermetus* sp.;

-bivalves: *Cardita calyculata* Linneo;

- polychaeta: Spirorbidae spp.

Continental reddish clinostratified coarse breccias (br in Fig. 6B) that are approximately 1.5 m thick and are interbedded with reddish silty-sandy deposits cover all marine deposits.

Figure 6

In the sector south of Montagna Spaccata, PS3 can be identified by the presence of two palaeo-littoral ridges north and south of the Gallipoli-Alezio ridge; they are arched in shape and have their concavities facing west, towards the sea (Fig. 2A, B, C). These littoral ridges extend parallel to PS3 towards the sea. We call the littoral ridge north of Gallipoli *Monte-Crocefisso* palaeo-littoral ridge (hereinafter MClr) and that south of Gallipoli *Carmine-Li Foggi* palaeo-littoral ridge (hereinafter CLlr). Both ridges are the local expression of the PS3 Mixed Deposit (PS3-MD; Figs. 3 and 7A, B), which is constituted, from bottom to top, by the PS3marine unit (PS3mu), Aeolian Unit 1 (AU1), and Aeolian Unit 2 (AU2) and lies on three older units wich represent the local substrate: Yellowish Sand (YS), Upper Palaeosol (UPA), and lacustrine silts (LS).

PS3 extends approximately 200 metres landward of the inner margin of CLlr, where the palaeovalleys of ancient ephemeral streams (locally called *lame*) abruptly end along an alignment at ca. +15 m (Fig. 7e).

The stratigraphy and chronology of the PS3-MD and the older underlying units in the sector south of Montagna Spaccata (where the PS3-MD forms the MClr and CLlr) are shown in Fig. 7; it is important to note that these older units on which the PS3-MD lies (YS, UPA, and LS) are not described in detail because they refer to a phase prior to the formation of PS3 and are not directly correlatable with palaeoshorelines recognised in the field; therefore, they are beyond the scope of this work.

The PS3-MD starts with thePS3mu, which lies in abrupt, erosional contact on the underlying UPA and LS (Fig. 7A, b, B). The base of the PS3muis in places constituted by a pebbly lag that is ca. 30 cm thick (Fig. 7b, c), where specimens of marine bivalve *Ostrea* sp. can be found sporadically. Above the pebbly lag, the unit passes to irregularly cemented calcarenites that have high- and low-angle cross-bedding, and contains rare specimens of *Ostrea* sp. In some cases, the calcarenites appear organised in westwards-dipping foresets (towards the current coastline). In section G4 (Fig. 7B), the pebbly lag is not present, and the basis of the PS3muis made up of irregularly cemented, coarse subhorizontal-bedded calcarenite, which forms load casts over the underlying UPA. This basal calcarenite passes upwards to irregularly cemented coarse calcarenite, alternating with gravel and calcirudite levels that are rich in mollusc shells and that have a low-angle, hummocky-like cross-lamination or they appear organised in westwards-dipping foresets (towards the current coastline). Between the basal, coarse subhorizontal-bedded calcarenite and the overlying hummocky/clinostratified calcarenites/calcirudites, there is a thin interval of light grey clays (cll) (Fig. 7B, f) showing wavy deformation structures at their interfaces with the overlying calcarenites.

The macrofaunal content of the PS3mu in this sector includes (apart from the already mentioned *Ostrea* sp.) only marine bivalves: *Barbatia barbata* (Linneo), *Chama gryphoides* (Linneo), *Acanthocardia tuberculata* (Linneo), *Glycymeris nummaria* (Linneo), *Chamelea gallina* (Linneo), *Loripes lucinalis* (Lamarck), *Donax trunculus* Linneo, *D. venustus* Poli, and *Lentidium mediterraneum* (Costa).

Above the PS3mu, we mapped the AU1, which outcrops only in the northern and southern parts of the CLlr and consists of fine, whitish/reddish calcarenite organised in wavy to cross-bedded cosets dipping in various directions. Within the unit, there are thin layers or lenses characterised by the presence of numerous voids crossed by cemented fossil root traces.

The observed fossil macrofauna is made up exclusively of rare specimens of terrestrial gastropods Helicidae.

Above the AU1, we mapped the AU2. South-eastwards-dipping foresets dominate the internal structure of this unit, which consists of fine, whitish–reddish calcarenite with thin layers or lenses characterised by the presence of numerous voids crossed by cemented fossil root traces. The observed fossil macrofauna consists exclusively of rare specimens of terrestrial gastropods Helicidae, while the microfauna is mainly made up of reworked or fragmented benthic foraminifers.

The depositional environment of AU1 and AU2 is coastal dunes.

Figure 7

4.1.4 Palaeoshoreline PS4 (elevation: ∼+22) and PS4 Mixed Deposit (PS4-MD)

In the sector from Montagna Spaccata northwards, this palaeoshoreline is mainly represented by a band of lithophagid borings within Mesozoic limestones, grouped into discontinuous clusters whose upper limit is ca. +22 m. a.p.s.l. At the Uluzzo locality, and specifically at the MS5 site (Figs. 8, 9), this palaeoshoreline is represented by a small residual wave-cut platform, a residual tidal notch, sea caves, lithophagid borings, the trace *Gastrochaenolites cor* Bromley and D'Alessandro with the original borer marine bivalve *Petricola lithophaga* (Retzius), and small patches of a syn- wave- cut platform deposit (Figs. 8, 9) composed of well-cemented calcirudite, which is the local expression of PS4-MD.

Figure 8

In the sector south of Montagna Spaccata, PS4 can be identified by the presence of two small and discontinuous relict littoral ridges north and south of Gallipoli, which are situated landwards with respect to the MClr and CLlr (Fig. 2B, C). The small remnants of these ridges seem to depict arched shapes with the concavity facing west, that is, towards the sea; they represent the PS4-MD in this sector; the few sections observable show aeolian whitish/reddish calcarenite, organised in wavy to cross-bedded cosets dipping in various directions but mostly landward-dipping. The observed macrofauna is exclusively made of very rare specimens of terrestrial gastropods Helicidae.

4.1.5 Palaeoshorelines PS5 (elevation: ～+41), PS6 (elevation: ～+62), and PS7 (elevation: ～+67)

These three palaeoshorelines are described together because of the common characteristics that they share in the sector from Montagna Spaccata northwards. In addition, PS6 and PS7 were observed in the field only at the Montagna Spaccata locality (Fig. 10), likely because the rocky slope reaches a higher elevation above present sea level and is poorly vegetated. All these palaeoshorelines are represented by bands of lithophagid borings grouped in discontinuous clusters; note that the elevations represent, as always, the points of maximum elevation of these bands above the present sea level.

In the sector south of Montagna Spaccata, the presence of these three palaeoshorelines may likely be derived from geomorphological evidence, such as slope breaks and the likely remains of the inner edges of marine terraces. The only exception is PS5, which, in this sector of the study area, is still visible to the north of San Mauro Abbey (Figs. 2A, 3) in the form of a band of lithophagid borings within Mesozoic limestones grouped into discontinuous clusters. In addition, a well-identified marine terrace deposit less than 1 km^2 wide that crops out between ca. +40 and +30 m may likely be correlated with PS5. This deposit, which we defined as the PS5 Marine Deposit (PS5-MaD), consists of yellowish-brownish fine calcareous-siliciclastic sands containing a few specimens of bivalves *Chlamys* sp., *Pecten* sp., and *Pseudamussium peslutrae* (Linneo). The microfauna is constituted of ostracods and foraminifers. Towards the top, the PS5-MaD becomes more silty/clayey and appears altered by the deposition of whitish caliche nodules, due to diagenetic processes.

Figure 9

Figure 10

4.2 Chronological analyses results and consequent chronological attributions

Our chronological analyses allow us to directly date some units associated with some of the recognised palaeoshorelines.

4.2.1 PS1 and PS1mu

The chronological analysis obtained via the isoleucine/alloisoleucine epimerisation method on shells of *Patella* sp. and *T. latus* (Gmelin) contained, respectively, in two samples taken from PS1mu at sites MS6 (Fig. 4A) and MS2 (Fig. 10; see also Fig. 2A for their locations) indicated aminozone E (Table 2A). This aminozone is associated with MIS 5.5 (Hearty et al., 1986; Hearty, 1987; Hearty and Dai Pra, 1992; Torres et al., 2013). At site G17 (Fig. 4B, see Fig. 2A for its location), the numerical age obtained from a sample of the LPA of 122.1±33.6 ky BP (Table 2A) allows us to assign the PS1mu more precisely to the late MIS 5.5, as the PS1mu overlies the LPA.

4.2.2 PS3 and PS3 Mixed Deposit (PS3-MD).

Regarding the PS3-MD, it has been possible to perform chronological analyses on the PS3mu, which constitutes the basal unit of the PS3-MD. At the Montagna Spaccata locality (MS1 site; Figs. 5 and 9; see Fig. 2A for its location) along the road cut (Fig. 6B), two chronological constraints have been obtained: (i) the isoleucine/alloisoleucine epimerisation on shells of *Patella* sp. contained in a sample taken from the PS3mu (Table 2A) indicated aminozone E (MIS 5.5); (ii) U-series dating applied to two specimens of *H. durotrix* Gosse anchored on the wave-cut platform on which the PS3mu lies (Fig. 6B) provided ages of 213.39±3.0 and 211.17±4.8ky BP (Table 2A), revealing MIS 7.3 (Waelbroeck et al., 2002; Grant et al., 2014).

In the sector south of Montagna Spaccata, the chronological analysis obtained with the isoleucine/alloisoleucine epimerisation method on shells of *Glycymeris* sp. contained in two samples taken from the PS3mu at site G4 (Fig. 7B; see Fig. 2A for its location) indicate aminozone E (MIS 5.5) (Table 2A).

4.2.3 Other units not associable with the recognised palaeoshorelines

The chronological analyses allow us to also assign ages to some other units that are not associable with the recognised palaeoshorelines, except for the already mentioned LPA.

In the sector south of Montagna Spaccata, specifically at site G17 near Punta Pizzo (Fig. 4B; see Fig. 2 for its location), the DMCU has been dated using the isoleucine/alloisoleucine epimerisation method on shells of *Glycymeris* sp. contained in a sample taken from this unit (Fig. 4B; Table 2A); this method indicates aminozone F, corresponding to MIS 7 (Hearty et al., 1986; Hearty, 1987; Hearty and Dai Pra, 1992; Torres et al., 2013). The U-series dating applied to *C. caespitosa* Linneo contained in the same sample provided an age ranging from a minimum of 211.97±3.6 ky BP to a maximum of 232.02±5.3 ky BP (Fig. 4B; Table 2A), which allows us to assign it to MIS 7.3 (Waelbroeck et al., 2002; Grant et al., 2014). This chronological analysis, with two different methods applied to the same sample (G17-2b; Table 2A), mutually reinforces the reliability of the dates obtained. As a consequence, the unit RS, underlying DMCU, dates back to MIS7.5 or to an older stage.

The DMCU was also dated at Torre Sabea (G20 site; see Fig. 2A for the location), where sample G20-1 (Table 2A) gave an age of 208.44±5.3 ky BP (MIS 7.3).

In the sector south of Montagna Spaccata, it has also been possible to perform chronological analyses on the YS and LS, which represent the substrate on which the PS3-MD (which, in this sector, forms the CLlr) was deposited.

For the YS, the chronological analysis with the amino acid racemisation method applied to ostracods contained in a sample taken from this unit (Fig. 7B; Table 2A) provided the age of 137.2±29.3 ky BP, which allows us to attribute it to MIS 6-MIS 5.5.

For the LS, the date obtained with the amino acid racemisation method applied to ostracods contained in a sample taken from this unit (Fig. 7B; Table 2A) provided the ages of 138.4±17.9 and 118.1±17.9 ky BP, which allows us to attribute it to MIS 6-MIS 5.5.

Table 2

5 DISCUSSION

5.1 Focus on *Palaeoshoreline PS3 (elevation: ～+15) and PS3 Mixed Deposit (PS3-MD)*

5.1.1 Sector south of Montagna Spaccata

The *Carmine-Li Foggi* palaeo-littoral ridge (CLlr) and *Monte-Crocefisso* palaeo-littoral ridge (MClr) constitute the geomorphological expression (Fig. 2A, B, C) of the PS3 Mixed Deposit (PS3-MD) in the sector south of Montagna Spaccata.

Our field observations and chronological analyses allow us to establish that CLlr and MClr are two sedimentary bodies made up of the PS3mu, AU1, and AU2. The CLlr and MClr lie on previous units dating back to MIS 6-5.5 and not associable with the recognised palaeoshorelines: YS, UPA, and LS. The scheme of the stratigraphic relationships between all units recognised within the PS3-MD (Fig. 7B) allows us to identify the correlations we have reconstructed between them.

The dates obtained from the PS3mu (MIS 5.5; Table 2A), the cll layer within the PS3mu (Fig. 7B, f), and the presence of a palaeoshoreline at ca. +15 m (PS3) elongated approximately 200 landward of the inner margin of CLlr (Fig. 7e) allow us to correlate PS3 and the PS3-MD (the latter morphologically represented by the CLlr and MClr) with each other and to reconstruct their parallel formation and evolution in the sector south of Montagna Spaccata.

The cll layer contributes to the reconstruction of the current elevation a.p.s.l. of the palaeoshoreline associated with the formation of the CLlr and MClr. The wavy deformation structures at the interface between the cll and the overlying calcarenites (Fig. 7B, f) typically form in the offshore transition due to storm waves (Henkel, 1970; Molina et al., 1998; Alfaro et al., 2002). This evidence indicates that the sea level was likely 6-10 m over the top of cll during its deposition (De Santis et al., 2022). Our field interpretation is that the cll indicates the maximum water depth and, therefore, the maximum marine transgression, while calcarenites/calcirudites above the cll represent the prograding beach deposits following the maximum marine transgression.

Therefore, the contact between the cll and the overlying calcarenites/calcirudites can be interpreted as indicative of the offshore transition of the palaeo-beach at the time of the maximum marine transgression. Today, after the tectonic uplift, this contact is ca. 8.5 m a.p.s.l. and we can assume a palaeo-depth, at the time of formation of this contact, of ca. 6-10 metres (Henkel, 1970; Molina et al., 1998; Alfaro et al., 2002). Adding the 8.5 metre-current elevation of the contact with the 6-10 metre-palaeo-depth, we obtain that the paleo-sea level today is uplifted within the range of 16.5 ± 2 m. The palaeoshoreline PS3, extending landward of the inner margin of CLlr at ca. +15 m, is the only one within this range, so we interpret 15 m as the current height a.p.s.l. reached, after the uplift, by the palaeoshoreline due to the sea level at the time of the maximum marine transgression, which started the formation of the CLlr and MClr.

Therefore, we conclude that the CLlr and MClr were formed immediately after the first MIS 5.5 highstand, which brought the sea on a palaeoshoreline (PS3) that today is ca. +15 m: soon after this first highstand was attained, the CLlr and MClr began to form as a barrier just offshore from the palaeoshoreline (Fig. 11 A-E), following the pattern of barrier formation reported in Roy et al. (1994) and Otvos (2012).

Fig. 11

5.1.2 Sector from Montagna Spaccata northwards; evidence of the reoccupation of the MIS 7.3 highstand by the MIS 5.5 highstand

In this sector, PS3 and the associated PS3-MD are more visible just at Montagna Spaccata (MS1 site; Fig. 6B). Here, the PS3-MD is represented only by the PS3mu, which dates back to MIS 5.5 (Table 2A). Nevertheless, on the wave-cut platform of Mesozoic limestones, two specimens of *H. durotrix* Gosse indicate MIS 7.3 (Table 2A). We interpret this apparent discrepancy as a case of the reoccupation of an older palaeoshoreline by a younger palaeoshoreline. The phases of palaeoshoreline formation and reoccupation can be summarised as follows (Fig. 12):

First, during the MIS 7.3 highstand, an inner edge with a syn-wave cut platform forms; in this phase, specimens of *H. durotrix* Gosse grow on the platform; note that this coral lives between 0 and 5 m below sea level (Picton and Morrow, 2016). As the current position of the fossils of *H. durotrix* Gosse is ca. +13 m, the near palaeoshoreline PS3 at +15 m (Fig. 6B) is the only one associable with fossils of this coral, as this situation indicates that the corals lived at ca. 2 m depth. The subsequent higher palaeoshoreline (PS4 at +22 m) cannot be associated with the fossils of *H. durotrix* Gosse because this would involve the corals living at a water depth of 9 m.

Second, the subsequent MIS 5.5 highstand settled more or less at the same position, reoccupying the palaeoshoreline of MIS 7.3. In this phase, the PS3muwas deposited on the previously formed wave cut platform, covering the fossil specimens of *H. durotrix* Gosse.

The reoccupation of PS3 dating back to MIS 7.3 by a subsequent highstand that reached PS3 again is well mapped only at Montagna Spaccata (MS1 site; Fig. 6B) because the Mesozoic limestone where palaeoshorelines are cut is prone to preserving better palaeo-landforms.

Fig. 12

However, more generally, evidence of the transgression of MIS 5.5 deposits on MIS 7.3 deposits in this study area is widely present. For example, at Torre Sabea (G20 site; see Fig. 2A for the location), the contact between the underlying DMCU and the overlying PS1mu can be observed in the field. At this site, the dating carried out on the DMCU (sample G20-1; Table 2A) gave an age of 208.44±5.3

ky BP (MIS 7.3), while the overlying PS1mu is attributable to MIS 5.5, which is also confirmed by the presence at this site of numerous specimens of *T. latus* (Gmelin), which, in Italy, is exclusive to MIS 5.5 (Hearty and Dai Pra, 1992; Antonioli et al., 2018). The same evidence is also found in the Uluzzo locality (MS11 site; see Fig. 2A for the location), where dating carried out on a marine deposit not attributable to any of the recognised units (sample MS11-1; Table 2A) gave ages of 223.84±7.2ky BP and 225.17±5.4 ky BP (MIS 7.3 onset). Our evidence and new absolute age controls from the Torre Sabea locality, in particular, confirm the stratigraphy, ages, and interpretation of that site reported in Hearty and Dai Pra (1992; see Fig. 9 of that work).

5.2 Uplift scenario; comparison between observed and expected palaeoshorelines

New chronological analyses, combined with the synchronous correlation method, have been used to test different sea level curves and uplift rate scenarios to produce the best match between observed and expected palaeoshorelines.

The best fitting scenario has been obtained using, as input into the terrace calculator, the sea-level curves of Waelbroeck et al. (2002) from present to 410 ky BP and Rohling et al. (2014) from 410 to 590 ky (Table 2, 1^{st} and 2^{nd} columns for sea level and age, respectively).

The scenario we reconstructed implies an uplift rate of 0.09 mm/yr from 590 to 130 ky BP (middle Pleistocene or MIS 15 - MIS 6 interval) and of 0.07 mm/yr from 130 ky BP onwards (late Pleistocene or MIS 5 - onwards).

The uplift rate of 0.07 mm/yr is derived from chronological analyses carried out on the PS3-MD (more specifically, on the PS3mu). Using the IE results from sites MS1 and G4 (Table 2A) and taking into account the link of origin between PS3 and the PS3-MD (see par. 5.1), we concluded that PS3 dates back to a first and higher peak of MIS 5.5, attained at ca. 127 ky BP (Waelbroeck et al., 2002), when the sea level reached an elevation of +6 m a.p.s.l (Waelbroeck et al., 2002).

The sea-level elevation attained during the first peak of MIS 5.5 is an object of debate. Some global compilations of RSL data combined with Glacial Isostatic Adjustment (GIA) modeling indicate that peak of global mean sea level during MIS 5.5 was higher than the previous long-standing estimate (4 to 6 m), in the range of ~6 to 9 m above present (Kopp et al., 2009; Dutton and Lambeck, 2012). This is in agreement with site specific, GIA-corrected coastal records in Seychelles at 7.6 ± 1.7 m (Dutton et al., 2015b). The Red Sea planktic $\delta^{18}O$ record places peak RSL values during MIS 5.5 at 6.7 ± 3.4 m (maximum probability with 95% probability envelope; Grant et al., 2012). Differences in RSL reconstructions obtained from several locations (Rovere et al., 2016) yield a range of interpretations about the evolution of global mean sea level during the MIS 5.5 highstand (Siddal et al., 2007; Stocchi et al, 2018), also comparing field data with numerical modelling (Stocchi et al, 2018). Differences in RSL reconstructions from site to site yield a range of interpretations about the evolution of global mean sea level during the MIS 5.5 highstand, going from a stable sea level (Stirling et al., 1998) to four peaks in sea level reflecting repeated sea-level oscillations (Thompson et al., 2011; Rohling et al., 2019). As yet, no consensus exists regarding this suite of scenarios.

In this work, for the application of the synchronous method, highstands from a sea-level curve have to be introduced as one of the inputs. Since the best fitting scenario between observed and expected palaeoshorelines has been obtained using as input the sea-level curve from Waelbroeck et al. (2002) from present to 410 ky BP, we used for MIS 5.5 the mean sea level reported in that curve, that is, +6 m a.p.s.l. In any case, this value is within the value range indicated in several literature works for the peak of global mean sea level during MIS 5.5 (Hearty et al., 2007; O'Leary et al., 2013; Dutton et al., 2015a and references therein; Rohling et al., 2019).

Based on the chronological analyses (IE) at sites MS2 and MS6 (Table 2A) and the presence of *T. latus* (Gmelin) at the MS2 site (Fig. 10), we concluded that PS1 and the associated PS1mu also belong to aminozone E (MIS 5.5). Nevertheless, given its minor elevation a.p.s.l. and, above all, the chronological constraint given by the age (122.1±33.6 ky BP) of the LPA, which at the G17 site underlies the PS1mu, we assign PS1 and the PS1mu to the second peak of MIS 5.5 (Hearty et al., 2007; O'Leary et al., 2013; Dutton et al., 2015a and references therein; Stocchi et al., 2018; Rohling et al., 2019), that is, ca. 120 ky BP, which has been recognised in other regions within the

Mediterranean realm (Cinque and Romano, 1990; Meschis et al., 2020). As a consequence, LPA indicates a sea-level fluctuation between the two sea-level highstands recognised in the study area within MIS 5.5. We interpret LPA as one of the palaeosols interbedded within marine deposits dating back to MIS 5.5 which had already been reported from the area of Gallipoli by Hearty and Dai Pra (1992) even if, at the site G17 (Fig. 4B), the LPA lies between the MIS 7 and 5.5. This is because here the deposits referable to the first highstand of MIS 5.5 are missing due to erosion and/or non-deposition.

Ultimately, the uplift rate of 0.07 mm/y is derived by assigning an age of 127 ky (MIS 5.5) and a palaeo-sea-level at +6 m (2nd column in Table 3) to PS3, which is currently at +15 m a.p.s.l; thus, the vertical displacement is ca. 9 m within 127 ky.

The uplift rate of 0.09 mm/y is derived from the evidence that PS3 is also the palaeoshoreline of MIS 7.3, as explained in paragraph 5.1.2. During MIS 7.3, the sea level reached an elevation of -4 m b.p.s.l. (Waelbroeck et al., 2002). Thus, the uplift rate of 0.09 mm/yr is derived by assigning a mean age of 212 ky (MIS 7.3) and a palaeo-sea-level at -4 m (2nd column in Table 3) to PS3, which is currently at +15 m a.p.s.l., thus yielding a vertical displacement of ca. 19 m within 212 ky.

It is important to emphasise that the two uplift rates are so similar to each other that, even assuming a constant average rate of 0.08 mm/y for the entire period (middle Pleistocene-onwards, or interval MIS 15-onwards; that is, 590 ky BP-onwards), the results of the synchronous method do not change.

Table 3

The expected palaeoshoreline elevations generated by our synchronous correlation method are listed in the 3rd column of Table 3.

We associated the expected palaeoshorelines generated by our synchronous correlation method (3rd column of Table 3 and Fig. 13) with the observed palaeoshorelines (4th column of Table 3 and Fig. 13) by seeking the best match between them. This match is mathematically expressed by the coefficient of determination (R^2 value) for linear regression analysis of the “observed” and the “expected” elevations of all palaeoshorelines (see Fig. 13).

Given the maximum uncertainty of ± 13 m in the sea-level curves we used (Waelbroeck et al., 2002; Rohling et al., 2014), we prudentially consider acceptable a gap of up to 10 m between an expected and the observed palaeoshoreline that we associate with it (compare the 3rd and 4th columns in Table 3).

Ultimately, the palaeoshorelines recognised in the field in this study are associated with sea-level highstands (Table 3 and Fig. 13), such as 120 ky BP (MIS 5.5, second peak; Hearty et al., 2007; Rohling et al., 2008; Kopp et al., 2009, 2013; O’Leary et al., 2013; Dutton et al., 2015a and references therein; Düsterhus et al., 2016), 127 ky BP (MIS 5.5, first peak), 212 ky BP (MIS 7.3), 330 ky BP (MIS 9.3), 410 ky BP (MIS 11), 525 ky BP (MS 13.3), and 590 ky BP (MIS 15).

Some expected palaeoshoreline elevations are lower or (nearly) equal to the next younger expected palaeoshorelines, suggesting that they may be overprinted or reoccupied, that is, partly or completely removed by erosion during the rising sea level of a subsequent highstand. Thus, except for PS3, none of the observed palaeoshorelines has been correlated with overprinted or reoccupied palaeoshorelines. The exception of PS3 results from a MIS 7.3 highstand reoccupied by the first peak of the MIS 5.5 highstand, and documented by our new absolute age controls. In addition, the synchronous correlation method predicts the presence of several currently submerged palaeoshorelines, which are probably completely overprinted.

Figure 13 shows, for two of the seven topographic profiles extracted from the DTM, the elevations of observed (coloured arrows) versus expected (horizontal lines) palaeoshoreline elevations. In this figure, the association between expected (and not overprinted) and observed palaeoshorelines is represented using the same colour for continuous horizontal lines and arrows, where the first represents the elevations of expected (and not overprinted) palaeoshorelines, and the second represents the corresponding observed palaeoshorelines.

Figure 13

Field measurements versus expected palaeoshoreline elevations show an R^2 value of ca. 0.99 (Fig. 14). This value confirms that the fits between the expected and observed palaeoshorelines are good, giving confidence to the uplift rates.

Figure 14

5.3 Terrace phases and vertical movements of the Apulian foreland in the middle-late Pleistocene; considerations of the MIS 7.3 highstand

The Apulian foreland represents an uncommon case of a foreland shared by two opposite- verging chains: the SW-verging Albanides- Hellenides and NE-verging southern Apennines. The deformation occurring within this type of foreland is uncommon and poorly understood.

To date, the Apulian foreland has been characterised by a scarcity of reliable chronological data concerning the marine terraces older than the last interglacial and, as a consequence, uplift rates have been estimated only for the late Pleistocene by using the elevation of the marine terrace related to the last interglacial period (MIS 5.5) (Hearty and Dai Pra, 1992; Belluomini et al., 2002).

The new chronological constraints and results of the synchronous correlation presented in this work allow us to update the results recently published in De Santis et al. (2021a).

The two uplift rates of 0.09 mm/yr from 590 to 130 ky and of 0.07 mm/yr from 130 ky BP onwards are more similar and have been obtained from precise chronological constraints. Although these data show a slight slowdown in the regional uplift, also an average constant uplift rate over time of 0.08 mm/yr may be claimed to explain the regional uplift for the last 590 ka for an almost tectonically stable region such as the Apulian foreland.

PS1 and PS2 (+6 and +7.5 m, respectively) both refer to the highstand at ca. 120 ky BP; the presence, in the study area, of sites where scattered lithophagid borings in the Mesozoic limestone are interposed between PS1 and PS2 seems to confirm this reconstruction, along with the stratigraphic relationship between the PS1mu and PS2mu. In addition, as PS3 (+15 m) is referred to 127 ky BP, we can confirm that, in the area of Gallipoli, there is evidence of at least two highstands during MIS 5.5.

Nevertheless, the chronological attribution and current elevation of PS3 (127 ky BP and +15 m a.p.s.l., respectively) suggest that they could represent the palaeoshoreline and deposit of MIS 5.5 found at an elevation that is one of the highest among those reported in previous studies between Taranto and Santa Maria di Leuca (Hearty and Dai Pra, 1992; Belluomini et al., 2002; Ferranti et al., 2006). One of the possible explanations could be that previous studies always considered MIS 5.5 deposits in a restricted coastal belt without recognising the real MIS 5.5 palaeoshoreline.

Our study highlights an important aspect of the MIS 7.3 highstand. Given the chronological constraint provided by the dating of *H. durotrix* Gosse for PS3, the latter can also be attributed to the MIS 7.3 highstand. Due to the almost -stability of the Apulia foreland, the only way to place the current position of the MIS 7.3 palaeoshoreline at +15 m is to postulate an elevation of the MIS 7.3 highstand close to the present sea level, as in Waelbroeck et al. (2002).

Indeed, entering into the synchronous method a MIS 7.3 highstand reconstructed many metres below the current sea level (i.e., ~ -29 metres in Grant et al., 2014) would imply a vertical displacement of the MIS 7.3 palaeoshoreline of ca. 40-45 m, with a mean uplift rate (between MIS 7.3 and today) of approximately 0.2 mm/yr. This value is very far from all uplift rates obtained for the coastal stretch where our study area is located (Ferranti et al., 2006; Cerrone et al., 2021b). In addition, the uplift rate of 0.2 mm/yr implies that the synchronous method assigns the +15 m palaeoshoreline to MIS 7.5, which does not match the chronological constraints of U-series dating applied to *H. durotrix* Gosse. This mismatch is due to the subsequent lowering of the uplift rate to 0.07 mm/y, which is also constrained by chronological analyses. However, more investigations are needed within the Apulian foreland to test whether MIS 7.3 is as high as we mapped it in this study.

In conclusion, the data arising for the Apulian foreland suggest a MIS 7.3 highstand near that reported in Waelbroeck et al. (2002), that is, near the present sea level.

A remarkable characteristic of the palaeoshorelines that we recognised is that they can be observed at the same elevation a.p.s.l. for the entire study area, which, from a structural point of view, spans horsts and grabens (Fig. 1) limited by normal faults (Ambrosetti et al., 1987); this feature indicates that these faults did not displace the coastal sector of the study area into blocks with differential uplift and suggests that, at least in the middle and late Pleistocene, this sector of the Salento Peninsula uplifted uniformly.

Palaeoshorelines dating back to the middle-late Pleistocene have been recognised in other peri-Mediterranean areas, and they are all characterised by geodynamic contexts different from the Apulian foreland. Table 4 summarises some examples of emerged palaeoshorelines, with the ages to which they have been attributed.

Table 4

All areas listed in Table 4 are characterised by uplift rates higher than those of the Apulian foreland. The main result of the difference in the uplift rates between the sites listed in Table 4 and the Apulia region is that, in the latter, a smaller number of highstands left a trace in the form of a palaeoshoreline. Due to the slow uplift rates, the palaeoshorelines have undergone overprinting or reoccupation or are now submerged: the synchronous correlation method highlights this situation. Extensive overprinting and reoccupation are symptomatic of slow uplift rates (Pedoja et al., 2018; Cerrone et al., 2021a,b).

CONCLUSIONS

The synchronous correlation method, applied for the first time extensively to the Apulian foreland, modifies the previously applied technique, known as "sequential correlation" (e.g., Roberts et al., 2013; Robertson et al., 2019), where it is assumed that starting from a single dated palaeoshoreline, the next higher and older palaeoshoreline belongs to the next older sea-level highstand. It is therefore probable that this classic methodological approach, if accompanied by the absence of reliable datings, does not highlight cases of overprinting or reoccupation, which instead are highly probable in geodynamic contexts characterised by fairly stable territories or with weak and constant vertical movements, such as that in the Apulian foreland.

Acknowledgements

We wish to thank all the staff at the Polo Scientifico e Tecnologico Magna Grecia (Taranto) for the topographic instruments. We also are very grateful to the three anonymous reviewers for their comments and suggestions that have allowed us to improve the quality of the paper.

Figure and table caption

Figure 1 - Study area. A: Regional context showing the main geological–structural domains in southern Italy. B: Simplified geological map of the Salento Peninsula (from Boenzi et al., 2010), showing the structural tectonic setup defined as "Serre Salentine": a series of horsts and grabens elongated in the NW–SE direction. C: Detailed geological map from Ciaranfi et al. (1992).

Figure 2 – A: 2-m +8-m digital terrain models (DTMs). B: 3D scene of the study area with sites and main localities cited in the text; the colours represent the elevation above the present sea level, as in the right up box in A.

Table 1- list of palaeoshorelines recognised with associated deposits and units (these latter are only if it has been possible to define them) and landforms in which palaeoshorelines and associated deposits/units appear. With the informal term

"mixed deposit" we mean a deposit correlated to a palaeoshoreline settled in different environments (es: marine +continental).

Fig. 3 - Reconstructed palaeoshorelines and associated units and the topographic profiles reported in Fig. 13. The panel on the top right shows the abbreviations of the recognised paleoshorelines and colors of representation and abbreviations of the associated units, described in detail in Section 4.1 and reported also in Tab. 1. Each palaeoshoreline is indicated with a continuous line where it is well recognisable in the field, with a dotted line where its position is detectable by geomorphological and/or geological indicators. See the text and Tab. 1 for the descriptions of the units associated with the recognised palaeoshorelines. Note that the units reported in this map are only those genetically associated with the recognised palaeoshorelines.

Figure 4- Field photographs of PS1 and PS1mu. A: sector from Montagna Spaccata northwards, specifically sites MS6 (left) and MS5 (right) at the Uluzzo locality (see Fig. 2A for the location). The upper limit of the band of lithophagid borings is indicated by black arrows; note the upper boundary of greyish PS1mu deposits, which follows the course of the band of lithophagid borings. Black horizontal lines with elevations in metres above the present sea level are indicated. B: Sector south of Montagna Spaccata: schematic stratigraphy of the Punta Pizzo locality, specifically site G17 (see Fig. 2A for the location); a: detail of the contact between two older Quaternary units: Reddish Sands (RS) and Discontinuous Marine Clastic Unit (DMCU). b: detail of the contact between the underlying LPA and the overlying PS1mu. c: detail of the basal part of the PS1mu, made up of centimetric clasts represented by fragments of Mesozoic limestone, rhodoliths, and heavily reworked and smoothed mollusc shells. These clasts are immersed in a matrix of reddish sand/silt and/or calcarenite/calcisiltite, evidently coming from the erosion of the underlying LPA. d: detail of the contact between the PS1mu and Mesozoic limestones (black arrows), with lithophagid borings. e: band of lithophagid borings at ca. +6 m. The legend of this figure is also used for Figures 6, 8, 9, and 11.

Figure 5- Field photographs of PS2, all taken in the sector from Montagna Spaccata northwards, specifically sites MS6 (upper photos) and MS5 (lower photo), both at the Uluzzo locality (see Fig. 2A for the location). The black arrows indicate the main clusters of lithophagid borings. Black horizontal lines with elevations in metres above the present sea level are indicated.

Figure 6 - Field photographs of PS3. A: sector from Montagna Spaccata northwards, specifically site MS5 at the Uluzzo locality (see Fig. 2A for the location). B: Montagna Spaccata; cut along the landward side of the coastal road, that is, the MS1 site (see Fig. 2A for the location). The red arrow indicates a probable residual tidal notch; the black arrows indicate lithophagid borings; dashed line follows the palaeo tidal notch and shore platform. c: cut along the seaward side of the coastal road, with the position of sample MS1-1 (*Hoplangia durotrix* Gosse; see Table 2A) reported in d, where lithophagid borings on the Mesozoic limestones are also visible. Black horizontal lines with elevations in metres above the present sea level are indicated. ML: Mesozoic limestones; PS3mu: PS3marine unit; br: continental breccias.

Figure 7 – A: Field photographs of sections at the G2-2 site (see Fig. 2A for the location) within the *Carmine-Li Foggi* palaeolittoral ridge (CLlr), formed by the following units grouped within the PS3 Mixed Deposit (PS3-MD): PS3marine unit (PS3mu), Aeolian Unit 1 (AU1), and Aeolian Unit 2 (AU2). The PS3-MD lies on older units: Yellowish sand (YS) and Upper Palaeosol (UPA). b: Detail of the succession, from bottom to top, of the units cropping out at site G2-2: Yellow Sands (YS), Upper Palaeosol (UPA), PS3marine Unit (PS3mu), Aeolian Unit 1 (AU1). c: Detail of the abrupt, erosional contact of the PS3mu on the underlying UPA, with the pebbly lag at the base of the PS3mu, which often forms a protruding shelf. B: Scheme of stratigraphic relationships between all units of the PS3 Mixed Deposit (PS3-MD) and older units cropping out at sites G2-2, G2-3 and G4 within the *Carmine-Li Foggi* palaeolittoral ridge (CLlr) (see Fig. 2A for the locations of sites G2-2, G2-3 and G4). e: Google Earth image of the trace of PS3 still visible approximately 200 metres landward of the inner margin of the southern sector of the CLlr, where the inactive valleys of ancient ephemeral streams (locally called *lame*) abruptly interrupt along an alignment at ca. +15 m. f: Field photographs of the G4 site (see Fig. 2A for the location) showing the cll layer within the PS3mu; the cll layer is very important to establishing a genetic link between the PS3 Mixed Deposit (PS3-MD) in this sector.

Figure 8 – A: Field photographs of PS4 at the Uluzzo locality in the sector from Montagna Spaccata northwards, specifically at the MS5 site (see Fig. 2A for the location and Fig. 9 for an overview of the MS5 site); the black squares labelled B and C contain details reported in photographs B and C. B: Sea cave. C: Small residual syn- wave- cut platform deposit (PS4-MD) characterised by the tace *Gastrochaenolites cor* (black arrow) with the original borer marine bivalve *Petricola lithophaga* (Retzius). Black horizontal lines with elevations in metres above the present sea level are indicated.

Figure 9 - Field photographs (up) and a sketch (down) of a cliff at the Uluzzo locality (MS5 site of Fig. 2A) in the sector from Montagna Spaccata northwards, showing the recognised palaeoshorelines and units (represented by the legend of Fig. 4). The legend on the left is also used for Figure 10.

Figure 10 – Google Earth image (top) of the Montagna Spaccata locality (MS1 and MS2 sites of Fig. 2A), showing the recognised palaeoshorelines and units (represented by the legend of Fig. 4). MS1 site is represented in detail in Fig. 6B. For the legend, see Fig. 9.

Table 2 – A: Samples on which chronological analyses were carried out with amino acid racemisation, isoleucine/alloisoleucine epimerisation, U-series dating, and relative results. The first part of the sample ID indicates the site from which the sample comes (reported in Fig. 2A). Amino acid racemisation was applied to ostracods, and due to the conversion algorithm of Ortiz et al. (2004), it gives numerical data. The isoleucine/alloisoleucine epimerisation allows us to attribute the samples to aminozones corresponding to specific MISs (Hearty et al., 1986; Hearty, 1987; Hearty and Dai Pra, 1992; Torres et al., 2000). The reported U-series ages are those corrected for detrital ^{230}Th using an initial ^{230}Th/^{232}Th activity ratio of 7 ± 50%. Samples MS1-2, MS2-1, and MS6-1 are from De Santis et al. (2021a)

B: D/L and D-allo/L-Ile ratios of all amino acids analysed for each sample reported in Table 1A; these ratios are the basis for calculating the numerical ages (if a conversion algorithm exists) or for aminozone determination; N: number of subsamples prepared for the analysis. C: U-series dating parameters obtained for the samples reported in Table 1A; N: numbers of subsamples prepared for the analysis. The ^{238}U and ^{232}Th concentrations were determined using the enriched ^{236}U and ^{229}Th isotopes, respectively.

$\delta^{234}U_m = \{[(^{234}U/^{238}U)_{sample}/(^{234}U/^{238}U)_{eq}]-1\}x1000$, where $(^{234}U/^{238}U)_{sample}$ is the measured atomic ratio and $(^{234}U/^{238}U)_{eq}$ is the atomic ratio at secular equilibrium

$\delta^{234}U_{(0)}$ is the initial value and is calculated by the equation $\delta^{234}U_{(0)} = \delta^{234}U_m \exp(\lambda_{234}t)$, where t is the age in years. and λ_{234} is the decay constant for ^{234}U

Ages $(ky)_{corr}$ are the ages corrected for detrital ^{230}Th using an initial ^{230}Th/^{232}Th activity ratio of 7 ± 50%

*denotes reanalysed sample solution

Fig. 11 – The formation phases of CLlr and MClr. A: Situation preceding the transgression. B: First highstand of MIS 5.5 (ca. 127 ky BP) and formation of palaeoshoreline PS3; formation of the cll level and overlying beach calcarenites

visible in the G4 section (Fig. 7B); C-D: formation of a barrier immediately after the maximum landward shift of the sea; E: uplift and present situation with palaeoshoreline PS3, as modelled by the first highstand of MIS 5.5, at ca. +15 m.

Fig. 12 – Reconstruction of the reoccupation of the MIS 7.3 palaeoshoreline by the MIS 5.5 palaeoshoreline at Montagna Spaccata (MS1 site, Fig. 6B; see Fig. 2A for the location). A: Pre-MIS 7.3; B: MIS 7.3 highstand; C: creation of an abrasion platform and tidal notch during the MIS 7.3 highstand; *H. durotrix* Gosse coral grew on the platform; D: phase of emersion; E: MIS 5.5 reoccupation by the sea of the MIS 7.3 palaeoshoreline (PS3) and deposition of the PS3marine unit (PS3mu); the underlying fossil specimens of *H. durotrix* Gosse are preserved only within holes in the platform. Compare this figure with Fig. 6.

Table 3 – Sea-level highstands (that is, expected palaeoshoreline elevations) and observed palaeoshorelines for the uplift scenario reconstructed in this work. The expected palaeoshoreline elevations are derived from synchronous correlation using sea-level highstands from Waelbroeck et al. (2002) from present to 410 ky BP and Rohling et al. (2014) from 410 to 590 ky (1^{st} and 2^{nd} columns for sea level and age, respectively) and an uplift rate of 0.09 mm/y from 590 to 130 ky BP (middle Pleistocene, interval MIS 15 - MIS 6) and of 0.07 mm/y from 130 ky BP onwards (late Pleistocene or MIS 5 - onwards). Note that some expected palaeoshoreline elevations are lower than or equal to the next younger expected palaeoshoreline, suggesting that they may well be overprinted or reoccupied; that is, removed by erosion during rising sea level by the subsequent highstand. Thus, none of the observed palaeoshorelines were correlated with overprinted/reoccupied palaeoshorelines, with the exception of PS3. Note also that, given the maximum uncertainty of ± 13 in sea-level curves that were used, we consider an acceptable gap of up to 10 m between an expected palaeoshoreline (3^{rd} column) and the observed palaeoshoreline that we associate with it (4^{th} column).

Figure 13 – Elevations of observed palaeoshorelines (coloured arrows) versus expected emerged palaeoshorelines (horizontal, coloured lines) using the synchronous method for topographic profiles of Figure 3. The scenario of expected palaeoshorelines was obtained using sea-level highstands from Waelbroeck et al. (2002) from present to 410 ky BP and Rohling et al. (2014) from 410 to 590 ky BP, and an uplift rate of 0.09 mm/y from 590 to 130 ky BP (middle Pleistocene or interval MIS 15 - MIS 6) and of 0.07 mm/y from 130 ky BP onwards (late Pleistocene or MIS 5 - onwards). Each horizontal line marked with a certain colour represents an expected palaeoshoreline elevation; the arrow of the same colour represents the corresponding observed palaeoshoreline. Note that some expected palaeoshoreline elevations are lower than or equal to the next younger expected palaeoshoreline, suggesting that they may well be overprinted or

reoccupied (dashed horizontal lines). Thus, none of the observed palaeoshorelines have been correlated with overprinted or reoccupied palaeoshorelines. The only exception is PS3, where reoccupation is well documented. The elevations in m. a.p.s.l. of the horizontal lines and arrows are the same as those in the 3rd and 4th columns in Table 3, respectively. Since both the expected and observed palaeoshorelines are at the same heights for the entire study area, they have been reported for only two topographic profiles.

Figure 14 – A: Graph showing linear regressions between observed and expected palaeoshoreline elevations. Good fits are quantified by R^2 values that are ≥ 0.99. B: Expected palaeoshoreline elevations; the graph also shows the submerged and overprinted palaeoshorelines. Both graphs are valid for all topographic profiles, as the palaeoshorelines observed in several profiles are always at the same elevation (m.a.p.s.l.).

Table 4- Some examples of emerged palaeoshorelines, with the ages to which they have been attributed, reconstructed uplift rates, and relative references.

References

Alfaro, P., Delgado, J., Estévez, A., Molina, J.M., Moretti, M., Soria, J.M., 2002. Liquefaction and fluidization structures in Messinian storm deposits of the Lower Segura Basin (Betic Cordillera, Southern Spain). International Journal of Earth Sciences 91, 505-513.

Ambrosetti, P., Bosi, C., Carraro, F., Ciaranfi, N., Panizza, M., Papani, G., Vezzani, L., Zanferrari, A., 1987. Neotectonic Map of Italy: Scale 1:500,000. Consiglio Nazionale delle Ricerche, Progetto Finalizzato Geodinamica, Sottoprogetto Neotettonica. Litografia Artistica Cartografica, Florence (Italy).

Amorosi, A., Antonioli, F., Bertini, A., Marabini, S., Mastronuzzi, G., Montagna, P.,Negri, A., Rossi, V., Scarponi, D., Taviani, M., Angeletti, L., Piva, A., Vai, G.B., 2014. The Middle-Upper Pleistocene Fronte Section (Taranto, Italy): An exceptionally preserved marine record of the Last Interglacial. Global and Planetary Change 119, 23-38.

Andersen, M.B., Stirling, C.H., Zimmermann, B., Halliday, A.N. 2010. Precise determination of the open ocean 234U/238U composition. Geochemistry, Geophysics, Geosystems 11, Q12003.

Antonioli, F., Ferranti, L., Stocchi, P., Deiana, G., Lo Presti, V., Furlani, S., Marino, C., Orru, P., Scicchitano, G., Trainito, E., 2018. Morphometry and elevation of the last interglacial tidal notches in tectonically stable coasts of the Mediterranean Sea. Earth-Science Reviews 185, 600–623.

Antonioli, F., Lo Presti, V., Rovere, A., Ferranti, L., Anzidei, M., Furlani, S., Mastronuzzi, G., Orru P., Scicchitano, G., Sannino, G., Spampinato, C.R., Pagliarulo, R., Deiana, G., de Sabata, E., Sansò, P., Vacchi, M., Vecchio, A., 2015. Tidal notches in Mediterranean Sea: a comprehensive analysis. Quaternary Science Reviews 119, 66-84.

Armijo, R., Meyer, B., King, G. C. P., Rigo, A., Papanastassiou, D. 1996. Quaternary evolution of the Corinth Rif and its implications for the Late Cenozoic evolution of the Aegean. Geophys. Journal International 126, 11–53.

Ascione, A., Romano, P., 1999. Vertical movements on the eastern margin of the Tyrrhenian extensional basin. New data from Mt. Bulgheria (Southern Apennines, Italy). Tectonophysics 315, 337–356. https://doi.org/10.1016/S0040-1951(99) 00279-6.

Azzaroli, A.,1968. Calcarenite di Gravina. Studi illustrativi della Carta Geologica d'Italia - Servizio Geologico d'Italia, Formazioni Geologiche, Fasc. 1, 183-187.

Belluomini, G., Caldara, M., Casini, C., Cerasoli, M., Manfra, L., Mastronuzzi, G., Palmentola, G., Sansò, P., Tuccimei, P., Vesica, P.L., 2002. The age of Late Pleistocene shorelines and tectonic activity of Taranto area, Southern Italy. Quaternary Science Reviews 21, 525-547.

Benjamin, J., Rovere, A., Fontana, A., Furlani, S., Vacchi, M., Inglis, R.H., Galili E., Antonioli, F., Sivan D., Miko, S., Mourtzas, N., Felja, I., Meredith-Williams, M., Goodman-Tchernov, B., Kolaiti, E., Anzidei, M., Gehrels, R., 2017. Late Quaternary sea-level changes and early human societies in the central and eastern Mediterranean Basin: An interdisciplinary review. Quaternary International 449, 29–57

Bianca, M., Catalano S., De Guidi, G., Gueli, A.M., Monaco, C., Ristuccia, G.M, Stella, G., Tortorici, G., Tortorici, L., Troja, S. O., 2011. Luminescence chronology of Pleistocene marine terraces of Capo Vaticano peninsula (Calabria, southern Italy). Quaternary International 232(1-2), 114-121.

Boenzi, F., Caldara, M., Pennetta, L., 1986. La trasgressione tirreniana nei dintorni di Castellaneta (Taranto). Geologia Applicata ed Idrogeologia 20(1) 1985, 163-175.

Boenzi, F., Caldara, M., Pennetta, L., 2010. L'ambiente fisico e la distribuzione dei vini nella regione pugliese. In: Storia regionale della vite e del vino in Italia: le Puglie. La Daunia, la Terra di Bari, la Terra d'Otranto, in: Calò, A., Bertoldi Le Noci, L (Eds.), Edizioni Pugliesi s.r.l. Martina Franca, pp. 17-31, ISBN 9788883481642.

Bright, J., Kaufman, D.S., 2011. Amino acid racemization in lacustrine ostracodes, part I: effect of oxidizing pre-treatments on amino acid composition. Quaternary Geochronology, 6, 154-173.

Bromley R.G., D'Alessandro A., 1987. Bioerosion of the Plio-Pleistocene transgression of Southern Italy. Riv. It. Paleont. Strat., 93(3), 379-442.

Brückner, H., 1980. Marine Terrassen in Süditalien. Eine quartärmorphologische Studie über das Küstentiefland von Metapont. Düsseldorfer Geographische Schriften, 14, 235 pp., Düsseldorf (PhD thesis).

Caldara, M., D'Alessandro, A., Di Geronimo, I., 1981. Paleocomunità circalitorali del Pleistocene di Gallipoli (Lecce). Bollettino Malacologico 17(7-8), 25-164.

Caldara, M., Iannone, A., Lopez, R., Simone, O., De Santis, V., Torres, T., Ortiz, J.E., 2013. New data on the Pleistocene of Trani (Adriatic coast, southern Italy). Italian Journal of Geosciences 132(2), 239-253.

Caldara, M., Mastronuzzi, G., Palmentola, G., Sansò, P., Tuccimei, P., Vesica, P.L., 2003. Reply to the comment by Hearty, P.J and Dai Pra, G. Quaternary Science Reviews 22(4-6), 2369-2371.

Caputo, R., Bianca, M., D'Onofrio, R., 2010. Ionian marine terraces of southern Italy: Insights into the Quaternary tectonic evolution of the area. Tectonics 29(4), TC4005.

.Cerrone, C., Ascione, A., Robustelli G., Soligo, M., Balassone, G., Tuccimei, P., 2021a. Late Quaternary uplift and sea level fluctuations along the Tyrrhenian margin of Basilicata-northern Calabria (southern Italy): new constraints from raised paleoshorelines. Geomorphology 395, 107978. https://doi.org/10.1016/j.geomorph.2021.107978

Cerrone, C., Vacchi, M., Fontana, A., Rovere, A., 2021b. Last Interglacial sea-level proxies in the Western Mediterranean. Earth System Science Data 13(9), 4485-4527.

Cheng, H., Lawrence Edwards, R., Shen, C.-C., Polyak, V. J., Asmerom, Y., Woodhead, J., Hellstrom, J., Wang, Y., Kong, X., Spötl, C., Wang, X., and Calvin Alexander, E., 2013. Improvements in ^{230}Th dating, ^{230}Th and ^{234}U half-life values, and U–Th isotopic measurements by multi-collector inductively coupled plasma mass spectrometry. Earth and Planetary Science Letters 371-372, 82-91.

Ciaranfi, N., Pieri, P., Ricchetti, G., 1992. Note alla carta geologica delle Murge e del Salento (Puglia centro-meridionale). Memorie della Società Geologica Italiana 41(1988), 449-460.

Cinque, A., Romano, P., 1990. Segnalazioni di nuove evidenze di antiche linee di riva in Penisola Sorrentina (Campania). Geografia Fisica e Dinamica Quaternaria 13,23-26.

Cowie, P.A., Roberts, G.P., 2001. Constraining slip rates and spacings for active normal faults. Journal of Structural Geology 23(12), 1901-1915.

Cowie, P. A., Roberts, G. P., Bull, J. M., Visini, F., 2012. Relationships between fault geometry, slip rate variability and earthquake recurrence in extensional settings. Geophysical Journal International 189(1), 143-160.

De Giosa, F., Scardino, G., Vacchi, M., Piscitelli, A., Milella, M., Ciccolella, A., Mastronuzzi, G., 2019. Geomorphological signature of late Pleistocene sea level oscillations in Torre Guaceto marine protected area (Adriatic Sea, SE Italy). Water 11(11), 2409.

De Santis, V., Caldara, M., 2016. Evolution of an incised valley system in the southern Adriatic Sea (Apulian margin): an onshore–offshore correlation. Geological Journal 51 (2), 263-284.

De Santis, V., Caldara, M., Pennetta, L., 2014a. The marine and alluvial terraces of Tavoliere di Puglia plain (southern Italy). Journal of Maps 10(1), 114-125.

De Santis, V., Caldara, M., Pennetta, L., 2020a. Continuous backstepping of Holocene coastal barrier systems into incised valleys: Insights from the Ofanto and Carapelle-Cervaro valleys. Water 12(6), 1799.

De Santis, V., Caldara, M., Pennetta, L., 2020b. Transgressive architecture of coastal barrier systems in the Ofanto incised valley and its surrounding shelf in response to stepped sea-level rise. Geosciences 10(12), 497.

De Santis, V., Caldara, M., Pennetta, L., Torres, T., Ortiz, J.E., 2013. Unconformity Bounded Stratigraphic Units in an Italian alluvial plain area: recognising and dating. Journal of Sedimentary Research 83, 96-114.

De Santis, V., Caldara, M., Torres, T., Ortiz, J.E., 2010. - Stratigraphic units of the Apulian Tavoliere Plain: chronology, correlation with marine isotope stages and implication regarding vertical movements. Sedimentary Geology 228, 255-270.

De Santis, V., Caldara, M., Torres, T., Ortiz, J.E., 2014b - Two middle Pleistocene warm stages in the Terraced Deposits of the Apulia Region (southern Italy). Quaternary international 332, 2-18.

De Santis, V., Caldara, M., Torres, T., Ortiz, J.E., Sánchez-Palencia, Y., 2018. A review of MIS 7 and MIS 5 terrace deposits along the gulf of Taranto based on new stratigraphic and chronological data. Italian Journal of Geosciences 137, 349-368.

De Santis, V., Caldara, M., Torres T., Ortiz J.E., Sánchez-Palencia Y., 2020c. The role of beach ridges, spits, or barriers in understanding marine terraces processes on loose or semiconsolidated substrates: Insights from the givoni of the Gulf of Taranto (southern Italy). Geological Journal 55(4), 2951-2975.

De Santis, V., Scardino, G., Meschis, M., Ortiz J.E., Sánchez-Palencia Y., Caldara M., 2021a. Refining the middle-late Pleistocene chronology of marine terraces and uplift history in a sector of the Apulian foreland (southern Italy) by applying a synchronous correlation technique and amino acid racemization to Patella spp. and Thetystrombus latus. Italian Journal of Geosciences 140 (3), 438-463

De Santis, V., Scardino, G., Ortiz, J.E., Sánchez-Palencia, Y., Caldara, M., 2021b. Pleistocene terracing phases in the metropolitan area of Bari - AAR dating and deduced uplift rates of the Apulian foreland. Rendiconti online della Società Geologica Italiana 54, 49-61.

De Santis, V., Scardino, G., Scicchitano, G., Montagna, P., Pons-Branchu, E., Ortiz J.E., Sánchez-Palencia Y, Lisco S, Moretti M., Caldara M., 2022. Last interglacial pressure pattern over the Mediterranean from aeolian sediments: A case study from Apulia. Palaeogeography, Palaeoclimatology, Palaeoecology 605, https://doi.org/10.1016/j.palaeo.2022.111228 .

Doglioni, C., Mongelli, F., Pieri, P., 1994. The Puglia uplift (SE Italy): an anomaly in the foreland of the Apenninic subduction due to buckling of a thick continental lithosphere. Tectonics 13(5), 1309-1321.

Doglioni, C., Tropeano, M., Mongelli, F., Pieri, P., 1996. Middle-late Pleistocene uplift of Puglia: an anomaly in the Apenninic foreland. Memorie della Società Geologica Italiana 51, 101-117.

Düsterhus, A., Tamisiea, M. E., Jevrejeva, S., 2016. Estimating the sea level highstand during the Last Interglacial: a probabilistic massive ensemble approach. Geophysical Journal International 206, 900–920.

Dutton, A., Carlson, A.E., Long, A.J., Milne, G.A., Clark, P.U., De Conto, R., Horton, B.P., Rahmstorf, S., Raymo, M.E., 2015a. Sea- level rise due to polar ice- sheet mass loss during past warm periods. Science 349(6244), aaa4019.

Dutton, A., Webster, J. M., Zwartz, D., Lambeck, K., Wohlfarth, B., 2015b. Tropical tales of polar ice: Evidence of last interglacial polar ice sheet retreat recorded by fossil reefs of the granitic Seychelles islands. Quaternary Science Review 107, 182–196.

Dutton A., Lambeck, K., 2012. Ice volume and sea level during the last interglacial. Science 337, 216–219

Evelpidou, N., Vassilopoulos, A., Pirazzoli, P.A., 2012. Holocene emergence in Euboea Island (Greece). Marine Geology 295–298, 14–19

Ferranti, L., Antonioli, F., Mauz, B., Amorosi, A., Dai Pra, G., Mastronuzzi, G., Monaco, C., Orru P., Pappalardo, M., Radtke, U., Renda, P., Romano, P., Sansò, P., Verrubbi, V., 2006. Markers of the last interglacial sea-level high stand along the coast of Italy: tectonic implications. Quaternary International 145-146, 30-54.

Ferranti, L., Burrato, P., Sechi, D., Andreucci, S., Pepe, F., Pascucci, V., 2021. Late Quaternary coastal uplift of southwestern Sicily, central Mediterranean Sea. Quaternary Science Reviews 255, 106812.

Ferranti, L., Oldow, J.S., 2006. Rates of late Neogene deformation along the southwestern margin of Adria, southern Apennines orogen, Italy, in: Pinter, N., Gyula, G., Weber J., Stein S., Medak D. (Eds.), The Adria Microplate: GPS Geodesy, Tectonics and Hazards. Nato Science Series: IV: Earth and Environmental Sciences 61. Springer, Dordrecht.

Gallen, S.F., Wegmann, KW, Bohnenstiehl, D.R., Pazzaglia, F.J., Brandon, M.T, Fassoulas, C., 2014. Active simultaneous uplift and margin-normal extension in a forearc high, Crete, Greece. Earth and Planetary Science Letters 398, 11-24.

Gignoux, M., 1913. Les formations marines: Pliocènes et Quaternaires de l'Italie du sud et de la Sicile. A. Rey; J.-B. Baillière, Lyon; Paris

Grant, K.M., Rohling, E.J., Bar-Matthews, M., Ayalon, A., Medina-Elizalde, M., Ramsey, C.B., Satow, C., Roberts, A.P., 2012. Rapid coupling between ice volume and polar temperature over the past 150,000 years. Nature. 2012 Nov 29; 491(7426).

Grant, K.M., Rohling, E.J, Ramsey, C.B., Cheng, H., Edwards, R.L., Florindo, F., Heslop, D., Marra F., Roberts, A.P., Tamisiea, M.E., Williams, F., 2014. Sea-level variability over five glacial cycles. Nature Communications 5, 5076.

Hearty, P.J., 1987. New data on the Pleistocene of Mallorca. Quaternary Science Reviews 6, 245-257.

Hearty, P.J., Dai Pra, G., 1987. Paleogeographic reconstruction of Quaternary environments in Toscana and north Lazio, central Italy. Bollettino del Servizio Geologico d'Italia 106, 189-224.

Hearty P.J., Dai Pra G., 1992. The age and stratigraphy of Middle Pleistocene and younger deposits along the Gulf of Taranto (Southeast Italy). Journal of Coastal Research 8(4), 82-105.

Hearty P.J., Hollin, J.T., Dumas, B., 1987. Geochronology of Pleistocene littoral deposits on the AIicante and Almeria coasts of Spain, in: Zazo, C. (Eds.), Late Quaternary Sea Level Changes in Spain. Trab. Neogeno-Cuaternario 10, 95-105.

Hearty, P.J., Hollin, J.T., Neumann, A.C., O'Leary, M.J., Mcculloch, M., 2007. Global sea-level fluctuations during the Last Interglaciation (MIS 5e). Quaternary Science Reviews 26, 2090-2112.

Hearty, P.J., Miller, G., Stearns, C., Szabo, B.J., 1986. Aminostratigraphy of Quaternary shorelines in the Mediterranean basin. Geological Society of America Bulletin 97, 850-858.

Henkel, D.J., 1970. The Role of Waves in Causing Submarine Landslides. Géotechnique 20(1), 75-80.

Iannone, A., Pieri, P., 1979. Considerazioni critiche sui tufi calcarei delle Murge. Nuovi dati litostratigrafici e paleoambientali. Geografia Fisica e Dinamica Quaternaria 2, 173-186.

Jaffey, A.H., Flynn, K.F., Glendenin, L.E., Bentley, W.C., Essling, A.M., 1971. Precision measurement of half-lives and specific activities of ^{235}U and ^{238}U. Physical Review C 4 (5), 1889–1906.

Kaufman, D.S., 2000. Amino acid racemization in ostracodes, in: Goodfriend, G., Collins, M., Fogel, M., Macko, S., Wehmiller, J., (Eds.), Perspectives in Amino Acid and Protein Geochemistry: New York, Oxford University Press, 145–160.

Kaufman, D.S., 2006. Temperature sensitivity of aspartic and glutamic acid racemization in the foraminifera Pulleniatina. Quaternary Geochronology 1, 188–207.

Kaufman, D.S., Manley, W.F., 1998. A new procedure for determining DL amino acid ratios in fossils using reverse phase liquid chromatography. Quaternary Science Reviews, 17, 987-1000.

Kershaw, S., 2000. Quaternary reefs of northeastern Sicily: structure and growth controls in an unstable tectonic setting. Journal of Coastal Research, 1037-1062.

Kopp, R.E., Simons, F.J., Mitrovica, J.X., Maloof, A.C., Oppenheimer, M., 2009. Probabilistic assessment of sea level during the last interglacial stage. Nature 462, 863–867.

Kopp, R.E., Simons, F.J., Mitrovica, J.X., Maloof, A.C., Oppenheimer M., 2013. A probabilistic assessment of sea level variations within the last interglacial stage. Geophysical Journal International 193, 711–716.

Lajoie, K.R., 1986. Coastal tectonics. Active tectonics, pp.95-124.

Largaiolli, T., Martinis, B., Mozzi, G., Nardin, M., Rossi, D., Ungaro, S., 1969. Note illustrative del della Carta Geologica d'Italia alla scala 1:100.000, F. 214 "Gallipoli". Servizio Geologico d'Italia, Roma.

Lorscheid, T., Stocchi, P., Casella, E., Gómez-Pujol, L., Vacchi, M., Mann, T., Rovere, A., 2017. Paleo sea-level changes and relative sea-level indicators: Precise measurements, indicative meaning and glacial isostatic adjustment perspectives from Mallorca (Western Mediterranean). Palaeogeography, Palaeoclimatology, Palaeoecology 473, 94–107.

Ludwig, K.R., Titterington, D.M., 1994. Calculation of ^{230}Th/U Isochrons, Ages, and Errors. Geochimica et Cosmochimica Acta 58, 5031-5042.

Marra, F., Florindo, F., Anzidei, M., Sepe, V., 2016. Paleo-surfaces of glacio-eustatically forced aggradational successions in the coastal area of Rome: assessing interplay between tectonics and sea-level during the last ten interglacials. Quaternary Science Review 148, 85-100.

Marra, F., Bahain, J.J., Jicha, B.R., Nomade, S., Palladino, D.M., Pereira, A., Tolomei, C., Pierre Voinchet, P., Anzidei, M., Aureli, D., Ceruleo, P., Falgueres, C., Florindo, F., Gatta, M., Ghaleb, B., La Rosa, M., Peretto, C., Petronio, C., Rocca, R., Rolfo, M.F., Salari, L., Smedile, A., Tombret, O., 2019. Reconstruction of the MIS 5.5, 5.3 and 5.1 coastal terraces in Latium (central Italy): A re-evaluation of the sea-level history in the Mediterranean Sea during the last interglacial. Quaternary International 525, 54-77.

Marra, F., Rolfo, F.M., Gaeta, M., Florindo, F., 2020. Anomalous Last Interglacial Tyrrhenian sea levels and Neanderthal settling at Guattari and Moscerini caves (central Italy). Scientific Reports 10:11929.

Meschis, M., Roberts, G. P., Robertson, J., Briant, R. M., 2018. The relationships between regional Quaternary uplift, deformation across active normal faults, and historical seismicity in the upper plate of subduction zones: the Capo D'Orlando fault. NE Sicily. Tectonics 37(5), 1231-1255.

Meschis, M., Scicchitano, G., Roberts, GP., Robertson, J., Barreca, G., Monaco, C., Spampinato, C., Sahy D., Antonioli F., Mildon Z.K., Scardino, G., 2020 Regional deformation and offshore crustal local faulting as combined processes to explain uplift through time constrained by investigating differentially uplifted late quaternary paleoshorelines: the Foreland Hyblean Plateau, SE Sicily. Tectonics 39, e2020TC006187.

Meschis, M., Roberts, G.P., Robertson, J., Mildon, Z.K., Sahy, D., Goswami, R., Sgambato, C., Faure Walker, J., Michetti, A.M., Iezzi, F., 2022. Out of phase Quaternary uplift-rate changes reveal normal fault interaction, implied by deformed marine palaeoshorelines. Geomorphology 108432, https://doi.org/10.1016/j.geomorph.2022.108432Molina, J. M., Alfaro, P., Moretti, M., Soria J. M., 1998. Soft-sediment deformation structures induced by cyclic stress of storm-waves in tempestites (Miocene, Guadalquivir Basin, Spain). Terra Nova 10(3), 145-150.

Murray-Wallace, C.V., Woodroffe, C.D., 2014. Quaternary Sea-Level Changes: A Global Perspective. Cambridge University Press.

Negri, A., Amorosi, A., Antonioli, F., Bertini, A., Florindo, F., Lurcock, P.C., Marabini, S., Mastronuzzi, G., Regattieri, E., Rossi V., Scarponi, D., Taviani, M., Zanchetta, G., Vai, G.B., 2015. A potential global boundary stratotype section and point (GSSP) for the Tarentian Stage, Upper Pleistocene, from the Taranto area (Italy): Results and future perspectives. Quaternary International 383, 145-157.

O'Leary, M., Hearty, P., Thompson, W., Raymo M.E, Mitrovica, J.X., Webster, J.M., 2013. Ice sheet collapse following a prolonged period of stable sea level during the last interglacial. Nature Geosciences 6, 796-800.

Ortiz, J.E., Gutiérrez-Zugasti, I., Torres, T., González-Morales, M., Sánchez-Palencia, Y., 2015. Protein diagenesis in Patella shells: implications for amino acid racemisation dating. Quaternary Geochronology 27, 105-118.

Ortiz, J.E., Torres, T., Pérez-González, A., 2013. Amino acid racemization in four species of ostracodes: taxonomic, environmental, and microstructural controls. Quaternary Geochronology 16, 129-143.

Ortiz, J.E., Torres, T., Julià, R., Delgado, A., Llamas, F.J., Soler, V., Delgado, J., 2004. Numerical dating algorithms of amino acid racemization ratios from continental ostracodes. Application to Guadix-Baza basin (southern Spain). Quaternary Science Reviews 23(5-6), 717-730.

Otvos, E.G., 2021. Coastal barriers-nomenclature, processes, and classification issues. Geomorphology 139–140, 39–52.

Pedoja, K., Jara-Muñoz, J., De Gelder, G., Robertson, J., Meschis, M., Fernandez-Blanco, D., Nexer, M., Poprawski, Y., Dugué, O., Delcaillau, B., Bessin, P., Benabdelouahed, M., Authemayou, C., Husson, L., Regard, V., Menier, D., Pinel, B., 2018. Neogene-Quaternary slow coastal uplift of western Europe through the perspective of sequences of strandlines from the Cotentin Peninsula (Normandy, France). Geomorphology 303, 338-356.

Pérès, J.M., 1967. The Mediterranean benthos. Oceanography Marine Biology Annual Review 5, 449–533.

Picton, B.E., Morrow, C.C., 2016. Hoplangia durotrix Gosse, 1860. In: Encyclopedia of Marine Life of Britain and Ireland. http://www.habitas.org.uk/marinelife/species.asp?item=D13860 Accessed on 2022-05-20.

Pons-Branchu E., Douville E., Roy-Barman M., Dumont E., Branchu P., Thil F., Frank N., Bordier L., Borst W., 2014. A geochemical perspective on Parisian urban history based on U-Th dating, laminae counting and yttrium and REE concentrations of recent carbonates in underground aqueducts. Quaternary Geochronology 24, 43-54.

Powell, J., Collins, M.J., Cussens, J., McLeod, N., Penkman, K.E.H., 2013. Results from an amino acid racemization inter-laboratory proficiency study; design and performance evaluation. Quaternary Geochronology 16, 183-197.

Progetto PST - Dati Lidar [WWW Document], 2021. Geoportale Nazionale. URL http://www.pcn.minambiente.it/mattm/progetto-pst-dati-lidar/

Ricchetti, G., Ciaranfi N., 2013. Note Illustrative della Carta Geologica d'Italia alla scala 1:50.000, F. 536 Ugento. 120 pp., LAC, Firenze.

Ricchetti, G., Ciaranfi, N., Luperto Sinni, E., Mongelli, F., Pieri, P., 1992. Geodinamica ed evoluzione sedimentaria e tettonica dell'avampaese apulo. Memorie Società Geologica Italiana, 41(1988), 57-82.

Roberts, G. P., Houghton, S. L., Underwood, C., Papanikolaou, I., Cowie, P. A., Van Calsteren, P., Wigley, T., Cooper, F.J., McArthur, J.M., 2009. Localization of quaternary slip rates in an active rift in 105 years: An example from central Greece constrained by ^{234}U- ^{230}Th coral dates from uplifted paleoshorelines. Journal of Geophysical Research 114, B10406.

Roberts, G. P., Meschis, M., Houghton, S., Underwood, C., Briant, R. M., 2013. The implications of revised Quaternary palaeoshoreline chronologies for the rates of active extension and uplift in the upper plate of subduction zones. Quaternary Science Reviews 78, 169-187.

Robertson, J., Meschis, M., Roberts, G. P., Ganas, A., Gheorghiu, D.M., 2019. Temporally constant quaternary uplift rates and their relationship with extensional upper- plate faults in south Crete (Greece), constrained with ^{36}Cl cosmogenic exposure dating. Tectonics 38(4), 1189-1222.

Robertson, J., Roberts, G. P., Iezzi, F., Meschis, M., Gheorghiu, D. M., Sahy, D., Bristow, C.,Sgambato, C., 2020. Distributed normal faulting in the tip zone of the South Alkyonides Fault System, Gulf of Corinth, constrained using 36Cl exposure dating of late-Quaternary wave-cut platforms 36: 104063.

Rohling, E., Grant, K., Hemleben, C., Siddal, M., Hoogakker, B.A.A., Bolshaw, M., Kucera M., 2008. High rates of sea-level rise during the last interglacial period. Nature Geosciences, 1, 38–42.

Rohling, E.J., Foster, G.L., Grant, K.M., Marino, G., Roberts, A.P., Tamisiea, M.E., Williams, F., 2014. Sea- level and deep- sea- temperature variability over the past 5.3 million years. Nature 508(7497), 477-482.

Rohling, E.J., Hibbert, F.D., Gran,t K.M., Galaasen, E.V., Irval, N., Kleiven, H.F., Marino G., Ninnemann, U., Roberts, A.P., Rosenthal, Y., Schulz, H., Williams, F.H., Yu, J., 2019. Asynchronous Antarctic and Greenland ice- volume contributions to the last interglacial sea-level highstand. Nature Communications 10(1), 5040.

Rovere, A., Antonioli, F., Bianchi, C. N., Shennan, I., Long, A. J., & Horton, B. P., 2015. Fixed biological indicators. Handbook of sea-level research, 268-280.

Rovere, A., Raymo, M.E., Vacchi, M., Lorscheid, T., Stocchi, P., Gómez-Pujol, L., Harris, D.L., Casella, E., O'Leary, M.J., Hearty, P.J., 2016. The analysis of Last Interglacial (MIS 5e) relative sea-level indicators: Reconstructing sea-level in a warmer world. Earth-Science Reviews 159, 404–427.

Roy, P. S., Cowell, P. J., Ferland, M. A., Thom, B. G., 1994. Wave dominated coast, in: Carter, R.W.G., Woodroffe, C.D. (Eds.), Coastal evolution, Late Quaternary shoreline morphodynamics, Cambridge University Press, Cambridge, pp. 121–186.

Scicchitano, G., C. R. Spampinato, L. Ferranti, F. Antonioli, C. Monaco, M. Capano, and C. Lubritto. "Uplifted Holocene shorelines at Capo Milazzo (NE Sicily, Italy): evidence of co-seismic and steady-state deformation." Quaternary International 232(1-2), 201-213.

M. Siddall, J. Chappell, E.-K. Potter. 2007. Eustatic sea level during past interglacials, in: Frank Sirocko, Martin Claussen, María Fernanda Sánchez Goñi, Thomas Litt. (Eds.), Developments in Quaternary Sciences (7), Elsevier, pp.75-92.

Stirling, C.H., Esat, T.M., Lambeck, K., McCulloch, M.T., 1998. Timing and duration of the Last Interglacial: Evidence for a restricted interval of widespread coral reef growth. Earth Planetary Science Letters 160, 745–762.

Stiros, S.C., Arnold, M., Pirazzoli, P.A., Laborel, J., Laborel, F., Papageorgiou, S., 1992. Historical coseismic uplift on Euboea Island, Greece. Earth and Planetary Science Letters, 108, 109-117.

Stocchi, P., Vacchi, M., Lorscheid, T., de Boer, B., Simms, A. R., van de Wal, R.S.W., Vermeersen, B.L.A., Pappalardo, M., Rovere, A., 2018. MIS 5e relative sea-level changes in the Mediterranean Sea: Contribution of isostatic disequilibrium. Quaternary Science Reviews, 185, 122-134.

Taviani, M., 2014. Unpersisting Persististrombus: a Mediterranean story. Vieraea 42, 9–18.

Thompson, W.G., Curran, H.A., Wilson, M.A., White, B. 2011. Sea-level and ice-sheet instability during the Last Interglacial: New Bahamas evidence. Nature Geosciences 4, 684.

Thompson, W.G., Spiegelman, M.W., Goldstein, S.L., Speed, R.C., 2003. An open-system model for U-series age determinations of fossil corals. Earth and Planetary Science Letters, 210, 365-381.

Torres, T., Llamas, J.F., Canoira, L., Coello, J., García-Alonso, P., Ortiz J.E., 2000. Aminostratigraphy of two marine sequences from the Mediterranean coast of Spain. Cabo de Huertas (Alicante) and Garrucha (Almería), in: Goodfriend, G.A., Collins, M.J., Fogel, M.L., Macko S.A., Wemiller J.F. (Eds.), Perspectives in Amino Acid and Protein Geochemistry. Oxford University Press, New York, pp. 263-278.

Torres T., Llamas J., Canoira L., García-Alonso P., García-Cortés A., Mansilla H., 1997. Amino acid chronology of the Lower Pleistocene deposits of Venta Micena (Orce, Granada, Andalusia, Spain). Organic Geochemistry 26, 85-97.

Torres, T., Ortiz, J.E., Arribas, I., 2013. Variations in racemization/epimerization ratios and amino acid content of Glycymeris shells in raised marine deposits in the Mediterranean. Quaternary Geochronology 16, 35-49.

Vacchi, M., Marriner, N., Morhange, C., Spada, G., Fontana, A., Rovere, A., 2016. Multiproxy assessment of Holocene relative sea-level changes in the western Mediterranean: Sea-level variability and improvements in the definition of the isostatic signal. Earth Science Reviews 155, 172–197.

Valenzano, E., Scardino, G., Cipriano, G., Fago, P., Capolongo, D., De Giosa, F., Lisco, S., Mele, D., Moretti, M., Mastronuzzi, G., 2018. Holocene morpho-sedimentary evolution of the Mar Piccolo basin (Taranto, Southern Italy). Geografia Fisica e Dinamica Quaternaria 41, 119-135

Waelbroeck, C., Labeyrie, L., Michel, E., Duplessy, J.C., McManus, J.F., Lambeck, K., Balbon, E., Labracherie, M., 2002. Sea-level and deep water temperature changes derived from benthic foraminifera isotopic records. Quaternary Science Reviews 21, 295-305.

Wehmiller, J. F., 1984. Interlaboratory comparison of amino acid enantiomeric ratios in fossil mollusks. Quaternary Research 22, 109-120.

Wehmiller, J.F., Miller, G., De Vogel, S., Kaufman, D.S., Brigth, J., Murray-Wallace, C.V., Ortiz, J.E., Penkman, K., 2010. Interlaboratory comparison of amino acid D/L values. Geological Society of America Annual Meeting, Denver, Abstracts with Programs 42(5), 86.

Westaway, R., 1993. Quaternary uplift of southern Italy. Journal of Geophysical Research: Solid Earth 98(B12), 21741-21772.

Whitacre, K.E., Kaufman, D.S., Kosnik, M.A., Hearty, P.J., 2017. Converting A/I values (ion exchange) to D/L values (reverse phase) for amino acid geochronology. Quaternary Geochronology 37, 1-6.

Zander, A., Fülling, A., Brückner, H., Mastronuzzi, G., 2006. OSL dating of Upper Pleistocene littoral sediments: a contribution to the chronostratigraphy of raised marine terraces bordering the Gulf of Taranto, South Italy. Geografia Fisica e Dinamica Quaternaria 29(1), 33-50.

Zazo, C., Goy, J.L., Dabrio, C.J., Bardajì, T., Hillaire-Marcel, C., Ghaleb, B., Gonza¤lez-Delgado, J.A., Soler, V., 2003. Pleistocene raised marine terraces of the Spanish Mediterranean and Atlantic coasts: records of coastal uplift, sea-level highstands and climate changes. Marine Geology 194, 103–133.

Fig. 1

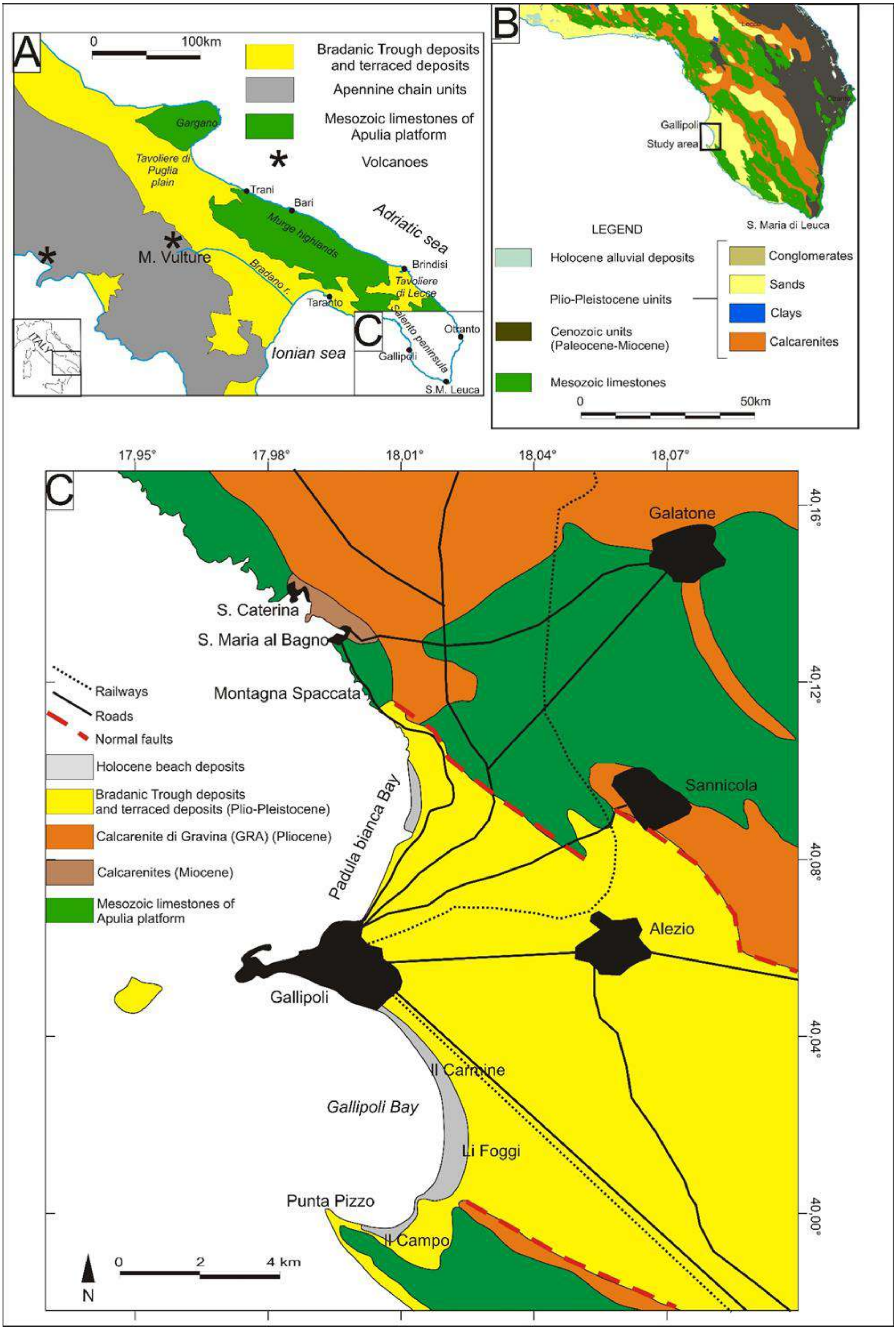
A
0
100km
Bradanic Trough deposits and terraced deposits
Apennine chain units
Mesozoic limestones of Apulia platform
Volcanoes
Gargano
Tavoliere di Puglia plain
Trani
Bari
Murge highlands
Adriatic sea
M. Vulture
Bradano r.
Brindisi
Tavoliere di Lecce
Taranto
Salento peninsula
Otranto
ITALY
Ionian sea
C
Gallipoli
S.M. Leuca
B
Gallipoli
Study area
S. Maria di Leuca
LEGEND
Holocene alluvial deposits
Plio-Pleistocene uinits
Conglomerates
Sands
Clays
Calcarenites
Cenozoic units (Paleocene-Miocene)
Mesozoic limestones
0
50km
17,95°
17,98°
18,01°
18,04°
18,07°
C
40,16°
40,12°
40,08°
40,04°
40,00°
Galatone
S. Caterina
S. Maria al Bagno
Montagna Spaccata
Railways
Roads
Normal faults
Holocene beach deposits
Bradanic Trough deposits and terraced deposits (Plio-Pleistocene)
Calcarenite di Gravina (GRA) (Pliocene)
Calcarenites (Miocene)
Mesozoic limestones of Apulia platform
Padula bianca Bay
Sannicola
Alezio
Gallipoli
Il Carmine
Gallipoli Bay
Li Foggi
Punta Pizzo
Il Campo
0
2
4 km
N

Fig. 2

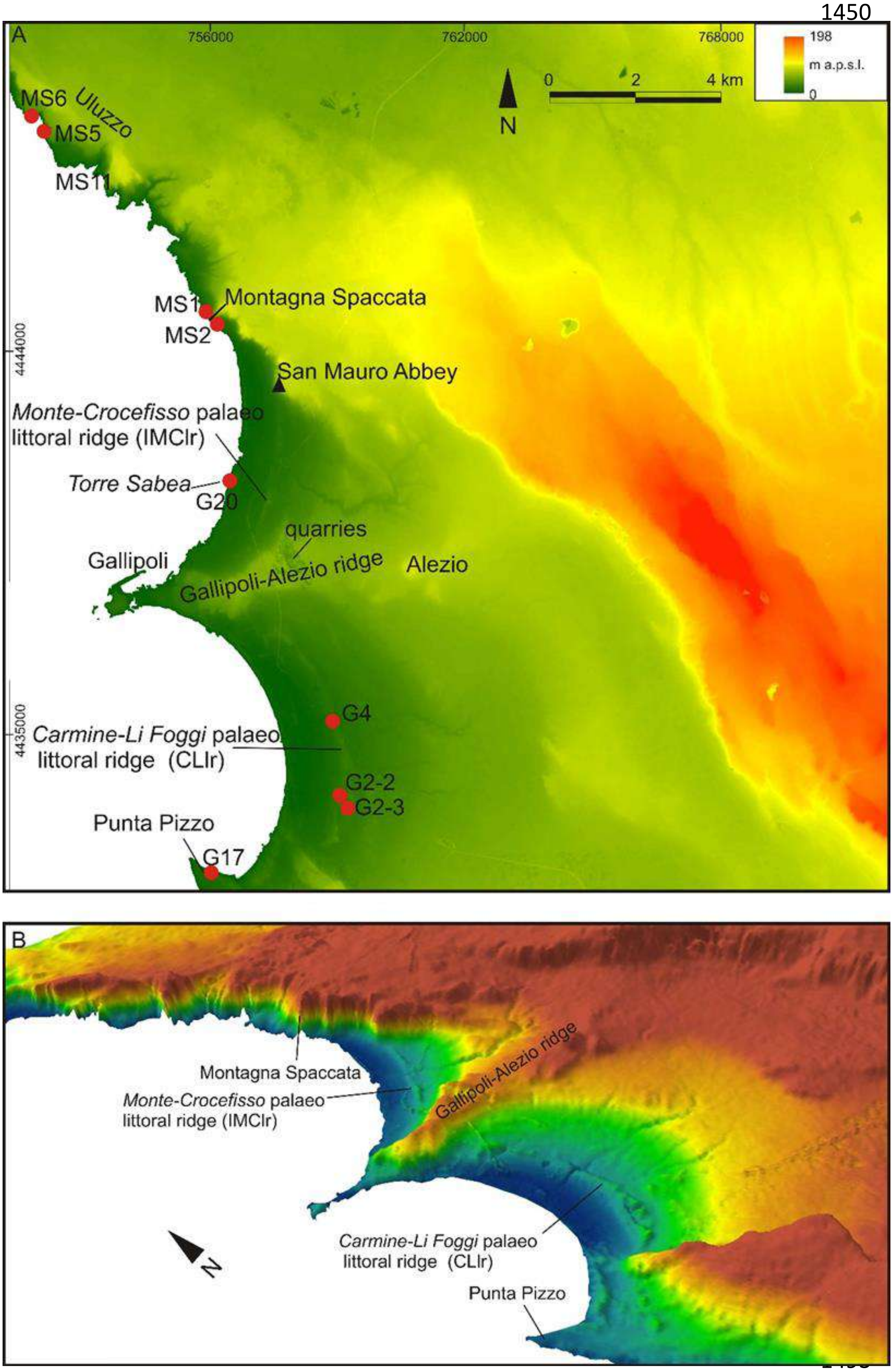
A
756000
762000
768000
198
m a.p.s.l.
0
0
2
4 km
N
MS6
Uluzzo
MS5
MS11
MS1
Montagna Spaccata
MS2
4444000
San Mauro Abbey
Monte-Crocefisso palaeo
littoral ridge (IMClr)
Torre Sabea
G20
quarries
Gallipoli
Gallipoli-Alezio ridge
Alezio
4435000
G4
Carmine-Li Foggi palaeo
littoral ridge (CLlr)
G2-2
G2-3
Punta Pizzo
G17
B
Montagna Spaccata
Monte-Crocefisso palaeo
littoral ridge (IMClr)
Gallipoli-Alezio ridge
N
Carmine-Li Foggi palaeo
littoral ridge (CLlr)
Punta Pizzo

Tab. 1

PALAEOSHORELINE	ASSOCIATED DEPOSITS	UNITS OF MIXED DEPOSITS (if has been possible to define them)	LANDFORMS IN THE SECTOR FROM BROKEN MOUNTAIN NORTHWARDS	LANDFORMS IN THE SECTOR SOUTH OF BROKEN MOUNTAIN
PS1 (+6 m)	PS1 marine unit (PS1mu)		Band of lithophagid borings	Band of lithophagid borings
PS2 (+7 m)	PS2 marine unit (PS2mu)		Band of lithophagid borings	Band of lithophagid borings
PS3 (+15 m)	PS3 Mixed Deposit (PS3-MD)	PS3 marine unit (PS3mu), Aeolian Unit 1 (AU1), Aeolian Unit 2 (AU2)	Band of lithophagid borings, tidal notches, wave-cut platform	*Monte-Crocefisso* palaeo littoral ridge (IMClr); *Carmine-Li Foggi* palaeo littoral ridge
PS4 (+22 m)	PS4 Mixed Deposit (PS4-MD)		Band of lithophagid borings, sea caves; patches of marine syn-wave cut platform deposits	Small and discontinuous relict littoral ridges with aeolian deposits
PS5 (+41 m)	PS5 Marine Deposit (PS5-MaD)		Band of lithophagid borings,	Band of lithophagid borings (near San Mauro abbey); marine terraced deposit less than 1 km^2 wide
PS6 (+62 m), PS7 (+67 m)			Band of lithophagid borings	Morphological inner edges

Fig. 3

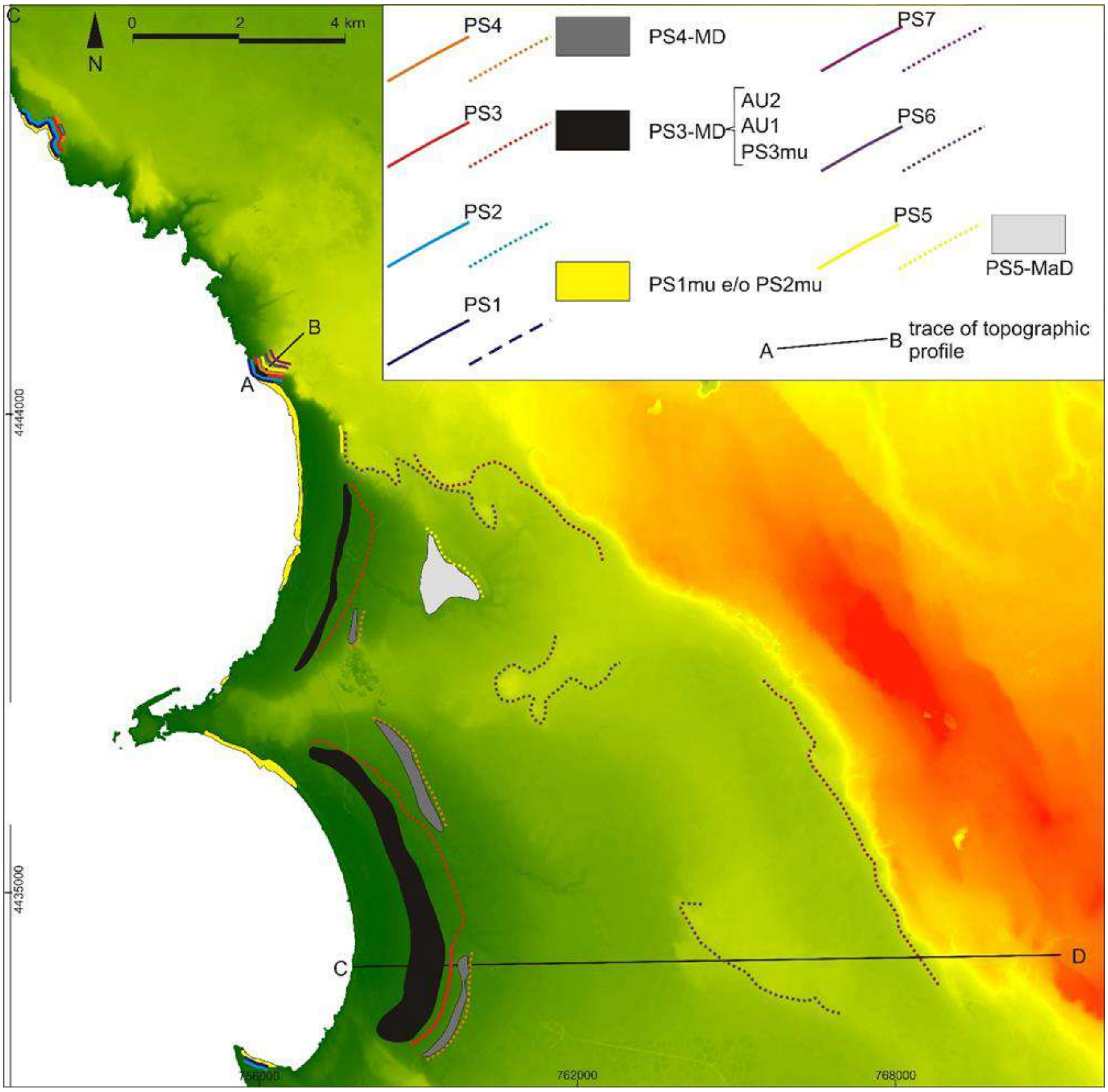

N
0
2
4 km
PS4
PS4-MD
PS7
PS3
PS3-MD
AU2
AU1
PS3mu
PS6
PS2
PS5
PS1mu e/o PS2mu
PS5-MaD
PS1
A
B
trace of topographic profile
C
D
4444000
4435000
756000
762000
768000

Fig. 4

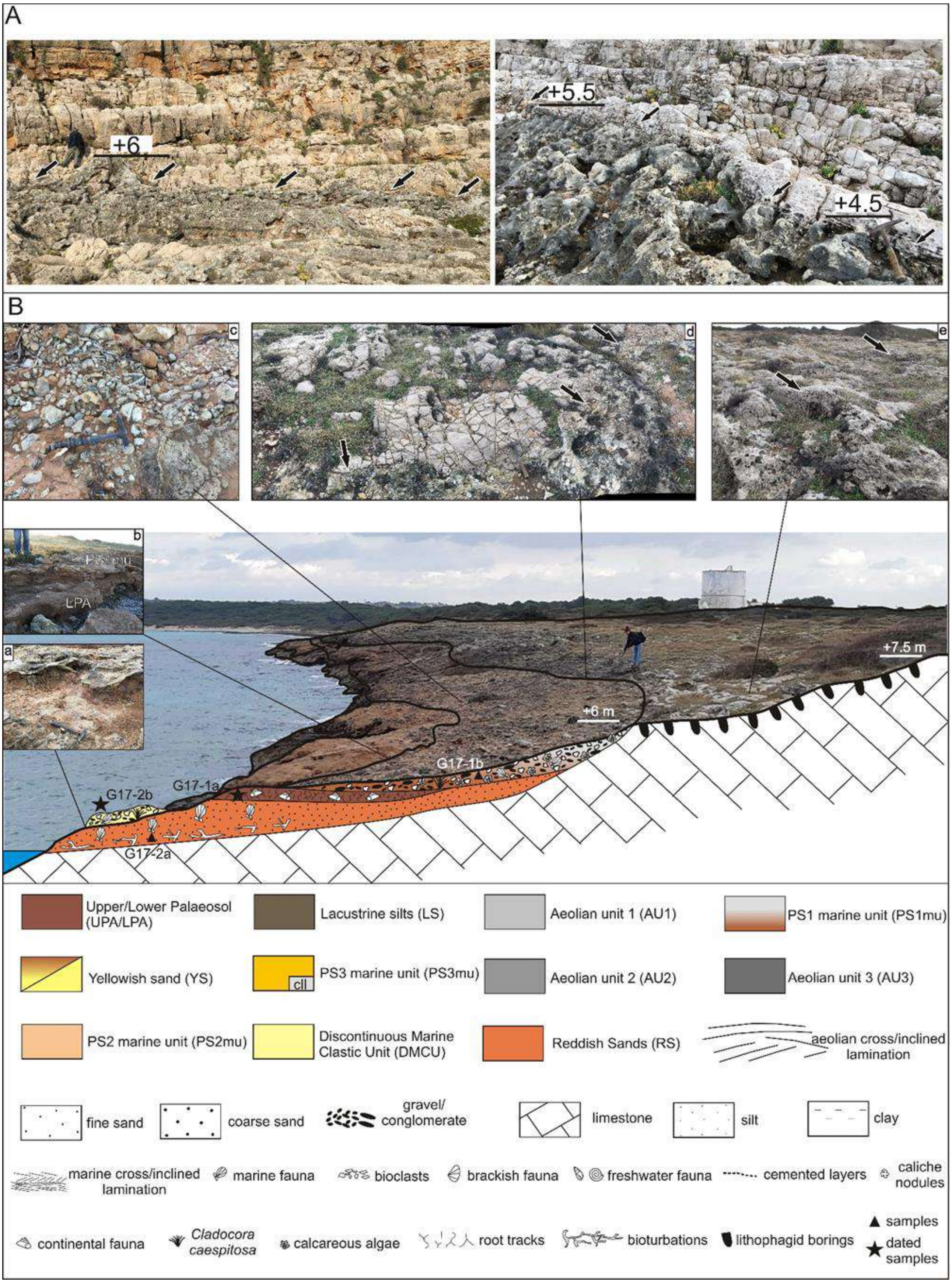

A
+6
+5.5
+4.5
B
c
d
e
b
PS1mu
LPA
a
+7.5 m
+6 m
G17-1b
G17-1a
G17-2b
G17-2a
Upper/Lower Palaeosol (UPA/LPA)
Lacustrine silts (LS)
Aeolian unit 1 (AU1)
PS1 marine unit (PS1mu)
Yellowish sand (YS)
PS3 marine unit (PS3mu)
cll
Aeolian unit 2 (AU2)
Aeolian unit 3 (AU3)
PS2 marine unit (PS2mu)
Discontinuous Marine Clastic Unit (DMCU)
Reddish Sands (RS)
aeolian cross/inclined lamination
fine sand
coarse sand
gravel/ conglomerate
limestone
silt
clay
marine cross/inclined lamination
marine fauna
bioclasts
brackish fauna
freshwater fauna
cemented layers
caliche nodules
continental fauna
Cladocora caespitosa
calcareous algae
root tracks
bioturbations
lithophagid borings
samples
dated samples

Fig. 5

Fig. 6

Fig. 7

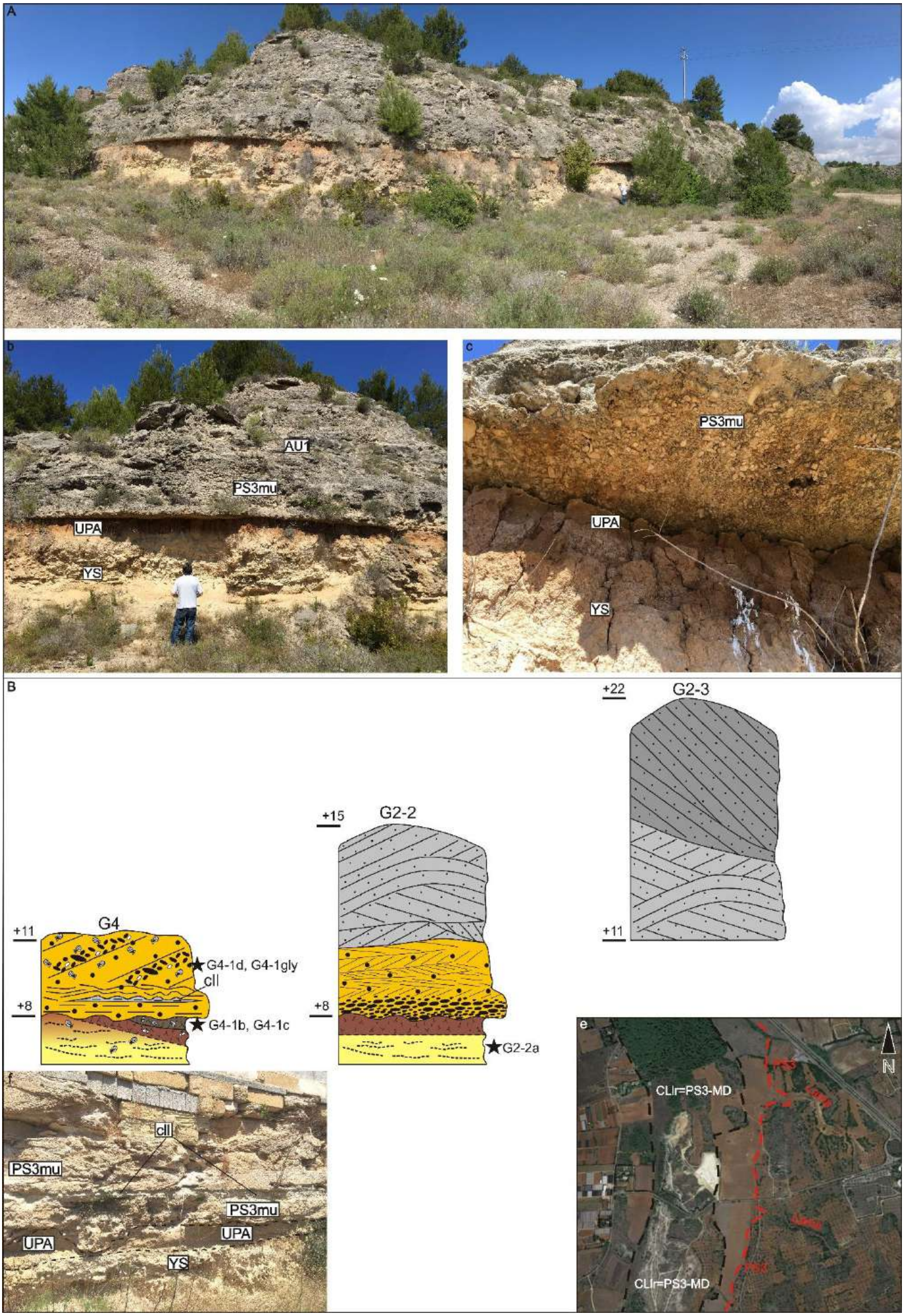
A
b
AU1
PS3mu
UPA
YS
c
PS3mu
UPA
YS
B
+22
G2-3
+11
+15
G2-2
+8
G2-2a
+11
G4
G4-1d, G4-1gly
cII
+8
G4-1b, G4-1c
f
cII
PS3mu
PS3mu
UPA
UPA
YS
e
N
CLIr=PS3-MD
CLIr=PS3-MD

Fig. 8

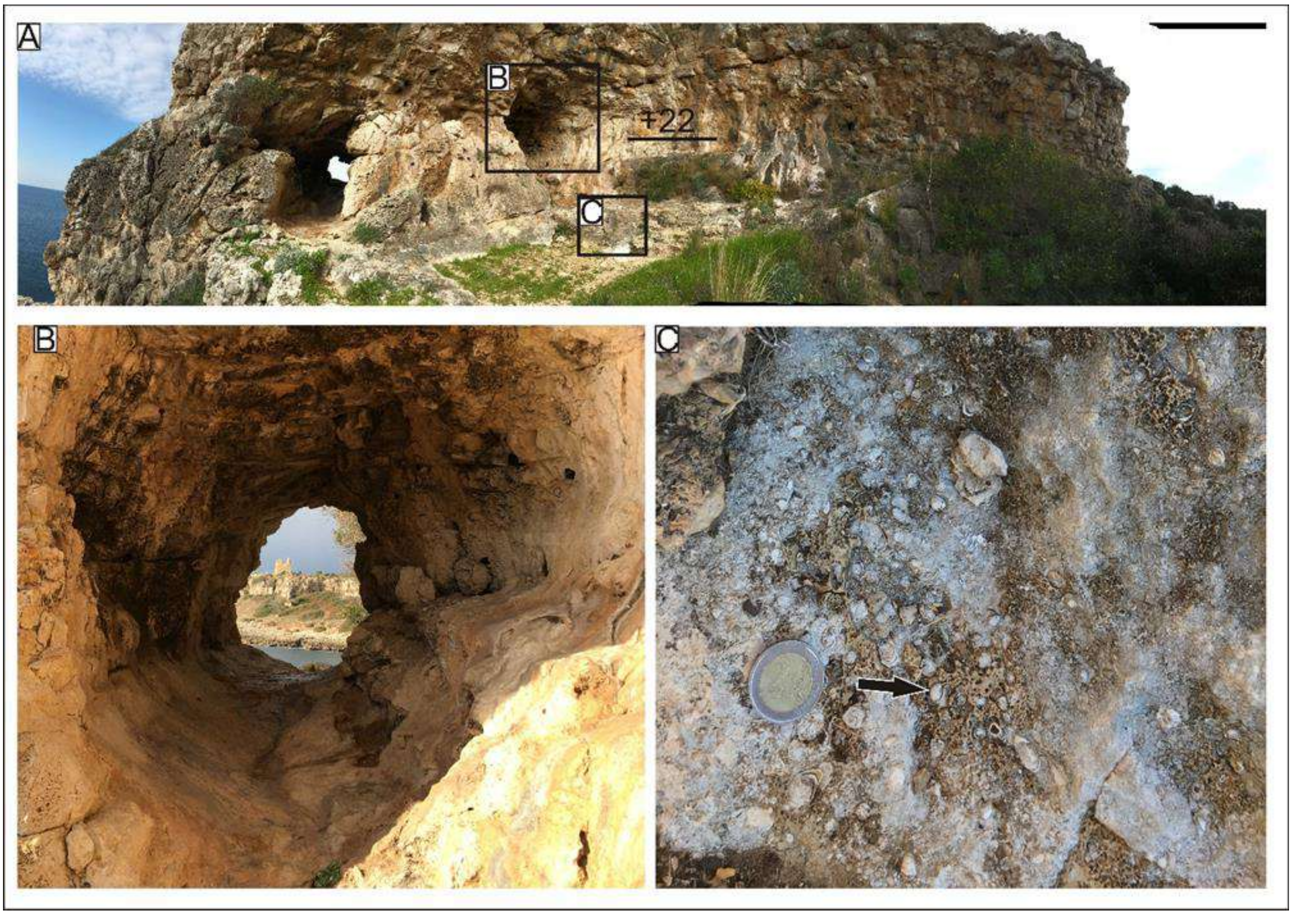

Fig. 9

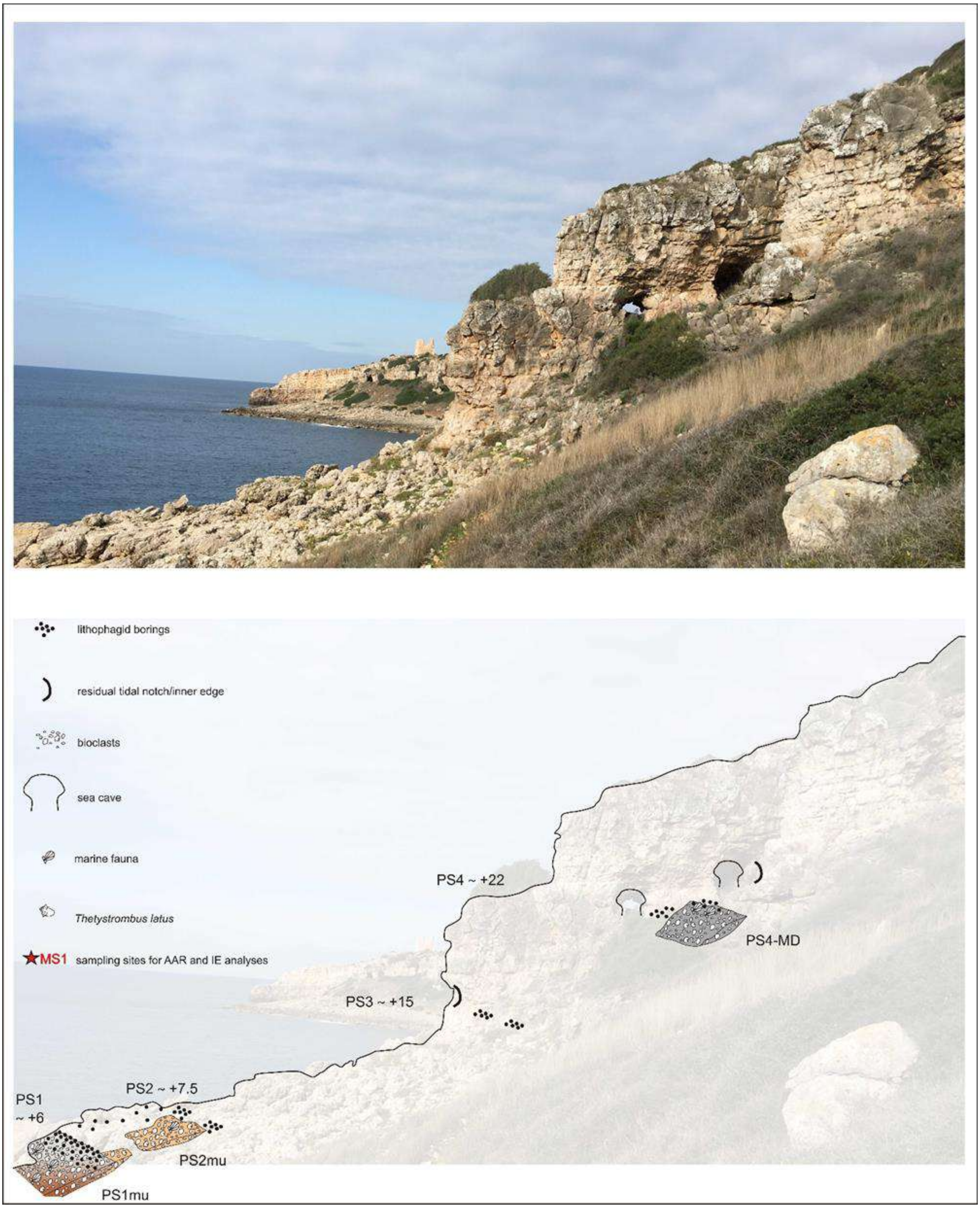
lithophagid borings
residual tidal notch/inner edge
bioclasts
sea cave
marine fauna
Thetystrombus latus
MS1 sampling sites for AAR and IE analyses
PS4 ~ +22
PS4-MD
PS3 ~ +15
PS2 ~ +7.5
PS1
~ +6
PS2mu
PS1mu

Fig. 10

Fig. 11

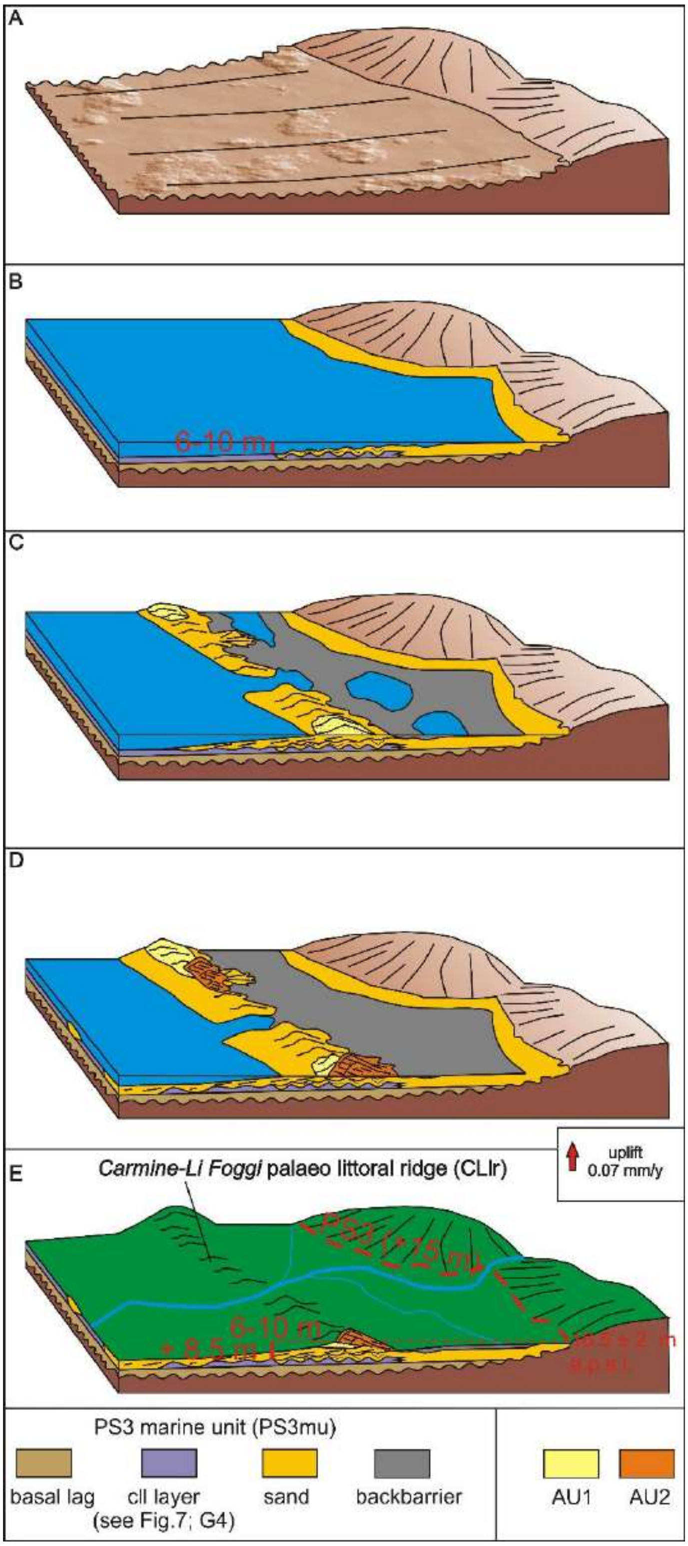
A
B
6-10 m
C
D
E
Carmine-Li Foggi palaeo littoral ridge (CLlr)
uplift
0.07 mm/y
6-10 m
PS3 marine unit (PS3mu)
basal lag
cll layer
(see Fig.7; G4)
sand
backbarrier
AU1
AU2

Tab. 2

TAB. 2A

	Sample ID/site	Unit	Palaeoshore line	Material for chronological analyses	Type of analysis	Age/Aminozone	Stage
South of Montagna Spaccata	G2-2a	YS		ostracod	AAR	137.2±29.3 ky BP	MIS 6-5.5
	G4-1c	LS		ostracod	AAR	138.4±17.9 ky BP	MIS 6-5.5
	G4-1b	LS		ostracod	AAR	118.1±17.9 ky BP	
	G4-1d	PS3mu	+15 m (PS3)	*Glycymeris* spp.	IE	E	MIS 5.5
	G4-1gly	PS3mu	+15 m (PS3)	*Glycymeris* spp.	IE	E	
	G17-1a	LPA		Helicidae	IE/AAR	122.1±33.6 ky BP	MIS 5.5
	G17-2b	DMCU		*Glycymeris* sp.	IE	F	MIS 7
	G17-2b	DMCU		*Cladocora caespitosa*	U-Th	232.02±5.3 ky BP 211.97±3.6 ky BP	MIS 7.3
	G20-1	DMCU		*Hoplangia durotrix*	U-Th	208.44±5.3 ky BP	MIS 7.3
From Montagna Spaccata northwards	MS1-2	PS3mu	+15 m (PS3)	*Patella* spp.	IE	E	MIS 5.5
	MS1-1	PS3 wave-cut platform	+15 m (PS3)	*Hoplangia durotrix*	U-Th	213.39±3.0 ky BP 211.07±4.8 ky BP	MIS 7.3
	MS2-1	PS1mu	+6 m (PS1)	*T. latus*	IE	E	MIS 5.5
	MS6-1	PS1mu	+6 m (PS1)	*Patella* spp.	IE	E	MIS 5.5
	MS11-1	Undefined		*Cladocora caespitosa*	U-Th	223.84±7.2 ky BP 225.17±5.4 ky BP	MIS 7.3

TAB. 2B

Sample ID	Taxa	N	D-allo/L-Ile	D/L Asp	D/L Glu	D/L Leu	D/L Phe
G2-2a	*Candona neglecta*	5		0.357±0.031	0.144±0.025		
G4-1c	*Cyprideis torosa*	6		0.386±0.009	0.120±0.003		
G4-1d	*Glycymeris* sp.	5	0.389±0.082	0.567±0.105	0.437±0.055		
G4-1gly	*Glycymeris* sp.	6	0.359±0.047	0.581±0.010	0.438±0.016		
G17-1a	Helicidae-Pulmonata	6	0.387±0.058	0.484±0.064	0.344±0.043	0.353±0.026	0.517±0.080
G17-2b	*Glycymeris* sp.	6	0.486±0.062	0.729±0.038	0.553±0.059		
MS1-2	*Patella* spp	8	0.242±0.094	0.561±0.060	0.307±0.073		
MS6-1	*Patella* spp	3	0.224±0.005	0.543±0.011	0.341±0.023		
MS2-1	*T. latus*	2	0.496±0.129	0.619±0.049	0.483±0.093		

TAB. 2C

Sample ID	Taxa	N	[^{238}U] µg/g	[^{232}Th] ng/g	$\delta^{234}U_m$	(^{230}Th/^{238}U)	(^{230}Th/^{232}Th)	$\delta^{234}U_{(0)}$	Age (ky)	Age (ky)$_{corr}$
G17-2b	*Cladocora caespitosa*	1	2.591±0.021	39.240±0.320	107.24±1.02	1.00723±0.0021	202.90±0.43	206.60±3.67	237.71±2.6	232.02±5.3
		2	2.854±0.025	46.363±0.373	103.29±1.71	0.97192±0.0013	182.11±0.24	188.04±3.67	215.30±2.0	211.97±3.6
G20-1	*Hoplangia durotrix*	1	4.403±0.036	8.260±0.068	83.52±0.78	0.95114±0.0019	1544.11±3.05	150.54±2.65	215.64±1.9	208.44±5.3
MS1-1	*Hoplangia durotrix*	1	4.758±0.038	63.815±0.514	87.37±1.12	0.95613±0.0011	218.43±0.26	159.69±2.44	216.21±1.6	213.39±3.0
		1*	4.768±0.038	63.806±0.518	88.05±2.17	0.95331±0.0028	218.10±0.66	159.89±4.50	213.86±3.5	211.07±4.8
MS11-1	*Cladocora caespitosa*	1	3.146±0.029	58.340±0.476	95.67±3.66	0.98447±0.0016	161.68±0.26	180.11±7.80	230.14±4.3	223.84±7.2
		1*	3.150±0.025	59.480±0.481	91.65±0.96	0.98231±0.0018	158.71±0.30	173.19±3.21	231.83±2.3	225.17±5.4

Fig. 12

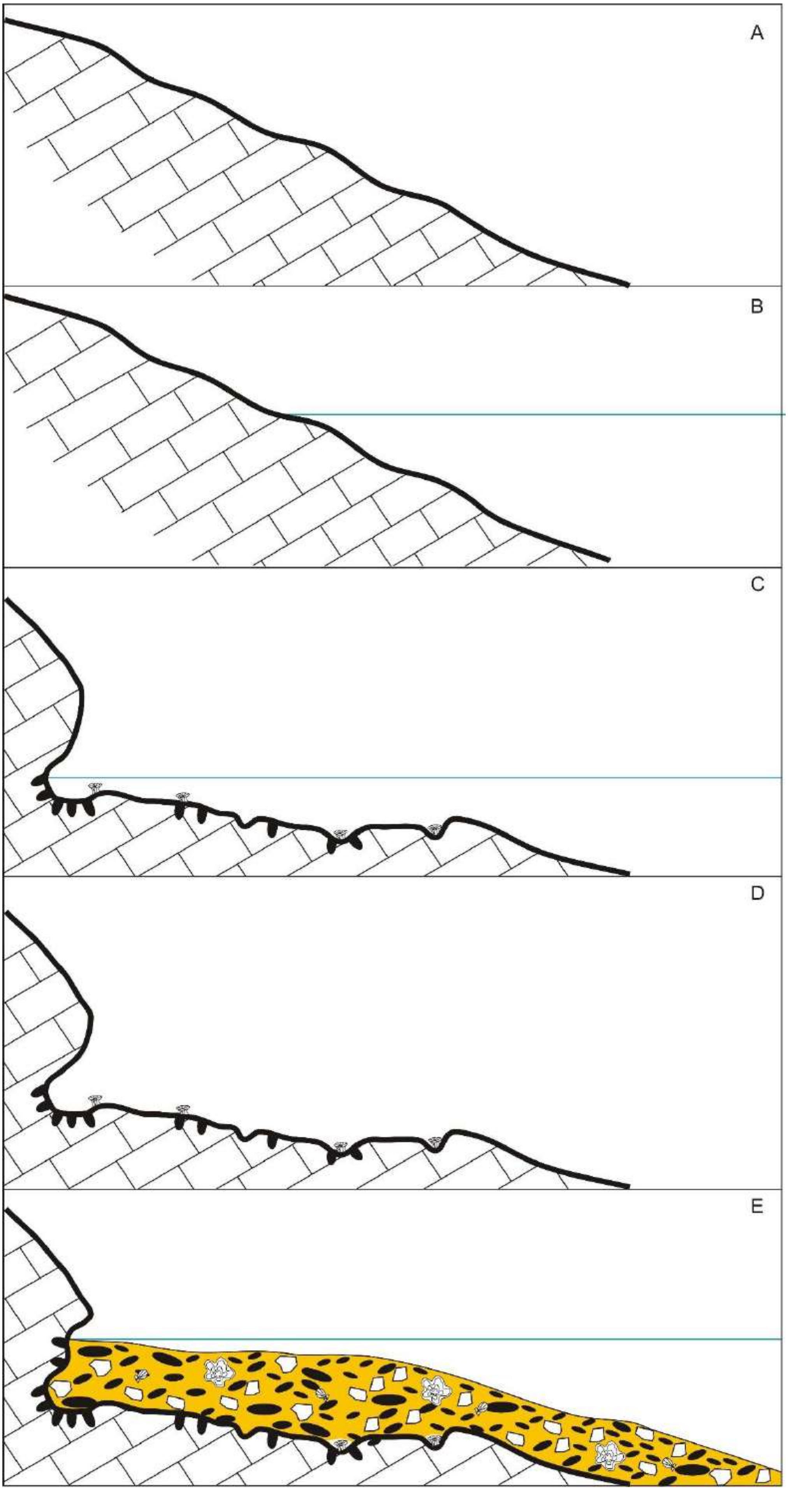

1703

Tab. 3

Ages of highstands (yrs); from Waelbroeck et al., 2002	Sea level relative to present sea level (m); from Waelbroeck et al., 2002	Expected highstand-palaeoshoreline elevations (m relative to present sea level)	DTM/field observed palaeoshoreline elevations (m) and our association with expected palaeoshorelines	Comments on our association between expected and observed palaeoshorelines	MIS
0	0	0	0		
30000	-80	-78		currently submerged	
50000	-60	-56		currently submerged	
76500	-30	-24		currently submerged	
100000	-25	-18		currently submerged	
115000	-21	-13		currently submerged	
120000	0	9	6/7.5	PS1 +PS2	5.5
127000	6	15	15	PS3	5.5
166000	-50	-37		currently submerged	6.5
196500	-10	5		overprinted	7.1
215000	-4	13	15	PS3 re-occupied by 127 ky BP highstand	7.3
235000	-12	7		overprinted	7.5
287000	-15	8		overprinted	8.5
303000	-15	4		overprinted	9.1
330000	5	32	22	PS4	9.3
410000	6	41	41	PS5	11
478000	0	41		re-occupied by 410 ky BP highstand	13.1
525000	20	65	62	PS6	13.3
550000	10	57		overprinted	15.1 (?)
560000	3	51		overprinted	15.1 (?)
590000	20	71	67	PS7	15.3 (?)

Fig. 13A, B

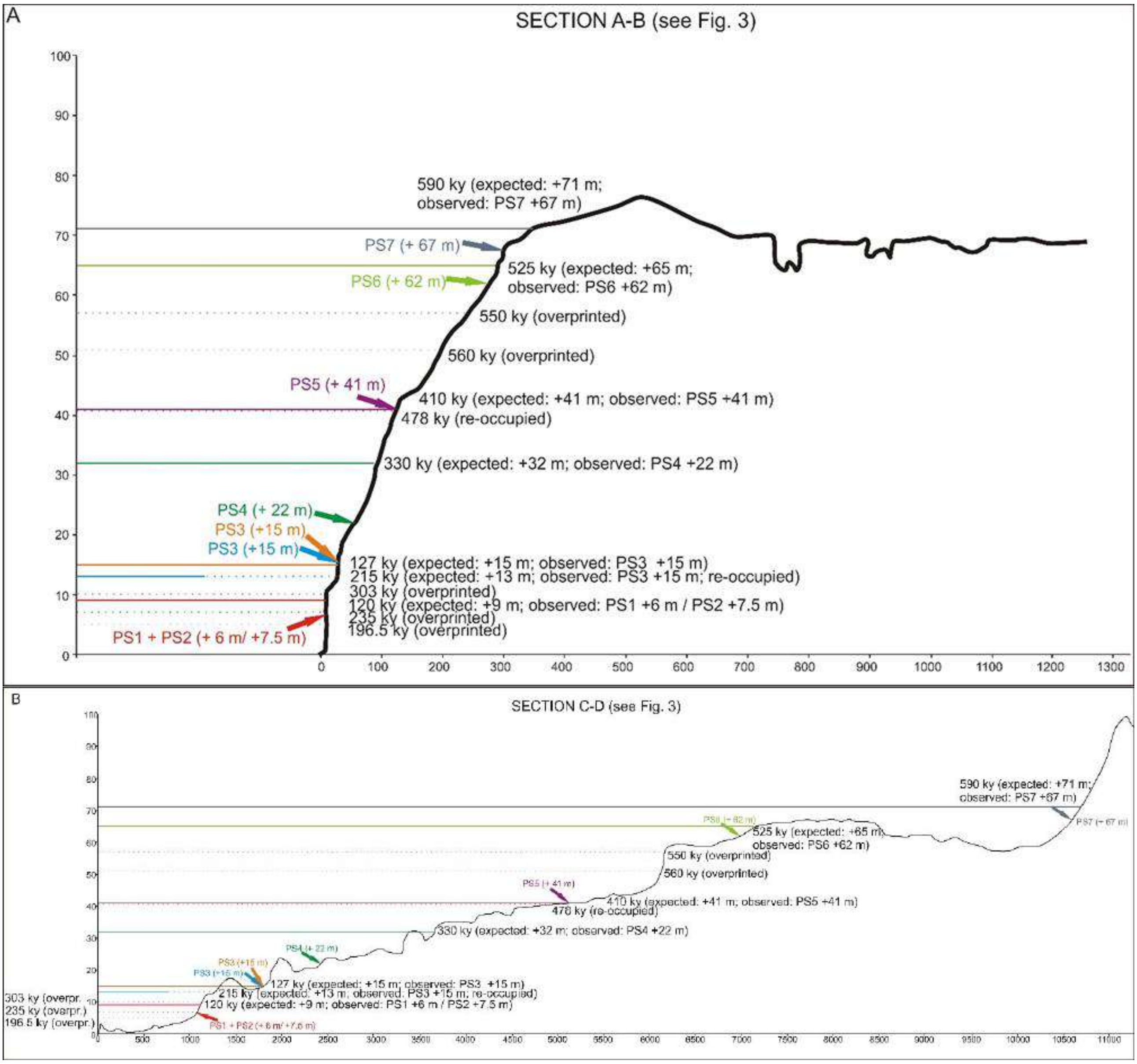
A
SECTION A-B (see Fig. 3)
590 ky (expected: +71 m;
observed: PS7 +67 m)
PS7 (+ 67 m)
525 ky (expected: +65 m;
observed: PS6 +62 m)
PS6 (+ 62 m)
550 ky (overprinted)
560 ky (overprinted)
PS5 (+ 41 m)
410 ky (expected: +41 m; observed: PS5 +41 m)
478 ky (re-occupied)
330 ky (expected: +32 m; observed: PS4 +22 m)
PS4 (+ 22 m)
PS3 (+15 m)
PS3 (+15 m)
127 ky (expected: +15 m; observed: PS3 +15 m)
215 ky (expected: +13 m; observed: PS3 +15 m; re-occupied)
303 ky (overprinted)
120 ky (expected: +9 m; observed: PS1 +6 m / PS2 +7.5 m)
235 ky (overprinted)
196.5 ky (overprinted)
PS1 + PS2 (+ 6 m/ +7.5 m)
B
SECTION C-D (see Fig. 3)
590 ky (expected: +71 m;
observed: PS7 +67 m)
525 ky (expected: +65 m;
observed: PS6 +62 m)
550 ky (overprinted)
560 ky (overprinted)
410 ky (expected: +41 m; observed: PS5 +41 m)
478 ky (re-occupied)
330 ky (expected: +32 m; observed: PS4 +22 m)
127 ky (expected: +15 m; observed: PS3 +15 m)
215 ky (expected: +13 m; observed: PS3 +15 m; re-occupied)
120 ky (expected: +9 m; observed: PS1 +6 m / PS2 +7.5 m)
303 ky (overpr.
235 ky (overpr.)
196.5 ky (overpr.)

Fig. 14

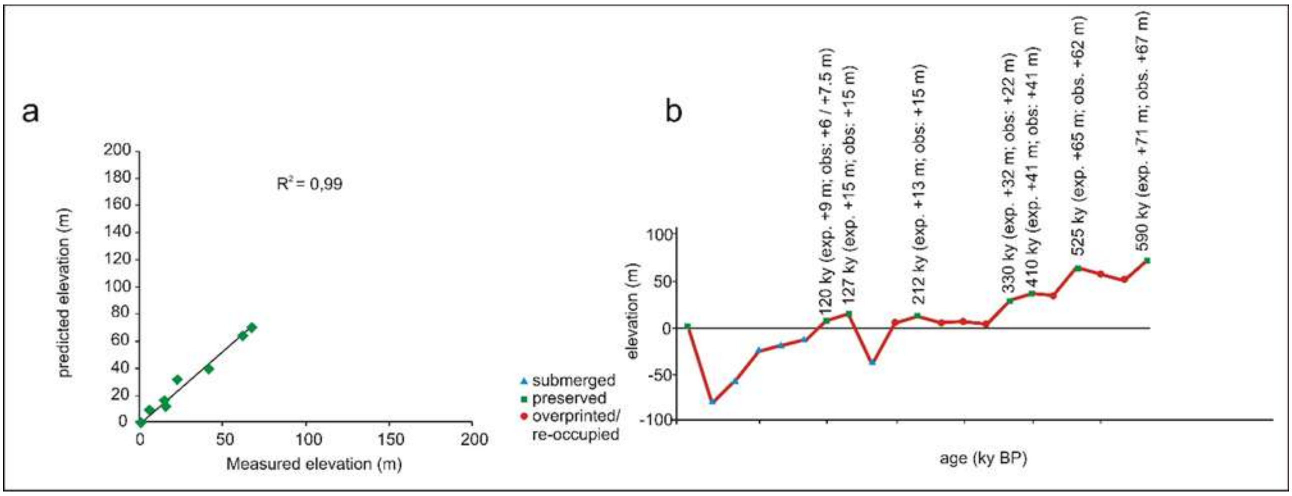

a
R² = 0,99
predicted elevation (m)
Measured elevation (m)
0
20
40
60
80
100
120
140
160
180
200
50
100
150
b
120 ky (exp. +9 m; obs: +6 / +7.5 m)
127 ky (exp. +15 m; obs: +15 m)
212 ky (exp. +13 m; obs: +15 m)
330 ky (exp. +32 m; obs: +22 m)
410 ky (exp. +41 m; obs: +41 m)
525 ky (exp. +65 m; obs. +62 m)
590 ky (exp. +71 m; obs. +67 m)
elevation (m)
-100
-50
submerged
preserved
overprinted/
re-occupied
age (ky BP)

Tab. 4

AREA	NUMBER OF PALAEOSHORELINE RECOGNISED	AGES (ky BP)	UPLIFT RATES (mm/y)	REFERENCES
Vibo Valentia (Tyrrhenian coast of the Calabria region, southern Italy)	11	50, 76.5, 100, 125, 178, 200, 217, 240, 285, 310, 340	between 0.4 and 1.75	Roberts et al., 2013
Capo D'Orlando (Tyrrhenian coast of the Sicilia region, southern Italy)	10	76.5, 100, 125, 178, 200, 217, 240, 285, 310, 340	between 0.4 and 0.89	Meschis et al., 2018
SE Sicily, along the Ionian coastal sector	9	119, 125, 200, 240, 310, 340, 410, 478, 525	between 0.16 and 0.41	Meschis et al., 2020
SW Sicily	11	82, 103, 124, 167, 197, 215, 236, 287, 313, 331, 406	between 0.46 and 0.82	Ferranti et al., 2021
Ionian coast of southern Italy	18	5-10, 30-35, 45-50, 55-65, 70-80, 80-85, 85-95, 10-105, 115-125, 165-180, 185-200, 225-240, 280-295, 305-315, 320-335, 390-410, 480-500, 570-590	between 0.2 and 2	Caputo et al., 2010
South Crete (Greece)	9	76.5, 100, 125, 175, 200, 240, 310, 340, 410	between 0.24 and 0.89	Robertson et al., 2019
Gulf of Corinth (Greece)	8	76, (possibly) 100, 125, 175, 200, 216, 240, 340	between 0.15 and 0.51	Roberts et al., 2009

Table 1

PALAEOSHORELINE	ASSOCIATED DEPOSITS	UNITS OF MIXED DEPOSITS (if has been possible to define them)	LANDFORMS IN THE SECTOR FROM BROKEN MOUNTAIN NORTHWARDS	LANDFORMS IN THE SECTOR SOUTH OF BROKEN MOUNTAIN
PS1 (+6 m)	PS1 marine unit (PS1mu)		Band of lithophagid borings	Band of lithophagid borings
PS2 (+7 m)	PS2 marine unit (PS2mu)		Band of lithophagid borings	Band of lithophagid borings
PS3 (+15 m)	PS3 Mixed Deposit (PS3-MD)	PS3 marine unit (PS3mu), Aeolian Unit 1 (AU1), Aeolian Unit 2 (AU2)	Band of lithophagid borings, tidal notches, wave-cut platform	*Monte-Crocefisso* palaeo littoral ridge (IMClr); *Carmine-Li Foggi* palaeo littoral ridge
PS4 (+22 m)	PS4 Mixed Deposit (PS4-MD)		Band of lithophagid borings, sea caves; patches of marine syn-wave cut platform deposits	Small and discontinuous relict littoral ridges with aeolian deposits
PS5 (+41 m)	PS5 Marine Deposit (PS5-MaD)		Band of lithophagid borings,	Band of lithophagid borings (near San Mauro abbey); marine terraced deposit less than 1 km^2 wide
PS6 (+62 m), PS7 (+67 m)			Band of lithophagid borings	Morphological inner edges

Table 2 Click here to access/download;Table (Editable version);Table 2.docx

TAB. 2A							
	Sample ID/site	**Unit**	**Palaeoshore line**	**Material for chronological analyses**	**Type of analysis**	**Age/Aminozone**	**Stage**
South of Montagna Spaccata	G2-2a	YS		ostracod	AAR	137.2±29.3 ky BP	MIS 6-5.5
	G4-1c	LS		ostracod	AAR	138.4±17.9 ky BP	MIS 6-5.5
	G4-1b	LS		ostracod	AAR	118.1±17.9 ky BP	
	G4-1d	PS3mu	+15 m (PS3)	*Glycymeris* spp.	IE	E	MIS 5.5
	G4-1gly	PS3mu	+15 m (PS3)	*Glycymeris* spp.	IE	E	
	G17-1a	LPA		Helicidae	IE/AAR	122.1±33.6 ky BP	MIS 5.5
	G17-2b	DMCU		*Glycymeris* sp.	IE	F	MIS 7
	G17-2b	DMCU		*Cladocora caespitosa*	U-Th	232.02±5.3 ky BP 211.97±3.6 ky BP	MIS 7.3
	G20-1	DMCU		*Hoplangia durotrix*	U-Th	208.44±5.3 ky BP	MIS 7.3
From Montagna Spaccata northwards	MS1-2	PS3mu	+15 m (PS3)	*Patella* spp.	IE	E	MIS 5.5
	MS1-1	PS3 wave-cut platform	+15 m (PS3)	*Hoplangia durotrix*	U-Th	213.39±3.0 ky BP 211.07±4.8 ky BP	MIS 7.3
	MS2-1	PS1mu	+6 m (PS1)	*T. latus*	IE	E	MIS 5.5
	MS6-1	PS1mu	+6 m (PS1)	*Patella* spp.	IE	E	MIS 5.5
	MS11-1	Undefined		*Cladocora caespitosa*	U-Th	223.84±7.2 ky BP 225.17±5.4 ky BP	MIS 7.3

TAB. 2B							
Sample ID	**Taxa**	**N**	**D-allo/L-Ile**	**D/L Asp**	**D/L Glu**	**D/L Leu**	**D/L Phe**
G2-2a	*Candona neglecta*	5		0.357±0.031	0.144±0.025		
G4-1c	*Cyprideis torosa*	6		0.386±0.009	0.120±0.003		
G4-1d	*Glycymeris* sp.	5	0.389±0.082	0.567±0.105	0.437±0.055		
G4-1gly	*Glycymeris* sp.	6	0.359±0.047	0.581±0.010	0.438±0.016		
G17-1a	Helicidae-Pulmonata	6	0.387±0.058	0.484±0.064	0.344±0.043	0.353±0.026	0.517±0.080
G17-2b	*Glycymeris* sp.	6	0.486±0.062	0.729±0.038	0.553±0.059		
MS1-2	*Patella* spp	8	0.242±0.094	0.561±0.060	0.307±0.073		
MS6-1	*Patella* spp	3	0.224±0.005	0.543±0.011	0.341±0.023		
MS2-1	*T. latus*	2	0.496±0.129	0.619±0.049	0.483±0.093		

TAB. 2C										
Sample ID	**Taxa**	**N**	**[^{238}U] µg/g**	**[^{232}Th] ng/g**	**$\delta^{234}U_m$**	**(^{230}Th/^{238}U)**	**(^{230}Th/^{232}Th)**	**$\delta^{234}U_{(0)}$**	**Age (ky)**	**Age (ky)$_{corr}$**
G17-2b	*Cladocora caespitosa*	1	2.591±0.021	39.240±0.320	107.24±1.02	1.00723±0.0021	202.90±0.43	206.60±3.67	237.71±2.6	232.02±5.3
		2	2.854±0.025	46.363±0.373	103.29±1.71	0.97192±0.0013	182.11±0.24	188.04±3.67	215.30±2.0	211.97±3.6
G20-1	*Hoplangia durotrix*	1	4.403±0.036	8.260±0.068	83.52±0.78	0.95114±0.0019	1544.11±3.05	150.54±2.65	215.64±1.9	208.44±5.3
MS1-1	*Hoplangia durotrix*	1	4.758±0.038	63.815±0.514	87.37±1.12	0.95613±0.0011	218.43±0.26	159.69±2.44	216.21±1.6	213.39±3.0
		1*	4.768±0.038	63.806±0.518	88.05±2.17	0.95331±0.0028	218.10±0.66	159.89±4.50	213.86±3.5	211.07±4.8
MS11-1	*Cladocora caespitosa*	1	3.146±0.029	58.340±0.476	95.67±3.66	0.98447±0.0016	161.68±0.26	180.11±7.80	230.14±4.3	223.84±7.2
		1*	3.150±0.025	59.480±0.481	91.65±0.96	0.98231±0.0018	158.71±0.30	173.19±3.21	231.83±2.3	225.17±5.4

Table 3

Ages of highstands (yrs); from Waelbroeck et al. (2002) and Rohling et al. (2014)	Sea level relative to present sea level (m); from Waelbroeck et al. (2002) and Rohling et al. (2014)	Expected highstand-palaeoshoreline elevations (m relative to present sea level)	DTM/field observed palaeoshoreline elevations (m) and our association with expected palaeoshorelines	Comments on our association between expected and observed palaeoshorelines	MIS
0	0	0	0		
30000	-80	-78		currently submerged	
50000	-60	-56		currently submerged	
76500	-30	-24		currently submerged	
100000	-25	-18		currently submerged	
115000	-21	-13		currently submerged	
120000	0	9	6/7.5	PS1 +PS2	5.5
127000	6	15	15	PS3	5.5
166000	-50	-37		currently submerged	6.5
196500	-10	5		overprinted	7.1
215000	-4	13	15	PS3 re-occupied by 127 ky BP highstand	7.3
235000	-12	7		overprinted	7.5
287000	-15	8		overprinted	8.5
303000	-15	4		overprinted	9.1
330000	5	32	22	PS4	9.3
410000	6	41	41	PS5	11
478000	0	41		re-occupied by 410 ky BP highstand	13.1
525000	20	65	62	PS6	13.3
550000	10	57		overprinted	15.1 (?)
560000	3	51		overprinted	15.1 (?)
590000	20	71	67	PS7	15.3 (?)

Table 4

AREA	NUMBER OF PALAEOSHORELINE RECOGNISED	AGES (ky BP)	UPLIFT RATES (mm/y)	REFERENCES
Vibo Valentia (Tyrrhenian coast of the Calabria region, southern Italy)	11	50, 76.5, 100, 125, 178, 200, 217, 240, 285, 310, 340	between 0.4 and 1.75	Roberts et al., 2013
Capo D'Orlando (Tyrrhenian coast of the Sicilia region, southern Italy)	10	76.5, 100, 125, 178, 200, 217, 240, 285, 310, 340	between 0.4 and 0.89	Meschis et al., 2018
SE Sicily, along the Ionian coastal sector	9	119, 125, 200, 240, 310, 340, 410, 478, 525	between 0.16 and 0.41	Meschis et al., 2020
SW Sicily	11	82, 103, 124, 167, 197, 215, 236, 287, 313, 331, 406	between 0.46 and 0.82	Ferranti et al., 2021
Ionian coast of southern Italy	18	5-10, 30-35, 45-50, 55-65, 70-80, 80-85, 85-95, 10-105, 115-125, 165-180, 185-200, 225-240, 280-295, 305-315, 320-335, 390-410, 480-500, 570-590	between 0.2 and 2	Caputo et al., 2010
South Crete (Greece)	9	76.5, 100, 125, 175, 200, 240, 310, 340, 410	between 0.24 and 0.89	Robertson et al., 2019
Gulf of Corinth (Greece)	8	76, (possibly) 100, 125, 175, 200, 216, 240, 340	between 0.15 and 0.51	Roberts et al., 2009

Figure 1 Click here to access/download;Figure (Color);Fig. 1.jpg

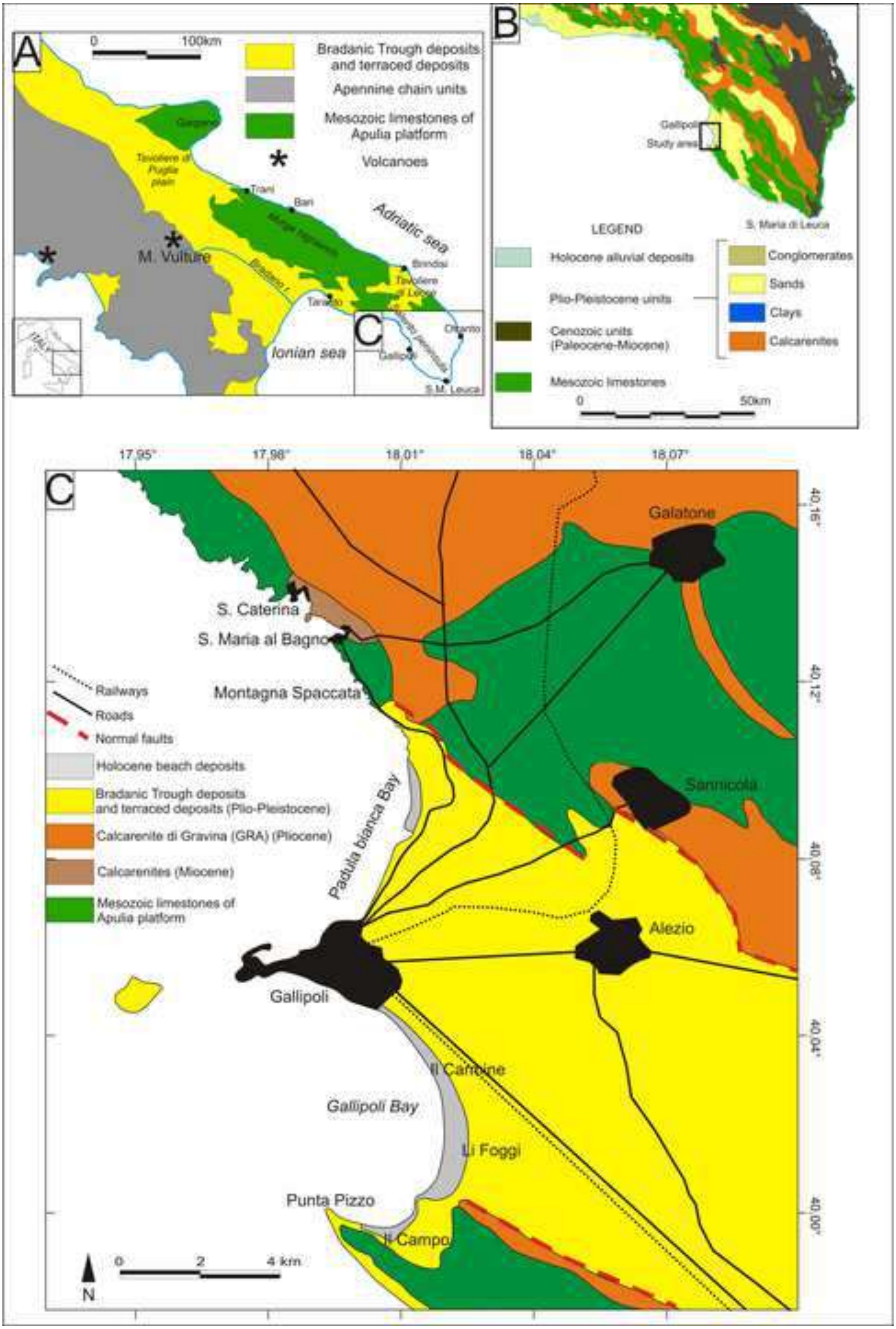

Figure 2

Click here to access/download;Figure (Color);Fig. 2.jpg

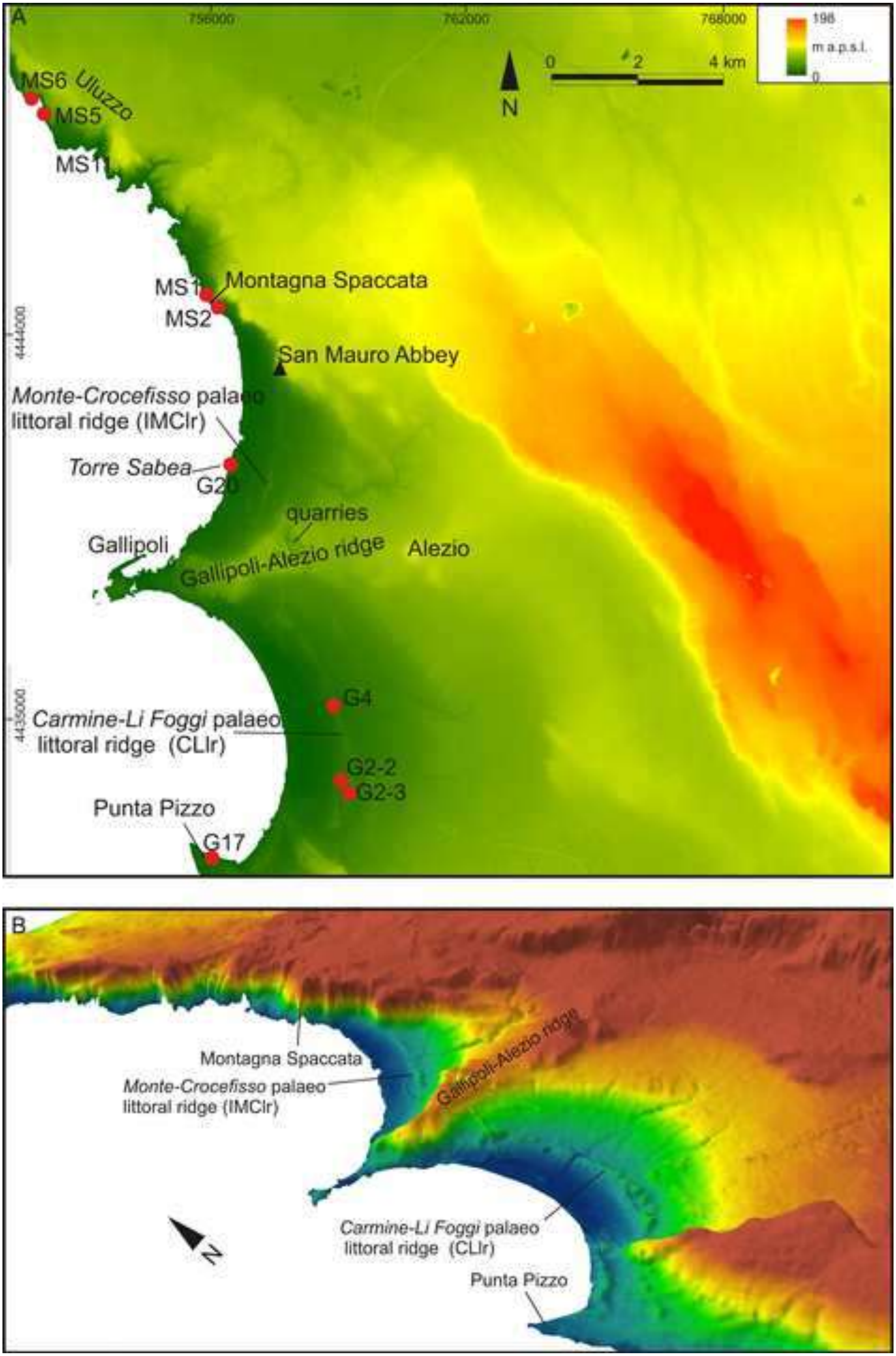

Figure 3

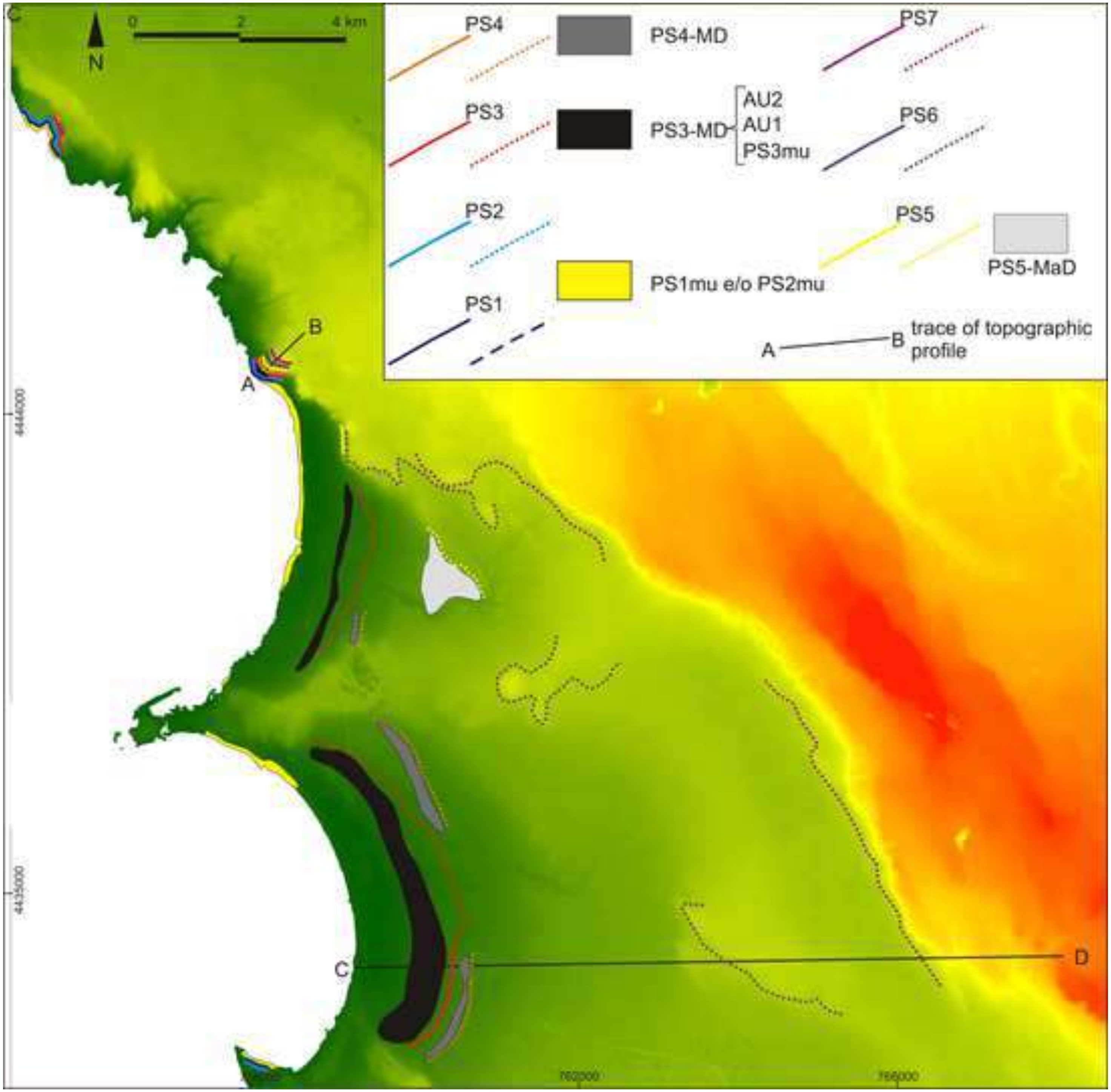
0
2
4 km
N
PS4
PS4-MD
PS7
PS3
PS3-MD
AU2
AU1
PS3mu
PS6
PS2
PS5
PS5-MaD
PS1mu e/o PS2mu
PS1
A
B
trace of topographic profile
C
D

Figure 4 Click here to access/download;Figure (Color);Fig. 4.jpg

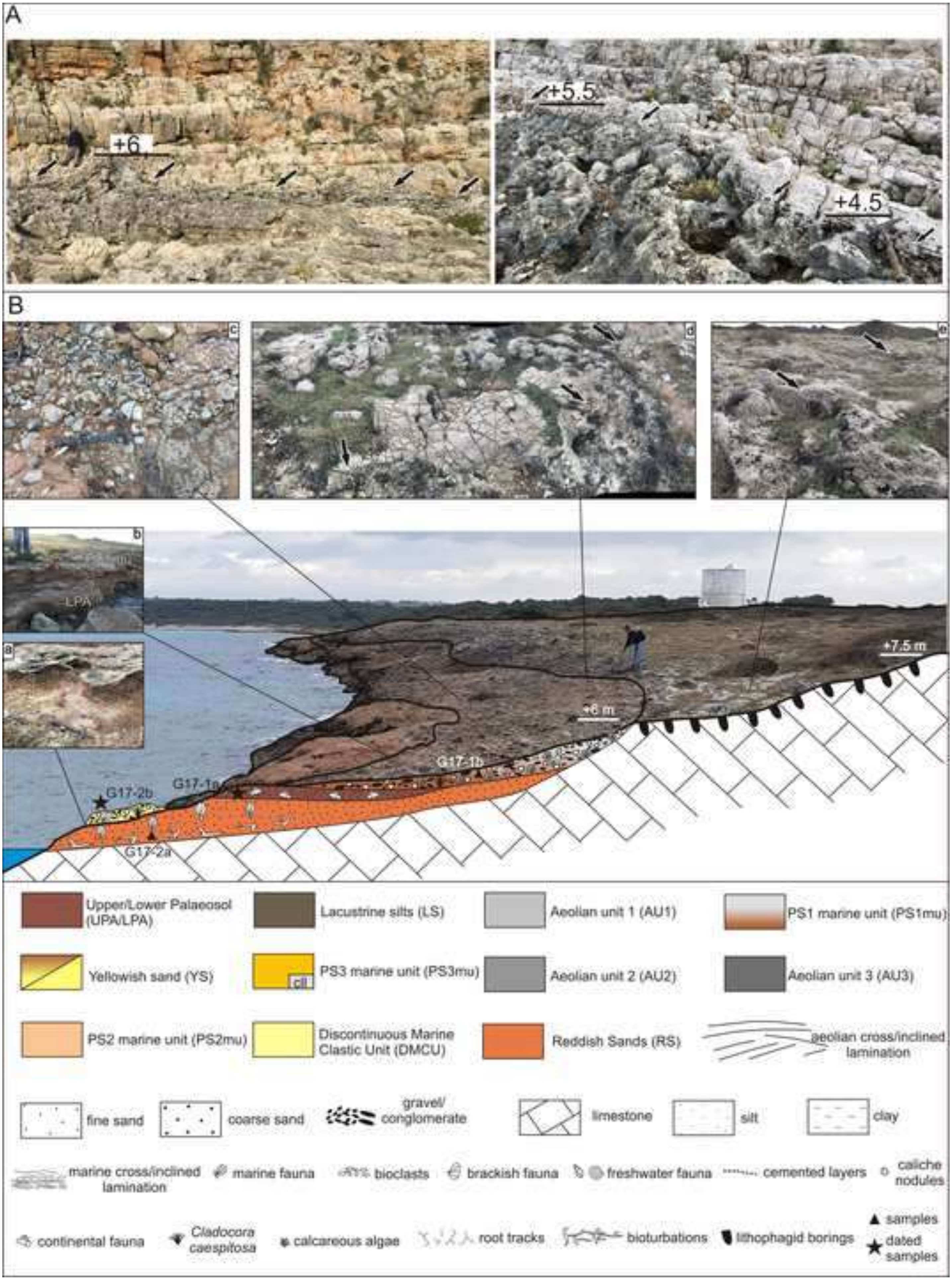

Figure 5


A
+15
B
ML
br
br
br
+15
PS3mu
br
MS1-2
ML
ML
d
c
PS3mu
MS1-1
ML

Figure 7

Click here to access/download;Figure (Color);Fig. 7.jpg

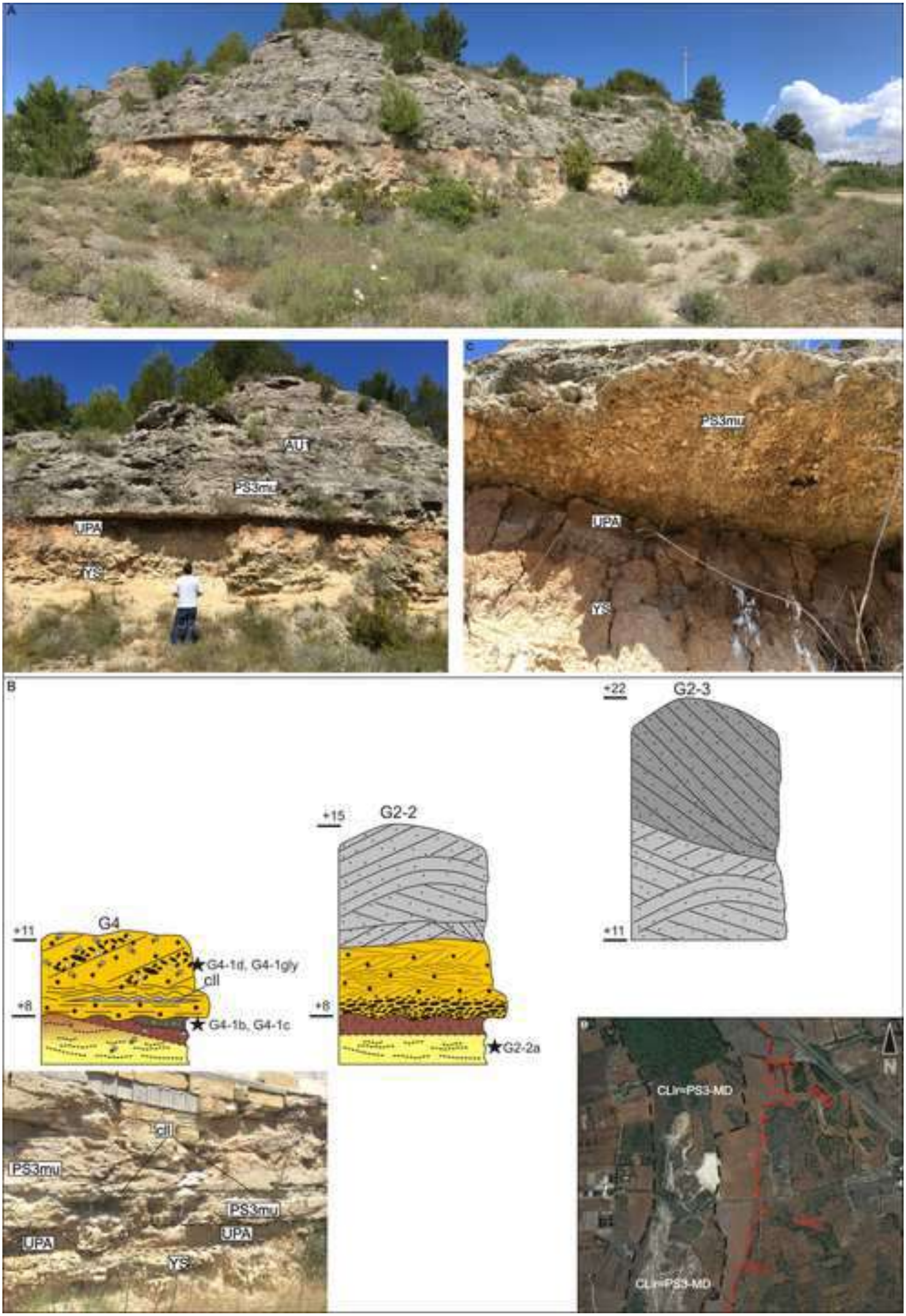

Figure 8 Click here to access/download;Figure (Color);Fig. 8.jpg

Figure 9

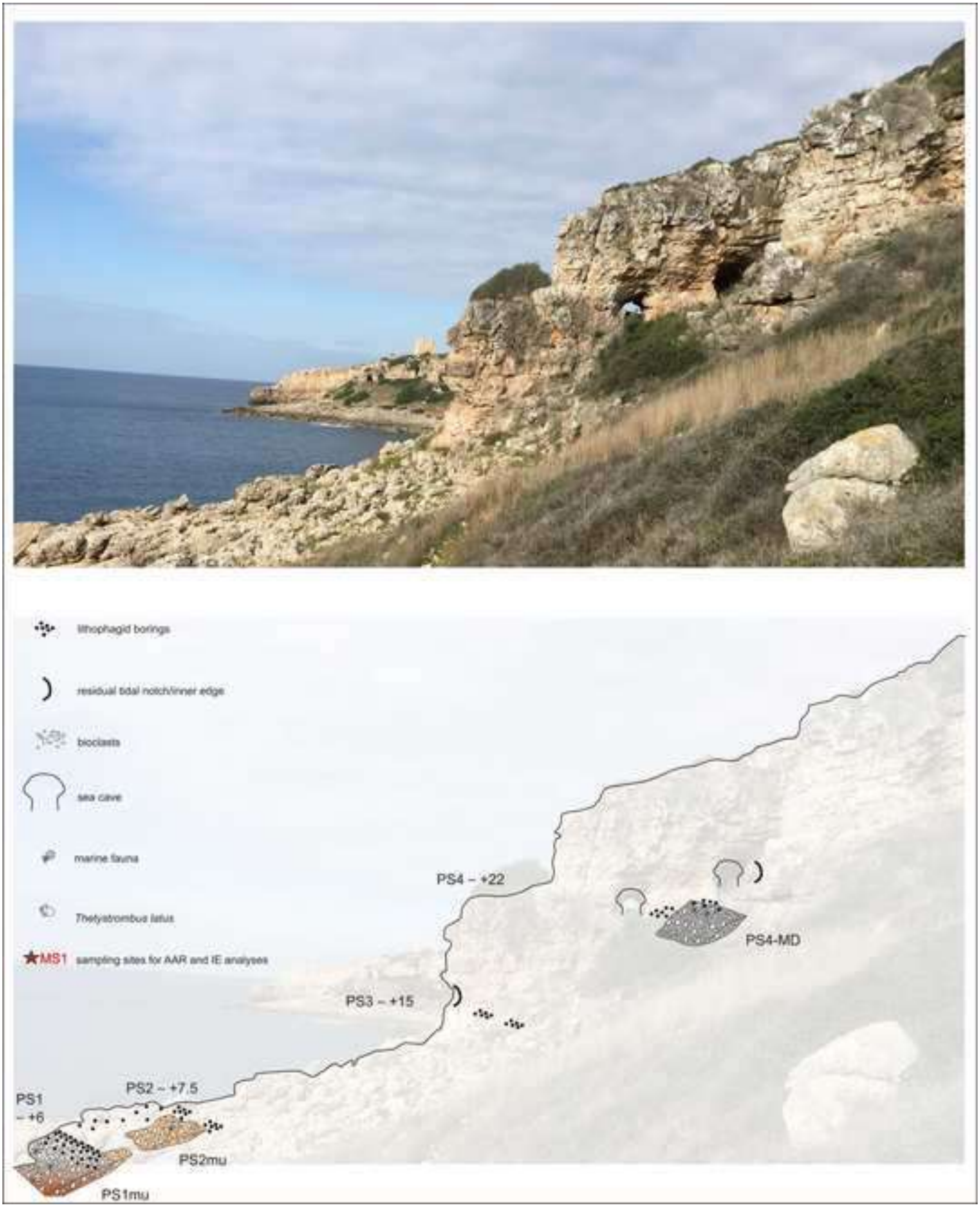
lithophagid borings
residual tidal notch/inner edge
bioclasts
sea cave
marine fauna
Thetystrombus latus
MS1 sampling sites for AAR and IE analyses
PS4 – +22
PS4-MD
PS3 – +15
PS2 – +7.5
PS1
– +6
PS2mu
PS1mu

Figure 10

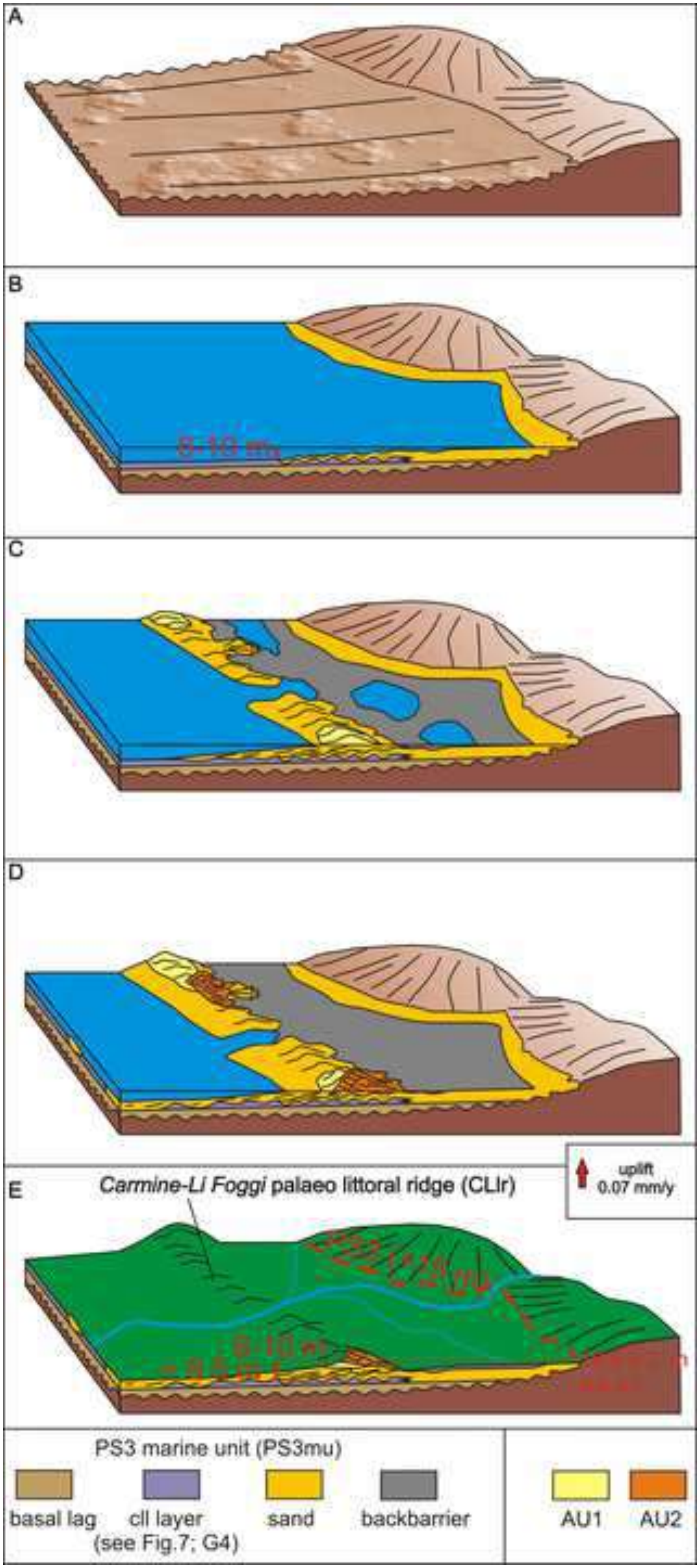
A
B
C
D
E
Carmine-Li Foggi palaeo littoral ridge (CLIr)
uplift
0.07 mm/y
PS3 marine unit (PS3mu)
basal lag
cll layer
(see Fig.7; G4)
sand
backbarrier
AU1
AU2

Figure 12

Click here to access/download;Figure (Color);Fig. 12.jpg

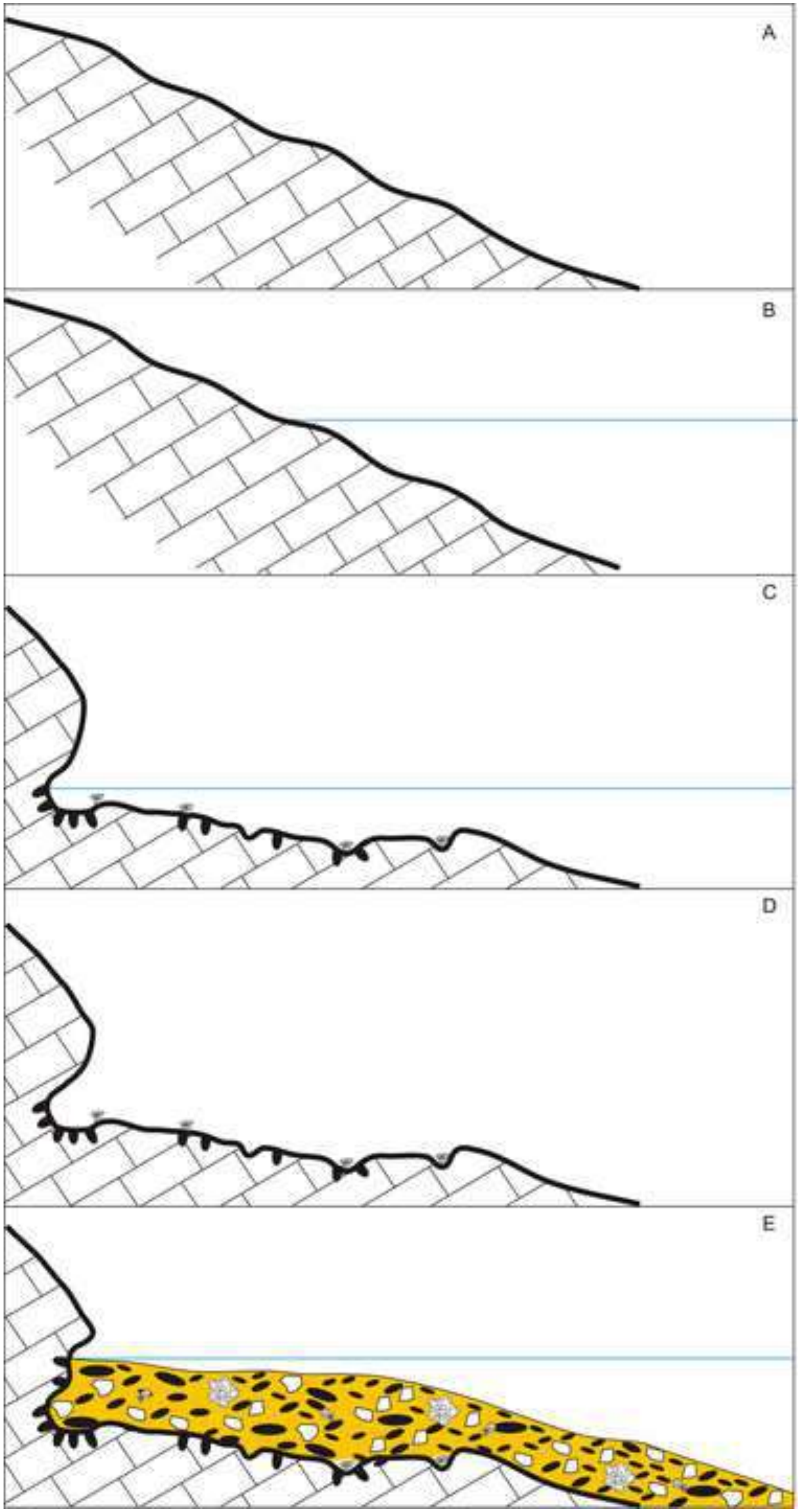

Figure 13A

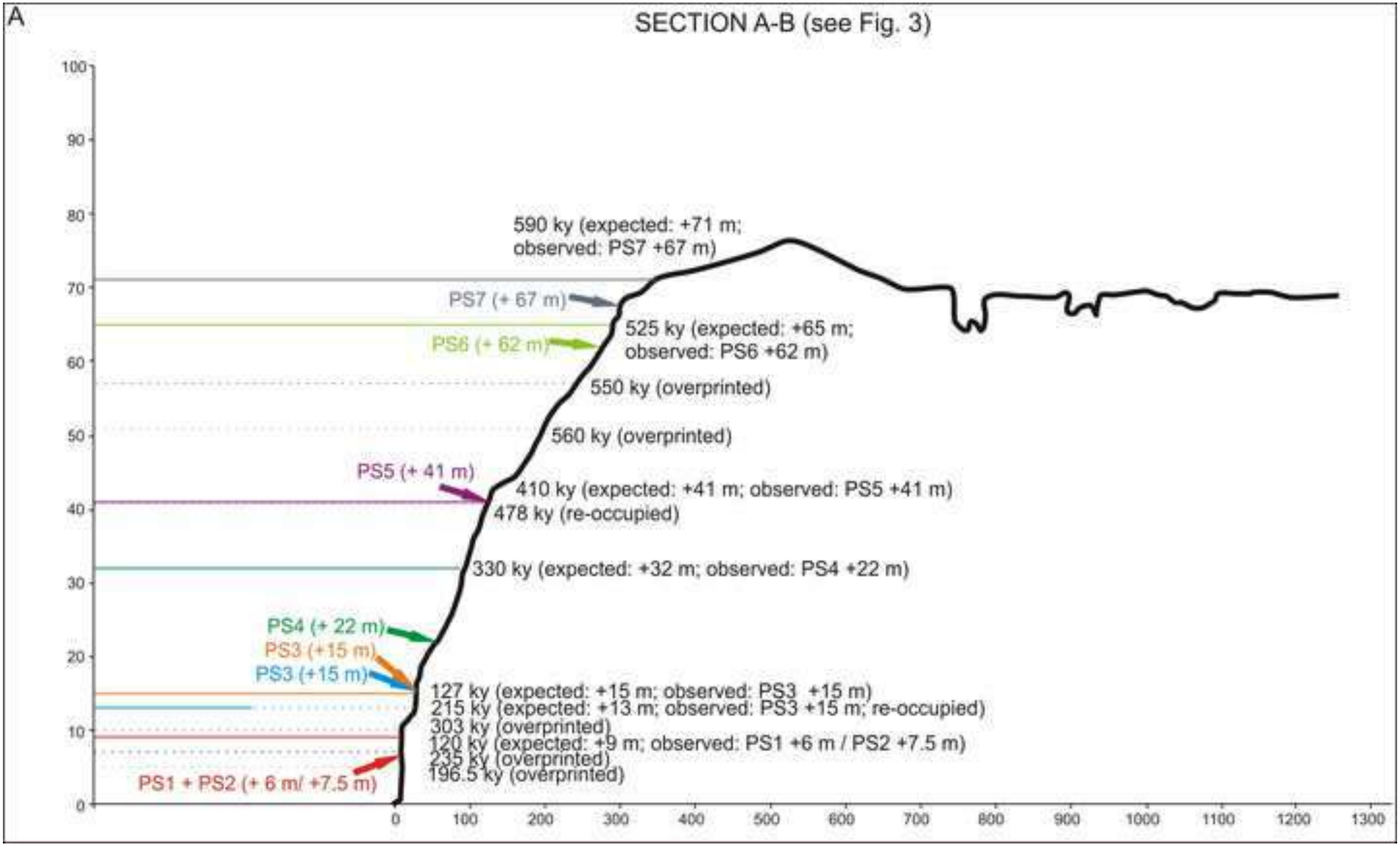
A
SECTION A-B (see Fig. 3)
100
90
80
70
60
50
40
30
20
10
0
0
100
200
300
400
500
600
700
800
900
1000
1100
1200
1300
590 ky (expected: +71 m;
observed: PS7 +67 m)
PS7 (+ 67 m)
525 ky (expected: +65 m;
observed: PS6 +62 m)
PS6 (+ 62 m)
550 ky (overprinted)
560 ky (overprinted)
PS5 (+ 41 m)
410 ky (expected: +41 m; observed: PS5 +41 m)
478 ky (re-occupied)
330 ky (expected: +32 m; observed: PS4 +22 m)
PS4 (+ 22 m)
PS3 (+15 m)
PS3 (+15 m)
127 ky (expected: +15 m; observed: PS3 +15 m)
215 ky (expected: +13 m; observed: PS3 +15 m; re-occupied)
303 ky (overprinted)
120 ky (expected: +9 m; observed: PS1 +6 m / PS2 +7.5 m)
235 ky (overprinted)
196.5 ky (overprinted)
PS1 + PS2 (+ 6 m/ +7.5 m)

Figure 13B

Click here to access/download;Figure (Color);Fig. 13B.jpg

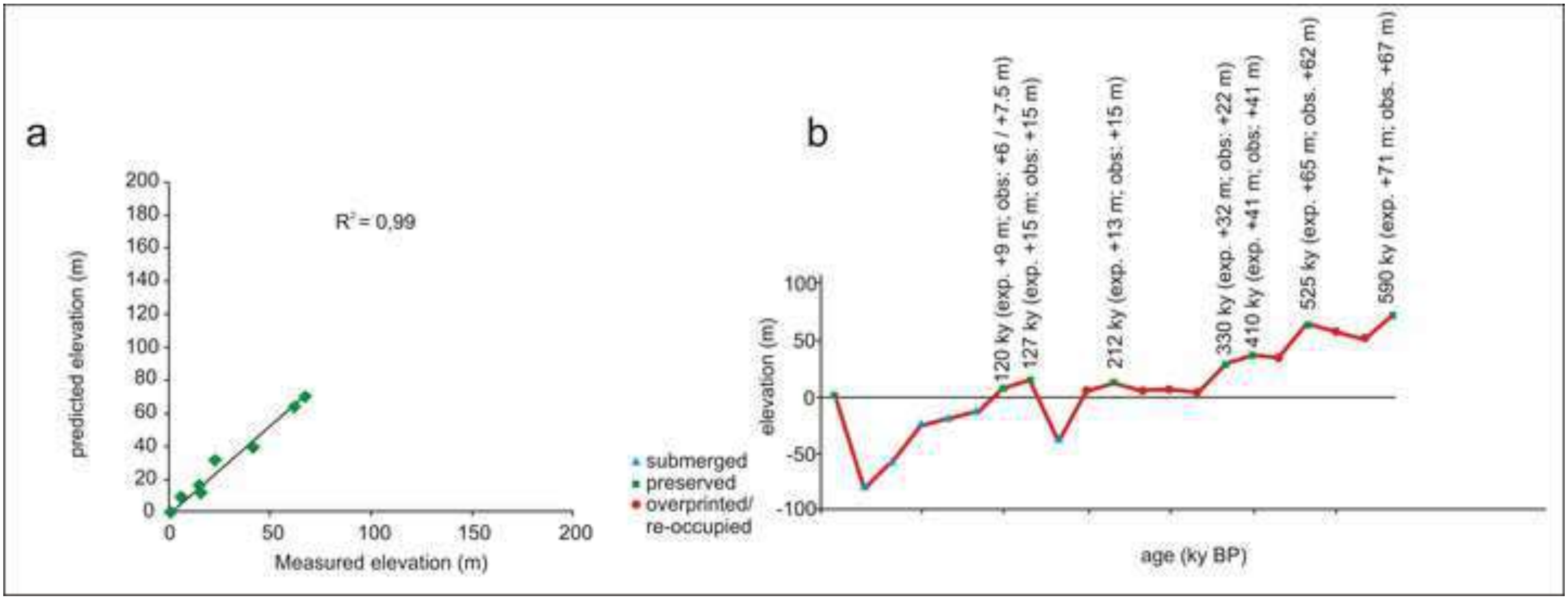

a
200
180
160
140
120
100
80
60
40
20
0
predicted elevation (m)
R² = 0,99
0
50
100
150
200
Measured elevation (m)
submerged
preserved
overprinted/
re-occupied
b
100
50
0
-50
-100
elevation (m)
age (ky BP)
120 ky (exp. +9 m; obs: +6 / +7.5 m)
127 ky (exp. +15 m; obs: +15 m)
212 ky (exp. +13 m; obs: +15 m)
330 ky (exp. +32 m; obs: +22 m)
410 ky (exp. +41 m; obs: +41 m)
525 ky (exp. +65 m; obs. +62 m)
590 ky (exp. +71 m; obs. +67 m)

Declaration of interests

☒The authors declare that they have no known competing financial interests or personal relationships that could have appeared to influence the work reported in this paper.

☐The authors declare the following financial interests/personal relationships which may be considered as potential competing interests: